



University of Zagreb

FACULTY OF SCIENCE
DEPARTMENT OF BIOLOGY

Ana Vujić

**Targeting DNA methylation and histone
modifications using CRISPR/dCas9
tools in the regulation of
glycosyltransferases gene expression
of HepG2 cells**

DOCTORAL THESIS

Mentor: Professor Vlatka Zoldoš, PhD

Zagreb, 2025



Sveučilište u Zagrebu

PRIRODOSLOVNO-MATEMATIČKI FAKULTET

BIOLOŠKI ODSJEK

Ana Vujić

**Promjena epigenetičkih modifikacija
DNA i histona upotrebom alata
CRISPR/dCas9 u istraživanju regulacije
gena za glikoziltransferaze u stanicama
HepG2**

DOKTORSKI RAD

Mentor: prof. dr. sc. Vlatka Zoldoš

Zagreb, 2025.

The work presented in this doctoral thesis was performed at the Division of Molecular Biology, Department of Biology, Faculty of Science, University of Zagreb, under the supervision of professor Vlatka Zoldoš as a part of postgraduate program in Biology at the Department of Biology, Faculty of Science, University of Zagreb.

Ovaj doktorski rad je izrađen na Zavodu za molekularnu biologiju Biološkog odsjeka Prirodoslovno-matematičkog fakulteta Sveučilišta u Zagrebu pod vodstvom prof. dr. sc. Vlatke Zoldoš u sklopu Sveučilišnog poslijediplomskog studija Biologije pri Biološkom odsjeku Prirodoslovno-matematičkog fakulteta Sveučilišta u Zagrebu.

Professor Vlatka Zoldoš, PhD is a full professor of Genetics, Epigenetics, and Molecular Cytogenetics at the Faculty of Science, University of Zagreb. She earned her doctoral degree within the framework of a collaborative Croatian-French dual mentorship program between the University of Zagreb and the University of Paris XI South, France. In 2007, she established the Laboratory for Epigenetics within the Department of Molecular Biology, which became a part of the Centre of Scientific Excellence in Personalized Healthcare in 2017. She is recognized as a pioneer in epigenetic research which uses cutting-edge CRISPR/dCas9 methodology for precise epigenome editing. Notably, in 2016, together with her research team, she was the first to develop CRISPR/dCas9-DNMT3A, a molecular tool designed for precise DNA methylation. Her primary research focus lies in understanding the intricate interactions between epigenetic mechanisms in the regulation of gene expression. Additionally, a significant part of her research is dedicated to investigating the epigenetic regulation of IgG glycosylation, with specific emphasis on how genetic and epigenetic dysregulation of this process contributes to the development of complex diseases such as chronic inflammation, diabetes, and cancer.

Professor Zoldoš has an extensive publication record, with over 50 scientific papers in high-impact international journals including Nature Communications, Nature Reviews Gastroenterology and Hepatology, Nucleic Acids Research, Current Opinion in Chemical Biology, and Epigenetics. Her work has been cited 2836 times (*h*-index 26), underscoring its significant influence in the field. Furthermore, she serves as an editor for several renowned scientific journals in the field. Her leadership and expertise are evident in her involvement in numerous projects. She has led or participated in 11 EU projects under FP7 and Horizon 2020 frameworks, as well as projects funded by EU structural funds, 2 bilateral projects, and 7 national projects (MZOS and HRZZ). She mentored 15 doctoral thesis and over 20 master's thesis.

ZAHVALE

Hvala mojoj mentorici, profesorici Vlatki Zoldoš, što mi je omogućila da budem dio istraživačke grupe laboratorija za Epigenetiku i u njoj napravim svoje prve znanstvene korake. Hvala na svim pruženim prilikama, na korisnim savjetima, ali i konstruktivnim kritikama. Hvala na potpori i motivaciji i što ste uvijek rado sa mnom dijelili svoju ljubav prema znanosti.

Veliko hvala mojoj Mariji na velikoj podršci i pomoći pri izradi ove doktorske disertacije i što je sa mnom nesebično dijelila svoje znanje, vrijeme i laboratorijske vještine još od izrade mog diplomskog rada. Hvala na svim savjetima i motivacijskim razgovorima, ali i smijehu uz koji su dugi sati u labosu prolazili puno brže.

Hvala mojim dragim kolegama iz grupe Goranu, Franu, Vedrani (mojoj Kokici), Niki, Karlu i Aleksandru na pomoći, podršci, na razgovorima, druženjima i smijehu.

Posebno hvala mojoj Aniki, što mi je uvijek prvo bila prijateljica, a tek onda kolegica. Hvala ti što si moja zagrebačka obitelj.

Veliko hvala svim mojim prijateljima koji su uvijek tu za mene kad mi je najteže, onima koji su sa mnom još od đачkih klupa do onih koji me prate od fakultetskih dana. Svatko od vas je na poseban način obogatio moj život i prava je sreća dijeliti s vama svoje uspjehe.

Najveće hvala mojoj obitelji, mami Zorici, tati Grgi i sestri Sofiji. Nijedno hvala koje napišem ne može zaista izraziti moju zahvalnost na bezuvjetnoj podršci i ljubavi koju mi pružate. Uz vas je svaki uspjeh sto puta ljepši, a svaka prepreka sto puta lakša.

University of Zagreb

Doctoral thesis

Faculty of Science

Department of Biology

TARGETING DNA METHYLATION AND HISTONE MODIFICATIONS USING
CRISPR/dCas9 TOOLS IN THE REGULATION OF GLYCOSYLTRANSFERASES GENE
EXPRESSION OF HEPG2 CELLS

ANA VUJIĆ

Faculty of Science, University of Zagreb

A complex gene-network comprising around 800 genes is involved in protein *N*-glycosylation, yet the regulatory mechanisms governing their contribution to the formation of complex *N*-glycome remain understudied. While genetic factors clearly influence glycosylation, environmental components mediated by epigenetic mechanisms play an even more prominent role. This research leveraged the precision of the CRISPR/dCas9 epigenome editing tools to investigate the role of DNA methylation and histone modifications in regulation of genes (*B4GALT1*, *FUT8*, *ST6GAL1*, *MGAT4A*, *MGAT4B*, *MGAT5*, *MGAT3*) encoding for glycosyltransferases involved in formation of complex *N*-glycans. Induced promoter methylation changes by DNMT3A-dCas9 and TET1-dCas9 altered transcriptional activity of all genes, with resulting changes in HepG2 total cell *N*-glycome, indicating regulatory role of DNA methylation in protein *N*-glycosylation. Additionally, *FUT8*, *B4GALT1* and *MGAT3* were subjected to targeted manipulation of histone acetylation and methylation. While these interventions did not consistently affect gene expression or histone marks, they remain promising tools that, with optimization, could advance studies of epigenetic regulation of protein *N*-glycosylation.

(136 pages, 29 figures, 7 tables, 328 references, original in English)

Keywords: DNA methylation, histone modifications, *N*-glycosylation, glycosyltransferases, CRISPR/dCas9

Supervisor: Professor Vlatka Zoldoš, PhD

Reviewers: Assistant Professor Ivan Gudelj, PhD

Associate Professor Nenad Malenica, PhD

Professor Inga Urlić, PhD

Prirodoslovno-matematički fakultet

Biološki odsjek

PROMJENA EPIGENETIČKIH MODIFIKACIJA DNA I HISTONA UPOTREBOM ALATA
CRISPR/dCas9 U ISTRAŽIVANJU REGULACIJE GENA ZA GLIKOZILTRANSFERAZE
U STANICAMA HEPG2

ANA VUJIĆ

Prirodoslovno-matematički fakultet

Složena genska mreža koja se sastoji od oko 800 gena uključena je u *N*-glikozilaciju proteina, međutim mehanizmi kojima su oni regulirani u formiranja kompleksnog *N*-glikoma su nedovoljno istraženi. Unatoč utjecaju genetičke komponente na glikozilaciju, okolišni faktori posredovani epigenetičkim mehanizmima imaju još veći utjecaj. Ovo istraživanje je iskoristilo preciznost alata za uređivanje epigenoma CRISPR/dCas9 kako bi istražilo ulogu metilacije DNA i histonskih modifikacija u regulaciji gena (*B4GALT1*, *FUT8*, *ST6GAL1*, *MGAT4A*, *MGAT4B*, *MGAT5*, *MGAT3*) koji kodiraju glikoziltransferaze uključene u formiranje kompleksnih *N*-glikana. Uvedene promjene u metilaciji promotora putem DNMT3A-dCas9 i TET1-dCas9 utjecale su na transkripcijsku aktivnost svih gena, što je rezultiralo promjenama u ukupnom staničnom *N*-glikomu HepG2 ukazujući na regulatornu ulogu metilacije DNA u *N*-glikozilaciji proteina. Također, geni *FUT8*, *B4GALT1* i *MGAT3* podvrgnuti su ciljanoj manipulaciji acetilacije i metilacije histona. Iako ove intervencije nisu dovele do konzistentne promjene u ekspresiji gena i histonskim oznakama, alati su se pokazali obećavajućima te bi, uz daljnju optimizaciju, mogli unaprijediti istraživanja epigenetičke regulacije *N*-glikozilacije proteina.

(136 stranica, 29 slika, 7 tablica, 328 literaturnih navoda, jezik izvornika: engleski)

Ključne riječi: metilacija DNA, histonske modifikacije, *N*-glikozilacija, glikoziltransferaze, CRISPR/dCas9

Mentor: prof. dr. sc. Vlatka Zoldoš

Ocjenjivači: doc. dr. sc. Ivan Gudelj

izv. prof. dr. sc. Nenad Malenica

prof. dr. sc. Inga Urlić

Table of Content

1. INTRODUCTION.....	1
2. LITERATURE OVERVIEW.....	6
2.1. Epigenetic mechanisms	6
2.1.1. DNA methylation	7
2.1.2. Histone modifications	12
2.1.2.1. Histone acetylation	14
2.1.2.2. Histone methylation	15
2.1.3. Interaction between DNA methylation and histone modifications	17
2.2. Protein <i>N</i> -glycosylation	20
2.2.1. Glycosyltransferases	22
2.2.1.1. FUT8 (α 1,6 fucosyltransferase).....	22
2.2.1.2. B4GALT1 (Beta-1,4-galactosyltransferase 1).....	22
2.2.1.3. ST6GAL1 (β -galactoside α -2,6-sialyltransferase 1)	23
2.2.1.4. MGAT5 (Alpha-1,6-mannosylglycoprotein 6-beta-N-acetylglucosaminyltransferase A).....	23
2.2.1.5. MGAT3 (Beta-1,4-mannosyl-glycoprotein 4-beta-N-acetylglucosaminyltransferase)	24
2.2.1.6. MGAT4A and MGAT4B (Alpha-1,3-mannosyl-glycoprotein 4-beta-N-acetylglucosaminyltransferase A and B)	24
2.2.2. Genetic and epigenetic regulation of protein <i>N</i> -glycosylation.....	25
2.3. CRISPR/dCas9 systems for epigenome editing	27
3. MATERIALS AND METHODS.....	34
3.1. Materials	34
3.1.1. Cell lines and bacterial strains	34
3.1.2. Single-guide RNA sequences, pyrosequencing primers and assays, and qPCR primers	34
3.1.3. Derived glycan traits	39
3.2. Methods	40
3.2.1. Cell culture conditions and transfection.....	40
3.2.2. Cloning of DNMT3A-dSpCas9 and TET1-dSaCas9 constructs for targeted cytosine methylation and demethylation.....	41
3.2.3. Cloning of a full-length HDAC3 catalytic domain.....	42
3.2.4. Cloning of dCas9 fusions with histone modifying enzymes	44
3.2.5. Determination of CpG methylation levels using bisulfite pyrosequencing	47
3.2.6. Analysis of gene expression on mRNA level.....	48

3.2.7. Analysis of gene expression on protein level.....	49
3.2.8. Analyses of histone modification levels	50
3.2.8.1. Native chromatin immunoprecipitation (N-ChIP)	50
3.2.8.2. CUT&RUN	52
3.2.8.3. Cross linking chromatin immunoprecipitation (X-ChIP).....	53
3.2.8.4 Analysis of immunoprecipitated fragments via qPCR	54
3.2.9. Analysis of the total <i>N</i> -glycome of HepG2 cells	55
3.2.10. Statistical analysis.....	57
4. RESULTS.....	58
4.1. Manipulations of promoter methylation of the candidate glyco-genes using CRISPR/dCas9 molecular tools.....	58
4.1.1. Targeting DNMT3A-dCas9 and TET1-dCas9 to the candidate glyco-gene promoters induces hyper- and hypomethylation.....	58
4.1.2. Targeted epigenetic manipulation of DNA methylation affects expression of glyco- genes	61
4.1.3. Effects of epigenetic manipulations on total <i>N</i> -glycome of HepG2 cell line	63
4.1.4. The <i>B4GALT1</i> and <i>FUT8</i> gene downregulation by hypermethylation and the <i>MGAT3</i> gene upregulation by hypomethylation resulted in changes at the protein level	72
4.2. Targeted manipulation of histone modifications in promoters of <i>FUT8</i> , <i>B4GALT1</i> , and <i>MGAT3</i> genes	73
4.2.1. Cloning of a full-length HDAC3 histone deacetylase domain.....	74
4.2.2. Targeting HDAC3-dCas9 to the <i>FUT8</i> and <i>B4GALT1</i> promoters and the effects on corresponding histone mark and gene transcriptional activity.....	75
4.2.3. Targeting RIOX1-dCas9 to the <i>FUT8</i> and <i>B4GALT1</i> promoters and the effects on corresponding histone mark and gene transcriptional activity.....	78
4.2.4. Targeting G9a-dCas9 to the <i>FUT8</i> and <i>B4GALT1</i> promoters and the effect on corresponding histone mark and gene transcriptional activity.....	80
4.2.5. Targeting p300-dCas9 and PRDM9-dCas9 to the <i>MGAT3</i> promoter and the effects on corresponding histone marks and gene transcriptional activity	81
4.2.6. Effects of targeted epigenetic manipulation of histone modifications on DNA methylation	83
5. DISCUSSION	85
6. CONCLUSIONS.....	103
7. REFERENCES.....	105
8. CURRICULUM VITAE.....	136

1. INTRODUCTION

Gene expression, a fundamental biological process, is intricately regulated at multiple levels, including epigenetic mechanisms. These mechanisms collaboratively establish chromatin compaction states, thereby dictating the activity of genes and regulatory elements within, ranging from densely packed heterochromatin to loosely organized euchromatin (1). Key epigenetic mechanisms encompass DNA methylation, histone modifications, histone variants, ATP-dependent chromatin remodeling, non-coding RNAs and nuclear architecture (2). In mammals, DNA methylation primarily occurs at the fifth carbon of cytosine residues, predominantly within CpG dinucleotides. CpG islands (CGIs), which are CpG-rich regions present in the promoters of most mammalian genes, are typically unmethylated (3–5). Conversely, high levels of DNA methylation within CGIs are associated with long-term and stable transcriptional repression, occurring either through direct steric hindrance of transcription factor binding or indirectly via the recruitment of methyl-binding domain (MBD) proteins (6). However, an increasing body of evidence suggests that the role of DNA methylation is context-dependent rather than strictly repressive, with hypermethylation of both promoter and distal regulatory regions also being associated with active transcription, while in other cases, gene expression remains unaffected by the presence or absence of DNA methylation (7–9). DNA methylation patterns are established during embryonic development by the *de novo* methyltransferases DNMT3A and DNMT3B and are subsequently maintained during cell division by DNMT1 (10,11). Conversely, DNA methylation is removed through either passive dilution during replication or active enzymatic removal by the ten-eleven translocation (TET) family of enzymes (3,12,13). Global changes in DNA methylation are commonly observed during both aging and disease development. Aging and cancer are characterized by a global loss of DNA methylation, which promotes genomic instability, along with site-specific hypermethylation of certain genes—particularly tumor suppressors (14,15).

Post-translational modifications of histone proteins constitute another major class of epigenetic modifications, predominantly occurring at their N-terminal tails (16). While a growing number of histone modifications have been described, the best-characterized include acetylation, methylation, and phosphorylation (17). Histone acetylation, occurring at lysine residues, is generally associated with active transcription and is dynamically regulated by the opposing activities of histone acetyltransferases (HATs) and histone deacetylases (HDACs) (16,18,19). In contrast, histone methylation has a dual signal for both activation and silencing, depending on the sequence context, specific residue to be methylated and a number of methyl

group added to it (20). For example, H3K9 di- and tri-methylation (H3K9me_{2/3}) are hallmarks of constitutive heterochromatin and gene silencing, though H3K9me₂ can also appear in euchromatic regions, marking weakly expressed or inactive genes (21). Histone lysine methyltransferases (HKMT) add methyl groups to lysins such as G9a which is responsible for the formation of H3K9me₂ in euchromatin (22). Conversely, methylation of lysine 4 in histone H3 (H3K4me) is associated with active transcription (23,24). Multiple HKMTs catalyze this modification; PRDM9, for instance, introduces H3K4me₃ at recombination hotspots during meiosis (25,26). Removal of this mark is mediated by histone lysine demethylases (KDMs), such as Ribosomal Oxygenase 1 (RIOX1), which is capable of demethylating H3K4me₁, me₂, and me₃ (16,27). Histone modifications do not function solely but intricately interact with each other as well as with DNA methylation (28). One well-established example is the antagonistic interaction between H3K4me₃ and DNA methylation, whereby H3K4me₃ strongly inhibits recruitment of DNMT3L necessary for forming a complex with DNMT3A and thus inhibiting its catalytic activity (29,30). A strong association is also established between DNA methylation and H3K9 methylation. For instance, G9a-dependent *de novo* CpG methylation is involved in silencing of imprinted genes, proviruses, and retrotransposons (31–33). This HKMT can directly interact with both *de novo* methyltransferases DNMT3A and DNMT3B, as well as with the maintenance methyltransferase DNMT1 (34–36).

Protein *N*-glycosylation, a pivotal post-translational modification, participates in myriads of molecular processes, spanning protein stabilization and folding to intricate immune responses. Analogous to the epigenome, protein *N*-glycosylation undergoes significant alterations during aging and disease progression, with aberrant *N*-glycosylation pattern also serving as a hallmark of virtually any type of cancer (37–39). Therefore, elucidating its regulation and the factors contributing to ubiquitously altered *N*-glycosylation pattern in disease and aging is of paramount importance. The regulation of *N*-glycosylation is highly complex and governed by the interplay of genetic and epigenetic mechanisms (40–45). The biosynthesis of *N*-glycans is achieved through a series of sequential enzymatic reactions involving diverse glycosidases and glycosyltransferases (46). Many glycosyltransferases are involved in formation of complex *N*-glycans, including B4GALT1, ST6GAL1, FUT8, MGAT4A/B, MGAT5, MGAT3, and others (47). Given the extensive array of proteins involved in *N*-glycan biosynthesis, recognition, and catabolism, coupled with strong environmental effect through epigenetic mechanisms, comprehending the regulation of this multifaceted process presents a

significant challenge. Despite substantial scientific efforts, the complete regulatory landscape of *N*-glycosylation is still not fully understood.

Several studies have attempted to link epigenetic mechanism to genes involved in *N*-glycosylation (glyco-genes further in text). Among these, microRNAs (miRNAs) have been identified as significant regulators of glyco-genes, particularly those encoding glycosyltransferases (48–52). In addition, it seems that subset of glyco-genes is regulated by promoter CpG methylation (44,45,53). However, most of these investigations are correlative in nature or rely on epigenetic inhibitors that induce global alterations in epigenetic marks (54,55). The use of such inhibitors complicates the attribution of observed transcriptional changes to specific genes or genomic regions due to their non-specific mode of action. The emergence of CRISPR/dCas9-based tools has revolutionized epigenetic research by enabling locus-specific modification of an epigenetic mark and directly linking it with gene expression, thus transforming the field from correlative to causative (56). Catalytically inactive Cas9 (dCas9), generated through point mutations in the nuclease domains of Cas9 protein, serves as a programmable "vehicle" for delivering epigenetic effector domains to target loci via sequence-specific single guide RNAs (sgRNAs). This system allows for precise manipulation of epigenetic modifications at defined genomic regions, thereby permitting direct investigation of their regulatory roles in gene expression and associated phenotypes (57,58). Numerous effector domains have been successfully fused to dCas9, resulting in targeted changes in epigenetic states and modulation of gene expression (for reviews see (56,57,59)). Notably, some of these tools have demonstrated the ability to reverse disease-associated phenotypes (60). Epigenetic effectors that have been tethered to dCas9 to date include domains that induce changes in DNA methylation, such as DNMT3A and TET1, as well as domains that induce changes in histone modifications, such as p300, HDAC3, PRDM9, and G9a (60–67).

The main goal of this thesis was to leverage the precision of the CRISPR/dCas9 system to introduce specific alterations in DNA methylation and histone modifications within strategic regions of genes encoding glycosyltransferases (referred to as glyco-genes further in text): *B4GALT1*, *FUT8*, *ST6GAL1*, *MGAT4A*, *MGAT4B*, *MGAT5*, and *MGAT3*. The aim was to assess whether a change of a specific modification would affect these genes' transcription and subsequently would it influence *N*-glycome of HepG2 cells. The successful demonstration of such effects would not only indicate that the genes are regulated by the affected epigenetic modifications but also support the regulatory role of the targeted genomic regions in glycosylation process. An additional goal was to investigate interplay between DNA

methylation and certain histone modifications, thereby providing further insight into the crosstalk between different epigenetic modifications and their role in the regulation of selected glyco-genes.

Specific goals of this study were:

- I. To target selected glyco-genes using DNMT3A-dCas9 and TET1-dCas9 molecular tools in order to methylate or demethylate specific cytosines in gene promoters, and to determine whether these interventions successfully altered CpG methylation levels.
- II. To evaluate the impact of targeted DNA methylation changes on the transcriptional activity of the selected genes, with the aim of identifying glyco-genes that are potentially regulated by DNA methylation.
- III. To analyze the whole-cell *N*-glycome in HepG2 cell line to determine the downstream effects of induced epigenetic changes.
- IV. To generate functional active form of full-length HDAC3-dCas9 fusion for targeted removal of histone acetylation marks.
- V. To identify glyco-genes that exhibit strongest downregulation upon DNMT3A-dCas9-mediated hypermethylation which resulted in altered corresponding *N*-glycan structures, and to target these genes with dCas9 fusions with histone effector domains: a) HDAC3-dCas9 for removal of histone acetylation; b) RIOX1-dCas9 for H3K4me3 removal; c) G9a-dCas9 for H3K9me2 introduction. The goal was to assess the impact of these engineered epigenetic alterations on gene transcriptional activity.
- VI. To target a strategic *MGAT3* gene region with dCas9 fusions with p300, to introduce histone acetylation, and PRDM9, to deposit H3K4me3, and to subsequently assess if they influence the *MGAT3* gene transcription.
- VII. To assess DNA methylation levels in promoter regions of the glyco-genes targeted with dCas9 fusions with histone modifiers in order to explore epigenetic crosstalk and its role in the transcriptional regulation of these genes.

All experiments were conducted on HepG2 cell line. Actively transcribed genes exhibiting low CpG methylation in their CpG islands in HepG2 cells, including *B4GALT1*, *FUT8*, *ST6GAL1*, *MGAT4A*, *MGAT4B*, and *MGAT5*, were targeted with DNMT3A-dSpCas9. Conversely, the only silenced gene in HepG2, *MGAT3*, displaying a high DNA methylation level at the same time, was targeted with TET1-dSaCas9. Epigenetically engineered cells using dCas9 fusions were harvested for subsequent analysis of DNA methylation, mRNA levels, and whole-cell *N*-glycome. Glyco-genes that were strongly downregulated after DNMT3A-dCas9-

mediated hypermethylation, which also resulted in significant changes of corresponding glycan structures, were selected for further experiments. Western blot analysis was employed to assess if the targeted hypermethylation resulted not only in mRNA but in protein level change as well. The selected glyco-genes appeared to be natively active in HepG2 cells, and their promoters are enriched in active histone marks H3K4me3 and H3K27ac. Therefore, for targeted removal of histone acetylation, full-length HDAC3 was N-terminally fused to dSpCas9 in both active and catalytically inactive forms (for inactive control), the latter generated by site-directed mutagenesis. Strategic gene regions were targeted with different dCas9 fusions: HDAC3-dSpCas9 to remove histone acetylation, RIOX1-dSpCas9 to remove H3K4me3, and G9a-dSpCas9 to deposit H3K9me2. The *MGAT3* gene, being natively silenced in HepG2 cells and not enriched with H3K27ac and H3K4me3 marks, was targeted with p300-dSaCas9 to induce histone acetylation and PRDM9-dSaCas9 to introduce H3K4me3. Following epigenetic engineering, the cells were collected for analysis of mRNA expression and enrichment of appropriate histone marks. Furthermore, to explore the interplay between different epigenetic marks, DNA methylation was analyzed in regions of promoters targeted with dCas9 fusions with histone modifiers.

In all experiments, two types of controls were included: i) a catalytically inactive version of the effector domain fused to the dCas9 ortholog (Inactive control); ii) a fusion with non-targeting sgRNA which does not bind to any region in the human genome (Non-targeting control). DNA methylation was assessed using bisulfite pyrosequencing. Histone modification levels (H3K27ac, H3K4me3, and H3K9me2) were measured using either native or cross-linked chromatin immunoprecipitation (NChIP or X-ChIP) or CUT&RUN analyses. Immunoprecipitated samples were analyzed by qPCR, and relative enrichment with the appropriate histone mark was calculated using the %INPUT method. Gene expression was evaluated by quantitative real-time PCR (RT-qPCR) using the $\Delta\Delta C_t$ method for relative quantification. The whole-cell *N*-glycome was analyzed by hydrophilic interaction ultra-high performance liquid chromatography (HILIC-UPLC).

2. LITERATURE OVERVIEW

2.1. Epigenetic mechanisms

Widely accepted definition of epigenetics refers to heritable changes in gene function that do not involve changes in the underlying DNA sequence (68). The eukaryotic genome is compactly organized within a three-dimensional higher-order structure called chromatin. A nucleosome, the basic unit of chromatin, comprises 147 base pairs of DNA wrapped around an octamer core composed of positively charged histone proteins, specifically two histone H2A-H2B dimers and one histone H3-H4 tetramer (69). Through action of different epigenetic mechanisms, chromatin coordinates all DNA-based processes which include transcription, chromosome segregation, DNA repair, and suppression of transposable elements (70–72). These epigenetic mechanisms include post-translational modifications of histones and incorporation of histone variants, DNA methylation, ATP-dependent chromatin remodeling, the implementation of RNAi pathways and non-protein coding RNAs and position of chromatin within nucleus, also called nuclear architecture (Figure 1) (2).

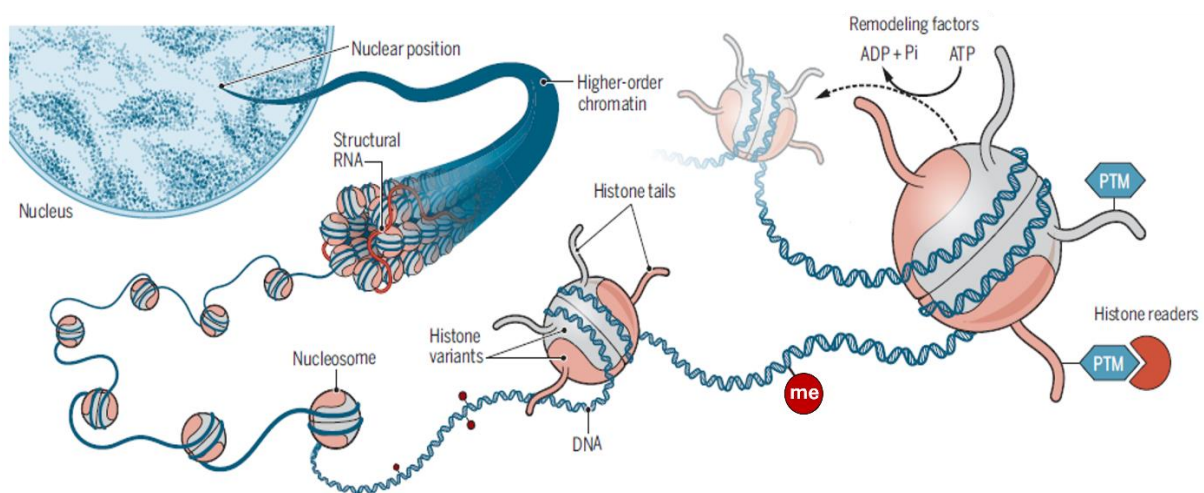


Figure 1. Epigenetic mechanisms. The schematic illustrates six epigenetic mechanisms involved in chromatin compaction and gene regulation. The key epigenetic mechanisms include: nuclear position, DNA methylation (me), chromatin remodeling complexes (remodeling factors), post-translational modifications of histones (PTM), histone variants and non-coding RNAs. Adapted from (73).

Epigenetic mechanisms regulate expression of a highly orchestrated set of genes as cells differentiate, resulting in distinct epigenetic signatures for each cell type (74). The establishment of these cell-type specific epigenetic signatures requires coordinated activities of enzymes responsible for depositing (writers), recognizing (readers), and removing (erasers)

epigenetic modifications. Once established, these modifications are maintained and transmitted through cell divisions (2,75). The accurate formation of the germline epigenome is crucial for proper gametogenesis and embryonic development (76,77). The activity of a specific genomic region is dictated by the level of chromatin compaction. Strictly defined, euchromatin is a more relaxed chromatin structure and comprises actively transcribed genes. In contrast, heterochromatin, which consists of many different classes of repetitive sequences, is highly condensed to silence these sequences (1). Heterochromatin is a crucial chromosomal feature maintaining genomic stability (71). Various combinations of epigenetic modifications contribute to distinct forms of heterochromatin and as such they are involved in suppression of repetitive elements, like transposons and satellite repeats (78,79). They also contribute to centromere formation and proper chromosome segregation (80,81). Additionally, epigenetic mechanisms regulate X chromosome inactivation in post-implantation female embryos and establish genomic imprints during gametogenesis, ensuring parent-specific gene expression, but are also involved in many other important nuclear processes (82–84).

2.1.1. DNA methylation

Methylated DNA bases including C5-methylcytosine (5mC), N4-methylcytosine (4mC), and N6-methyladenine (6mA) are present in many genomes, however 5mC is the most prevalent DNA modification in eukaryotic genomes (11). DNA methylation is established through the covalent attachment of a methyl group to the fifth carbon atom of the cytosine pyrimidine ring within the DNA molecule. In mammals, most DNA methylation occurs within CpG dinucleotides, with over 80% of CpGs methylated in most somatic tissues. Highly methylated sequences include satellite DNA and other repetitive elements such as transposons and retrotransposons, intergenic DNA and exons (3). However, CpG islands (CGIs) and other regulatory sequences are exceptions to this global cytosine methylation, showing significantly lower 5mC levels. CGIs are genomic regions rich in CpG content, typically spanning around 1 kb on average. More than two thirds of mammalian genes possess CGI associated promoters (4). Approximately 15% to 21% of CpGs exhibit variations in methylation levels across human tissues. These CpG sites cluster into tissue specific differentially methylated regions (DMRs) which are predominantly located distally to the transcriptional start sites and often coincide with enhancers (85,86).

The presence of 5mC at CGIs and high levels of DNA methylation in general are associated with long term, stable gene repression and is especially important in three major classes of genes in somatic tissues including those on inactive X chromosome, imprinted genes

and germline-specific genes (6). Studies suggest that DNA methylation interferes with gene expression through two distinct mechanisms. One hypothesis is that the presence of a methyl group alters the binding affinity and specificity of transcription factors (TFs) responsible for initiation of gene transcription. Many TFs recognize CpG-rich sequence motifs, and some of them are incapable of binding the DNA when methylated (Figure 2a-b) (87). The second mechanism involves proteins belonging to the methyl-CpG-binding domain (MBD) family which, through interaction with 5mC, play different roles in epigenetic remodeling and transcriptional repression (Figure 3). MBD proteins recognize 5mC and recruit various co-repressor complexes which, in turn, facilitate chromatin condensation, leading to gene silencing. For instance, MBD2 is associated with a corepressor complex NuRD comprised of histone deacetylases and the large chromatin remodeling protein Mi-2 (88).

While dense promoter DNA methylation is generally associated with transcriptional repression, evidence indicates that methylation at one or more specific CpG sites is sufficient to fine-tune gene expression. For instance, methylation at a single CpG in the *ESR1* promoter inhibits Ets-2 binding, reducing transcription, and similar site-specific methylation downregulates *XAF1* in gastric and colon cancers (89,90). Despite this classical repressive role, genome-wide studies have challenged this simple gene-silencing paradigm, revealing that the transcriptional consequences of DNA methylation are more nuanced and context-dependent (9). In tumors, hypermethylation does not always silence genes but rather reinforces their inactive state (91). Furthermore, the presence or absence of promoter methylation doesn't always correlate with transcriptional status. For example, although *Nanog* and *OCT4* are silenced in adult mammary tissues, their promoters remain largely unmethylated (8). Intriguingly, increasing evidence demonstrates that promoter hypermethylation correlates with transcriptional activity in various contexts such as carcinogenesis, metastasis, development, and induced pluripotent stem cells (iPSCs) (7). In acute myeloid leukemia, the *AWT1* promoter is hypermethylated despite high gene expression (92). Notably, several oncogenes show transcriptional activation upon promoter hypermethylation (7). *TERT*, which encodes telomerase reverse transcriptase, exhibits a strong positive correlation between promoter methylation and expression across tumor types and telomerase-positive normal tissues (93). A specific 433 bp region located immediately upstream of the *TERT* core promoter—THOR (TERT Hypermethylated Oncological Region)—contains 52 CpG sites that are hypermethylated in TERT-expressing cancer cell lines compared to normal counterparts (94). The prevailing proposed mechanism for methylation-induced transcriptional activation

suggests that methylation may block binding of transcriptional repressors, thereby facilitating gene activation (Figure 2c-d). Additionally, DNA methylation can modulate the activity of distal regulatory elements, which can influence gene expression in both repressive and activating manners (7). For instance, hypermethylation of CTCF binding sites in glioma disrupts insulator function, leading to enhancer-mediated *PDGFRA* activation (95). Conversely, in Tet2-deficient mouse embryonic stem cells (mESC), hypermethylation of specific enhancers is associated with decreased H3K27ac levels and reduced expression of nearby genes, exemplified by the enhancer of *Lefty1* gene (96). These studies collectively underscore the complex and context-dependent role of DNA methylation in gene regulation, extending beyond simple gene silencing where depending on locus site, chromatin contexts and presence of different transcription factors, DNA methylation can produce distinct effects on gene expression.

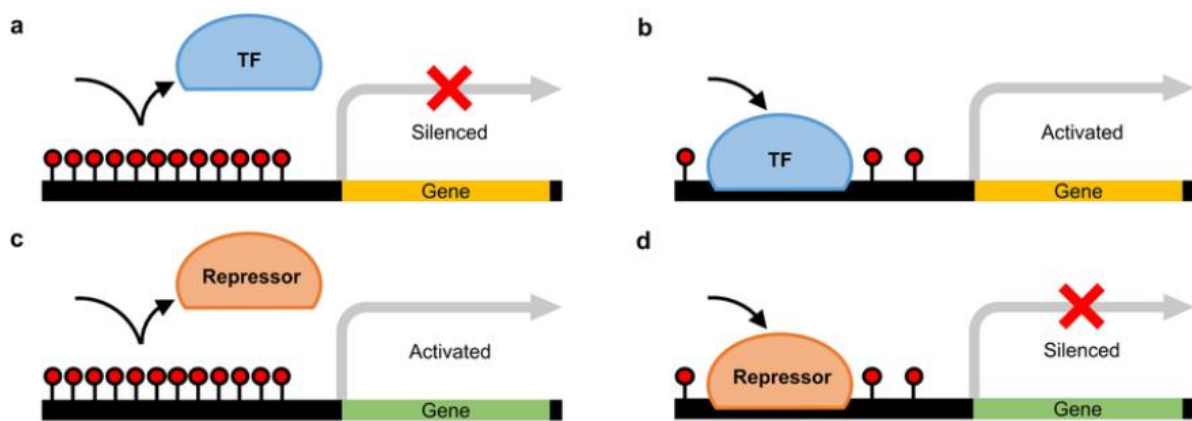


Figure 2. Effects of promoter DNA methylation on transcription factor binding and gene expression. Promoter methylation is typically linked to transcriptional repression. One established mechanism involves interference with transcription factor (TF) binding, where methylation of CpG sites (red circles) impedes TF binding and thus inhibits gene expression (a), whereas unmethylated CpG sites permit TF binding and activate transcription (b). However, emerging evidence indicates that promoter methylation can also facilitate gene expression by preventing the binding of transcriptional repressors. In such cases, 5mC blocks repressor binding, thereby enabling transcription (c), while the absence of methylation allows repressor recruitment, leading to gene silencing (d). Adapted from (97).

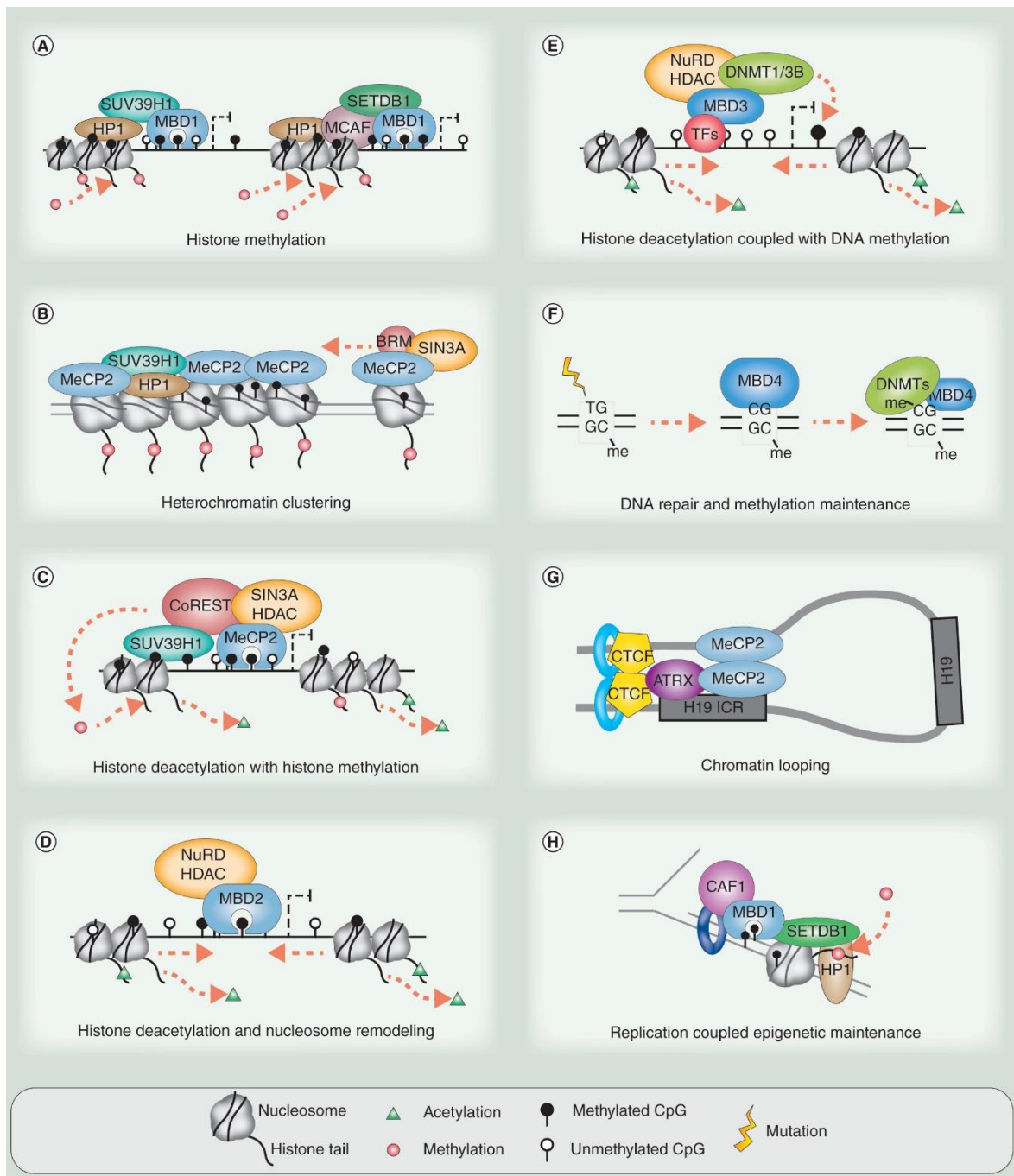


Figure 3. Diverse roles of MBD family proteins in epigenetic remodeling and transcriptional repression. (a) MBD1 mediates transcriptional repression by recruiting histone methyltransferases (SUV39H1, SETDB1) and heterochromatin protein 1 (HP1) to DNA-methylated regions, promoting heterochromatin formation. (b) MeCP2 interacts with SUV39H1-HP1 to induce heterochromatin clustering at its binding sites. (c) MeCP2 also coordinates histone methylation and deacetylation through interactions with cofactors such as CoREST at methylated DNA sites. (d) MBD2 represses transcription by recruiting the NuRD complex, composed of histone deacetylases and the Mi-2 chromatin remodeler. (e) MBD3,

while also engaging the NuRD/Mi-2 complex, promotes histone deacetylation and *de novo* DNA methylation *via* recruitment of DNMT1 and DNMT3B. Its promoter binding is mediated by transcription factors. (f) MBD4 contains a C-terminal glycosylase domain that repairs spontaneous 5-mC→T mutations. It also interacts with DNMTs to facilitate remethylation. (g) MeCP2 contributes to transcriptional repression by inducing chromatin loop formation. It recruits the nucleosome remodeler ATRX which creates open DNA and binding sites for members of the cohesin complex and CTCF protein. (h) MBD1 associates with replication forks through interaction with CAF-1, a replication-coupled chromatin remodeler, ensuring methylation of newly incorporated histones. Adapted from (98).

During embryogenesis, the mammalian genome undergoes two waves of epigenetic reprogramming marked by changes in DNA methylation. Epigenetic reprogramming involves global genome demethylation which allows *de novo* establishment of cell-type-specific methylation. The first wave occurs in preimplantation embryos, and the second during the development of primordial germ cells (PGCs) (3,6). DNA methylation patterns in embryonic development are established by the activity of *de novo* DNA methyltransferases (DNMT), namely DNMT3A and DNMT3B (10). These patterns are subsequently maintained by DNMT1. The human genome encodes two other DNMTs, DNMT2 and DNMT3L, which are non-canonical family members that lack the intrinsic methyltransferase activity (11). However, DNMT3L interacts with and stimulates the activity of DNMT3A and DNMT3B, particularly in the germline (99,100). All DNMTs use S-adenosylmethionine (SAM) as a methyl group donor and share the same catalytic mechanism for DNA methylation. Typically, they consist of an N-terminal regulatory domain and a C-terminal catalytic domain (11).

DNA methylation can be removed through both active and passive mechanisms. Passive demethylation occurs when DNA methylation maintenance machinery is absent or inhibited causing gradual dilution of methylation marks during DNA replication (3). Active DNA demethylation is mediated by enzymes from the ten-eleven translocation (TET) family. The mammalian genome encodes three members of TET family: TET1, TET2, and TET3 (101,102). TET proteins convert 5mC to 5-hydroxymethylcytosine and further to 5-formylcytosine and 5-carboxylcytosine. These oxidized forms are then removed through replication-dependent dilution or thymine-DNA glycosylase (TDG)-mediated base excision repair (13,103). The precise targeting of TET proteins to genomic elements is achieved through the CXXC domain found in TET1 and TET3 proteins. The CXXC domain exhibits a preference for binding to unmethylated CpGs (104,105).

Major targets of DNA methylation in mammalian genomes are transposable elements (TEs). 5mC serves as the primary strategy for long-term silencing of TEs in higher eukaryotes (106,107). X chromosome inactivation (XCI) is another process dependent on DNA methylation where DNA methylation acts as a final step, locking down silenced genes in the late stage of XCI (108). Parental allele-specific DNA methylation is essential for imprinted gene expression and as such it persists through the wave of genomic reprogramming during embryogenesis. Imprinted genes are often found in clusters and regulation of their expression relies on germline-derived differential DNA methylation at cis-regulatory elements called imprinting control regions (109). These germline differentially methylated regions (gDMRs) serve as the primary signal, establishing secondary epigenetic modifications and recruiting specific transcription factors that orchestrate imprinted expression. The human genome harbors around 35 gDMRs associated with imprinted loci (110,111).

Mutations in DNA methylation pathways (including genes for DNMT, TET, and MBD proteins) can cause various congenital syndromes involving immunodeficiency, growth problems, and neurodegeneration (6). Furthermore, aberrant DNA methylation pattern is a prevalent feature in virtually every type of cancer, marked by global genome hypomethylation and localized hypermethylation of specific CGIs (112). Global hypomethylation leads to activation and transposition of TEs promoting genomic instability and chromosome rearrangements, typical for cancer cells. Hypermethylation of CGIs associated with tumor-suppressor genes is most common epigenetic mechanism contributing to carcinogenesis (113). These widespread alterations in cancer methylation patterns may be driven by mutations in the DNA methylation machinery such as TET mutations observed in myeloid malignancies (114) and DNMT3A mutations in acute myeloid leukemia (115).

2.1.2. Histone modifications

N-terminal tails protruding from nucleosomes are the primary sites for histone post-translational modifications (PTMs). Amino acid residues of N-terminal ends are modified by the addition of various chemical groups or small proteins (Figure 4). PTMs regulate chromatin-based processes *in cis* by altering the structural and physical properties of nucleosomes or *in trans* by serving as docking sites for recruitment of different effector proteins (116). In chromatin, PTMs occur in various combinations, giving rise to the „histone code“ hypothesis which proposes that distinct PTMs, on one or more tails, act sequentially or in combination to form a “code” that dictates the functional state of a particular genomic region, such as active transcription or silenced chromatin (117). To date, many histone modifications have been

discovered and characterized including: acetylation, phosphorylation, methylation, SUMOylation, ubiquitination, malonylation, ADP-ribosylation, biotinylation, butyrylation, citrullination, O-GlcNAcylation, crotonylation, formylation, hydroxyisobutyrylation, 2-, hydroxyisobutyrylation, isomerization, glutarylation, lactylation, S-palmitoylation, Propionylation, succinylation, polyADP-ribosylation, carbamoylation, deamidation and *N*-glycosylation. For comprehensive catalogue of these histone modifications including their number and position in histone proteins see (17) and (118) and references within. Most studied modifications whose regulatory role was explored in this research as well include methylation and acetylation.

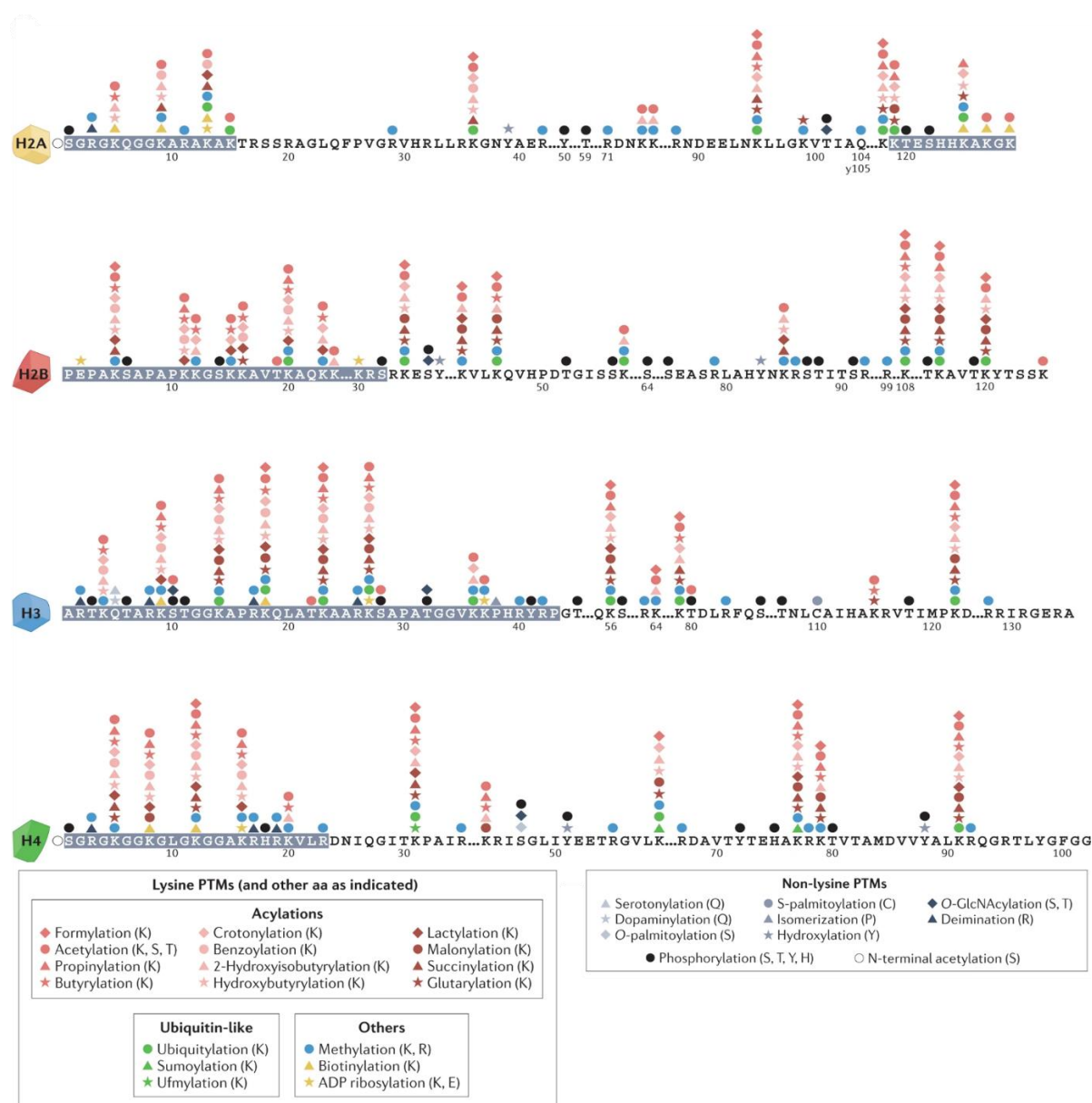


Figure 4. Post-translational modifications of histones H2A, H2B, H3 and H4. The figure illustrates the amino acid sequences of histones H2A, H2B, H3, and H4, along with their

associated post-translational modifications (PTMs). Amino acids within the histone tails are highlighted in gray. Modifications are represented by symbols as detailed in the figure legend. Adapted from (119).

2.1.2.1. Histone acetylation

Histone acetylation is a reversible histone modification established at ϵ -amino group of lysine residues. Acetylation neutralizes the positive charge of the lysine residues, weakening the interactions between DNA and histones. This promotes chromatin opening and facilitates transcription, therefore, histone acetylation is associated with gene activity (16). Acetylation also promotes an open chromatin state by acting as a docking site for bromodomain-containing transcription factors (120). Dynamic process of lysine acetylation is regulated by antagonistic action of histone acetyltransferases (HATs) and histone deacetylases (HDACs). Humans possess three major families of HATs: GNAT, EP300/CBP, and MYST (18). Human HDACs are classified into four major families based on their homology with yeast HDAC. Class I, Class II and Class IV HDACs rely on Zn^{2+} as a cofactor in their active sites while Class III, also known as sirtuins, utilize NAD^{+} as a cofactor and exhibit a distinct catalytic mechanism compared to other HDAC families (19). Because HDACs lack an intrinsic DNA binding ability, their recruitment to DNA relies on different protein complexes (121).

Acetylation sites on H3 and H4 histone tails are best studied, and they include marks such as H3K27ac and H3K9ac (25). H3K27ac, introduced by the action of CBP/p300, usually co-occurs with H3K4me3 at promoters and enhancers of actively transcribed genes. Enhancers marked with H3K4me1 and H3K27ac are categorized as active enhancers (122). H3K27ac is recognized by Bromodomain and extra terminal domain (BET) proteins which act as a scaffold that facilitates the assembly of TFs and RNA polymerase II to initiate gene expression (25,123). H3K9ac is another well-characterized mark that co-localizes with H3K4me3 at promoters of actively transcribed genes and is involved in regulation of gene expression patterns during cell differentiation, gene activation and DNA repair (124,125). There is substantial evidence of crosstalk between histone acetylation and phosphorylation, where these modifications cooperatively regulate chromatin structure and gene expression. A well-characterized example involves phosphorylation of histone H3 at serine 10 (H3S10ph), which promotes acetylation at lysine 14 (H3K14ac) by enhancing recruitment of the histone acetyltransferase GCN5 (126,127). This interplay is also crucial in transcriptional elongation, as seen with the *FOSL1* gene: phosphorylation of H3S10 at the *FOSL1* enhancer, leads to recruitment of the acetyltransferase MOF and subsequent acetylation of H4K16 which in turn, facilitates the

recruitment of the positive transcription elongation factor P-TEFb, promoting RNA polymerase II pause release (128). Additionally, phosphorylation of serine 31 on the histone variant H3.3 enhances the activity of p300, further promoting enhancer acetylation (129).

Disruption of „acetylation homeostasis“, characterized by balanced concentration, enzymatic activity and proper recruitment of HATs and HDACs, leads to various neurodegenerative diseases, developmental disorders, and cancers. A well-characterized epigenetic abnormality in cancer is a combined loss of acetylating proteins and gain in HDAC activity. Aberrant HDAC activity plays a key role in silencing tumor suppressor genes, promoting cancer initiation and progression (121).

2.1.2.2. Histone methylation

Methylation can occur on all basic residues of histone proteins including arginine, lysine and histidine. However, lysine methylation of histones H3 and H4 is a pivotal posttranslational modification with numerous lysine residues undergoing mono-, di- and trimethylation, resulting in distinct transcriptional regulation outcomes (20). Best-studied methylation marks associated with actively transcribed gene regions include H3K4, H3K36, and H3K79, while methylation at H3K9, H3K27 and H4K20 is typically correlated with silenced gene regions and condensed chromatin (16). The catalytic activity of histone lysine methyltransferases (HKMT) mediates lysine residue methylation and is comprised of SET-domain-containing and DOT1-like proteins. Histone lysine demethylases (KDMA) are responsible for removal of methyl mark with two so far identified family of demethylases including amine oxidases and Jumonji C (JmJC)-domain-containing, iron-dependent dioxygenases (25). Like other PTMs, histone methyl marks exert their function through interaction with proteins that specifically recognize these marks *via* methyl-binding domains such as PHD fingers, WD40 repeats, CW domains and PWWP domains (20).

Constitutive heterochromatin is defined by H3K9 dimethylation (H3K9me2) and trimethylation (H3K9me3), primarily at non-coding regions like TEs, pericentric satellites, and subtelomeric repeats. Notably, H3K9me2 can also mark silenced or weakly expressed genes within euchromatin (21). The HKMTs that specifically methylate H3K9 in mammals include Suppressor of variegation 3–9 homologue 1 and 2 (SUV39H1, SUV39H2), SET domain bifurcated 1 and 2 (SETDB1, SETDB2), G9a, and G9A-like protein (GLP). SUV39H1/H2 catalyzes the formation of H3K9me2 and H3K9me3 in pericentromeric heterochromatin (130). The chromodomain of HP1 protein recognizes these marks, recruiting more SUV39H1/H2 and other proteins (chromatin remodelers, transcriptional repressors, HDACs), thereby promoting

the propagation of heterochromatin formation (131,132). Histone methyltransferases G9a and GLP can form hetero- or homodimers, catalyzing the formation of H3K9me1 or H3K9me2 in euchromatin, thereby promoting the silencing of genes within these regions (22). Through automethylation at their Lys165 residue, G9a and GLP can also interact with HP1 protein (133). These HKMTs are also essential for H3K9me2 formation in regions containing Class III endogenous retroviruses (ERVs) (134,135). Furthermore, they play a crucial role in transcriptional silencing and DNA methylation of integrated vectors of the Moloney murine leukemia virus (34).

Histone modification H3K4me is associated with active genes. H3K4me3 marks promoters of actively transcribed and poised genes, while H3K4me1 and H3K4me2 are enriched in enhancers and the 5' end of transcribed genes, respectively (23,24). These marks are recognized by protein readers containing methyl-binding domains, facilitating chromatin opening and transcriptional activation. Human genome encodes for 11 different H3K4 methyltransferases including MLL1-4, SET1A and B, SMYD1-3, SET7/9 and PRDM9 (25). PRDM9 is a critical player in a meiotic recombination, it tri-methylates Lys4 in H3 in specific genomic locations facilitating the initiation of meiotic recombination (26). Different KDMs can remove H3K4 methylation marks, and these include KDM, KDM2 and KDM5 family of KDMs, so as KDM ribosomal oxygenase 1 (RIOX1) that contains JmjC domain and can demethylate both H3K4me2 and me3 (16,136). RIOX also demethylates H3K4me1 and exhibits partial activity on H3K36me2. RIOX1-mediated demethylation of H3K4me3 inhibits SP7/OSX-driven activation of genes involved in osteoblast differentiation and plays a role in regulating DNA repair pathways following ionizing radiation (27,136). KDMs can associate with Polycomb group (PcG) of proteins, H3K9 HKMTs and repressive complexes that contain HDACs, suggesting that coordinated regulation of methylation and acetylation promotes gene repression (20). H3K4 methylation has a crucial role in animal development and, apart from transcription, it has been linked to various cellular processes such as DNA recombination, repair and replication (137). A very important feature in animal developmental process is the existence of genes bivalently marked with both H3K4me3 and H3K27me3. These seemingly contradictory marks poise genes for future expression, often found in promoters of genes with low expression in early embryos (e.g., SOX, PAX, POU). During differentiation, lineage-specific decisions are made by selective removal of either H3K4me3 or H3K27me3 (74). Apart from poised, H3K27me3 is also associated with silenced promoters and enhancers. This

repressive methyl mark is introduced by the action of EZH2 enzyme within the PRC2 complex (25).

In addition to DNA methylation, histone methylation also plays an important role in both X chromosome inactivation and genomic imprinting. In X inactivation, the long non-coding Xist RNA, transcribed from the silenced X chromosome, recruits PRC2 complex which then deposits H3K27me3 on the silenced X, while this mark silences the *Xist* gene itself on the active X chromosome (138,139). In genomic imprinting, H3K9 methylation cooperates with DNA methylation to silence genes in a parent-of-origin-dependent manner (74). Interestingly, H3K27me3 plays a key role in a DNA methylation-independent imprinting mechanism (140). Aberrant regulation of histone methylation, driven by factors like promoter hypermethylation, mutations in histone-modifying enzymes, or mutations in histone methylation sites, leads to abnormal gene expression in various cancers (16). For instance, imbalances between H3K27me3 and H3K4me3 marks at bivalent promoters contribute to cancer development (141). Mutations in HKMTs are frequently observed in tumors. (16).

2.1.3. Interaction between DNA methylation and histone modifications

Different epigenetic mechanisms do not operate independently, and numerous studies have confirmed the extensive crosstalk between DNA methylation and histone modifications (28) (Figure 5). The most well-documented interplay between CpG methylation and histone modifications involves the action of DNA methyltransferases during *de novo* methylation, especially concerning the H3K4 methylation mark. Many groups have demonstrated an antagonistic relationship between CpG methylation and H3K4 methylation, particularly within CpG islands (29,30,142–144). Oocytes lacking H3K4 demethylase activity exhibit elevated levels of H3K4 methylation, which hinders *de novo* DNA methylation and disrupts the establishment of genomic imprinting (145,146). DNMT3 enzymes harbor an ADD (ATRX-DNMT3-DNMT3L) domain that binds the H3 histone tail, facilitating *de novo* methylation. However, H3K4me3 disrupts this interaction (29,144). A point mutation in the ADD domain of DNMT3L impairs its ability to bind to histones, consequently impeding both CpG and non-CpG methylation (147). Another study identified point mutations within the ADD domain of DNMT3A, rendering it unresponsive to H3K4 methylation (148). Structural analyses show that unmodified H3 tails promote DNMT3A activity by relieving its autoinhibitory conformation. In the absence of unmodified H3K4, the ADD domain binds the catalytic domain, blocking DNA binding. Binding the ADD domain to unmodified H3K4 triggers a conformational change

that disrupts this interaction, releasing autoinhibition of DNMT3A and enabling DNA methylation (30).

Gene bodies of actively transcribed genes display two key features: enrichment of the histone mark H3K36me3 and high levels of CpG methylation (149). The PWWP domain, found both in DNMT3A and DNMT3B, interacts with H3K36me3 (149–151). In yeast, DNMT3B binding and *de novo* methylation correlates with H3K36me3 patterns dependent on the histone methyltransferase SET2 (152). DNMT3A, despite recognizing both H3K36me2 and H3K36me3, shows higher affinity towards H3K36me2 and targets these regions for *de novo* methylation. Loss of NSD1/2, histone 3 lysine 36 (H3K36) methyltransferases, redistributes DNMT3A from H3K36me2-enriched intergenic regions to H3K36me3-enriched genic regions (142,153). Notably, *NSD1* mutations are linked to abnormal DNA methylation patterns in developmental syndromes and carcinomas (142).

As an integral part of constitutive heterochromatin, DNA methylation and H3K9 methylation are strongly associated. This association is often achieved through interaction between different DNA methyltransferases and members of SET-containing SUV39 protein family (28,142). SUV39H1 or SUV39H2 directly recruit DNMT3A (28,154), and their double knockout in mice abolishes DNMT3B localization and *de novo* DNA methylation (155). *Setdb1* deletion in mESCs results in hypomethylation of long terminal repeat (LTR) retrotransposons, class I and II ERVs, and some imprinted genes (156). *De novo* CpG methylation also depends on G9a, even in the absence of G9 methyltransferase activity (31,35). G9a dependent *de novo* CpG methylation is involved in silencing of imprinted genes, provirus and retrotransposons in mESC (33–35). Lack of G9a in embryos leads to decrease in CpG methylation in promoters of germline-specific genes (157). G9a interacts with DNMT3A and DNMT3B either directly (31) or indirectly through HUSH complex member MMP8 or UHRF1 (32,158).

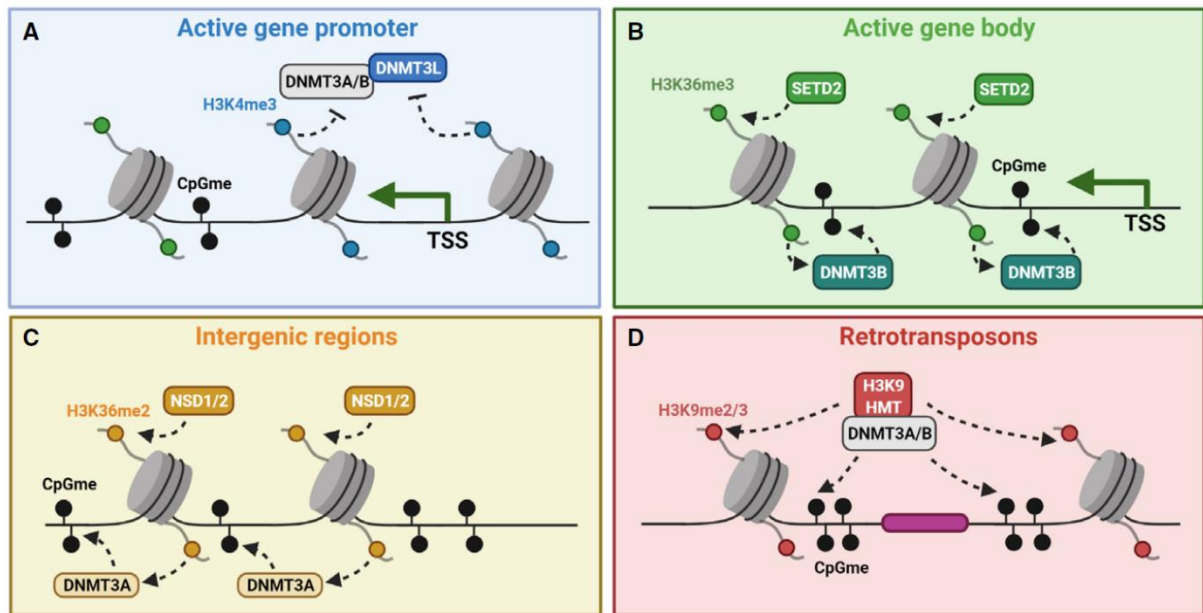


Figure 5. Crosstalk between *de novo* DNA methylation and histone modifications. (a) H3K4 methylation hinders the binding of the ADD domain of DNMT3 methyltransferases, thereby inhibiting *de novo* DNA methylation. (b) The PWWP domain of DNMT3B interacts with H3K36me3, a histone modification enriched in the gene bodies of actively transcribed genes, facilitating DNMT3B localization to these regions. (c) In intergenic regions, H3K36me2 modification interacts with the PWWP domain of DNMT3A, directing its localization to these genomic regions. (d) Interactions between H3K9 methyltransferases and DNMT3A/B lead to co-localization of H3K9me3 and DNA methylation at repetitive elements and retrotransposons, resulting in their transcriptional silencing. Adapted from (142).

Maintenance of DNA methylation patterns also depends on various histone modifications. UHRF1, a key protein in DNMT1-mediated DNA methylation maintenance, plays a significant role in these interactions. Through its RING domain, UHRF1 ubiquitinates Lys18 and Lys23 in histone H3 which are then recognized by RFTS (Replication Foci Targeting Sequence) domain of DNMT1 facilitating its chromatin targeting and stimulating its methyltransferase activity (159,160). The tandem Tudor (TTD) and PHD finger domains of UHRF1, connected by a linker region, recognize H3K9me3 and unmodified H3R2 respectively (161,162). The H3K9me2-specific methyltransferase G9a/GLP can directly interact with DNMT1 while recent findings also indicate that DNMT1 alone can bind specifically to H3K9me3 through its RFTS domain (163,164).

2.2. Protein *N*-glycosylation

Glycosylation, one of the most prevalent post-translational modifications, involves the covalent attachment of complex oligosaccharides to proteins. This includes the addition of *N*-linked glycans, *O*-linked glycans, phosphorylated glycans, glycosaminoglycans, and glycosylphosphatidylinositol (GPI) anchors to peptide backbones, as well as C-mannosylation of tryptophan residues (37,165). *N*-glycosylation specifically refers to the attachment of oligosaccharides to asparagine residues via a β -1-N linkage. *N*-linked glycans share a common GlcNAc₂Man₃ core structure, to which additional monosaccharides can be added or removed (37).

Protein *N*-glycosylation is involved in myriads of molecular processes such as protein stability and folding (166,167). Various chaperones, glycosidases, and glycosyltransferases interact with *N*-glycans on glycoprotein surfaces, facilitating folding and quality control in the endoplasmic reticulum (ER) (168). Furthermore, *N*-glycans play a pivotal role in receptor function, influencing ligand binding, oligomerization, and signaling, with glycan branching significantly impacting receptor turnover and downstream signaling (46,169). It also has a major role in immune processes, for instance *N*-glycans mediate essential cell-cell interactions through lectin recognition, a fundamental aspect of self/non-self-recognition. Aberrant protein *N*-glycosylation can lead to the development of autoimmune diseases. Involvement of *N*-glycans in major histocompatibility complex interactions is crucial for the development of adaptive immune responses (170). Virtually all immune cell surface proteins are modified by *N*-glycans which tightly control and fine-tune the immune system (171). One of the most extensively studied glycoproteins is immunoglobulin G (IgG), a key player in the adaptive immune system. Glycosylation of both the Fab and Fc regions significantly impacts IgG functions, with Fc glycosylation particularly influencing effector functions through interactions with Fc γ receptors acting as a switch between pro- and anti-inflammatory responses (172–174). Changes in IgG glycosylation have been associated to aging and numerous diseases (175–177).

Aberrant *N*-glycosylation of many different proteins is implicated in a wide spectrum of human diseases. Alterations in glycosylation patterns of various glycoproteins, as well as in the global *N*-glycome, are observed in congenital disorders of glycosylation (CDGs), infectious, autoimmune, inflammatory diseases, and cancer (37,39). Aberrant protein *N*-glycosylation is hallmark of cancer, with changes in glycan expression linked to cancer proliferation, invasion, metastasis, and the regulation of cell proliferation, adhesion and migration (178,179). In most cancers, these changes involve sialylation, fucosylation and glycan branching (178). The unique

aberrant glycosylation pattern along with the modified expression of glycosyltransferases and glycosidases are used as cancer biomarkers (180,181).

Biosynthesis of *N*-glycans takes place in the endoplasmic reticulum (ER) and the Golgi apparatus through a series of stepwise reactions involving various glycosidases and glycosyltransferases (46). The glycosylation process begins in the ER, where a lipid-linked precursor (Glc3Man9GlcNAc2-P-P-dolichol) is assembled, flipped to the ER lumen, and transferred to a nascent polypeptide by oligosaccharyltransferase. The glycoprotein undergoes initial processing in the ER and further maturation in the Golgi, where its glycan structure is trimmed and modified (46,182). Elongation and branching of a glycan, resulting in a hybrid or complex *N*-glycan structure, is catalyzed by mannosidases and multiple glycosyltransferases through the addition of GlcNAc, galactose, sialic acid, and fucose sugars (Figure 6) (47). Glycosyltransferases, such as FUT8, B4GALT1, ST6GAL1, MGAT3, MGAT4A/B, and MGAT5, are localized in the Golgi apparatus and exhibit a characteristic type II transmembrane protein structure. This structure includes an N-terminal cytoplasmic domain, a transmembrane domain, a stem region, and a C-terminal catalytic domain oriented toward the trans-Golgi lumen (183–186). The degree of processing and branching of *N*-glycans depends on their accessibility to Golgi glycosyltransferases, with those having greater access being more likely to be processed into complex *N*-glycans (46).

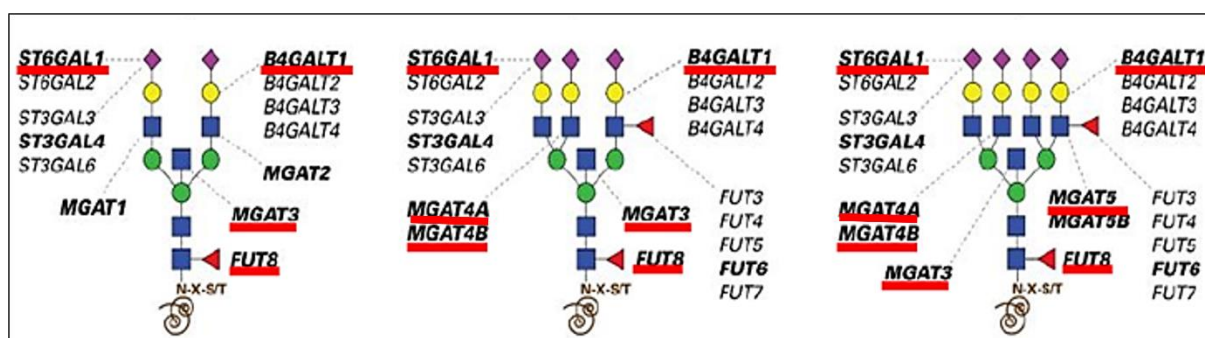


Figure 6. Genes involved in the formation of complex *N*-glycans. Figure illustrates the complex *N*-glycan structures and the genes encoding glycosyltransferases involved in their formation. The epigenetic regulation of glycosyltransferases underlined in red is a central focus of this dissertation and their function is discussed in greater detail within the text. Adapted from (187).

2.2.1. Glycosyltransferases

2.2.1.1. *FUT8* (α 1,6 fucosyltransferase)

The *FUT8* gene is located on chromosome 14q23.3 (188). It encodes for α 1,6 fucosyltransferase which catalyzes the transfer of a fucose residues from GDP- β -L-fucose to the innermost GlcNAc residue of *N*-glycans via an α 1,6 linkage (189). It is the only enzyme responsible for core-fucosylation of mammalian *N*-glycoproteins (190). Core fucosylation is a critical biological modification implicated in various physiological and pathological processes. Knockout (KO) of *FUT8* in mice leads to development of severe phenotypes showing that core fucosylation is crucial for growth factor receptor activity (191–193). *FUT8* is upregulated in various cancers including lung, liver, colorectal, ovarian, prostate, breast, melanoma, thyroid, and pancreatic cancer (194). It influences cell adhesion and migration by modulating E-cadherin turnover and α 3/ β 1 integrin activity (195,196). Additionally, FUT8 regulates transforming growth factor- β 1 receptor (TGF- β 1) and epidermal growth factor (EGF) with its upregulation often observed during epithelial-mesenchymal transition (EMT) in multiple cancers (197–200). The best-known role of core fucosylation is its ability to alter antibody-dependent cellular cytotoxicity (ADCC). Specifically, the absence of core fucose on the *N*-glycan of IgG significantly enhances ADCC activity (189,201). Increased core-fucosylation is also emerging as a promising biomarker for cancer detection and monitoring. The core fucosylated form of α -fetoprotein (AFP-L3) has already been approved by the U.S. Food and Drug Administration (FDA) for the early detection of hepatocellular carcinoma (HCC) (38,194).

2.2.1.2. *B4GALT1* (Beta-1,4-galactosyltransferase 1)

Galactosylation of *N*-glycans is carried out by a set of seven distinct β -1,4-galactosyltransferases in mammalian cells with B4GALT1 being the predominant isoenzyme (202,203). B4GALT1 catalyzes the transfer of a galactose moiety from UDP-galactose to a GlcNAc residue via a β 1–4 linkage (184,204,205). Substrate binding induces conformational changes within the enzyme during its catalytic cycle. B4GALT1 forms both high molecular weight oligomers and homodimers (184). The human *B4GALT1* gene is located on chromosome 9p13. Its promoter contains multiple transcription start sites (TSS) within the 33167138–33167403 bp range, a region overlapping its CGI (206). This area is a part of the 1.454 kb transcriptional regulatory region (TR1-PE1) at the 5' end of *B4GALT1*, which functions as a bidirectional promoter driving its own transcription and the transcription of its antisense long non-coding RNA (B4GALT1-AS). The *B4GALT1* gene encodes two protein isoforms: a long

form (399 amino acids) and a short form (386 amino acids) (207). B4GALT1 has a vital role in numerous biological processes including cell growth, sperm-egg interaction, inflammation, embryogenesis, morphogenesis, central nervous system development, cell migration and cell adhesion (207,208). Abnormal expression of *B4GALT1* is associated with development and malignant progression of several tumors, such as hepatocellular carcinoma, breast cancer, and glioblastoma (209–211).

2.2.1.3. *ST6GAL1* (β -galactoside α -2,6-sialyltransferase 1)

The *ST6GAL1* encodes for β -galactoside α -2,6-sialyltransferase 1, an enzyme that catalyzes transfer of a sialic acid moiety from an activated donor to the 6'-hydroxyl group of a disaccharide containing a terminal galactose forming an α 2,6-linkage (185). Given that the addition of sialic acid by ST6GAL1 requires the presence of terminal galactose, it is not surprising that B4GALT1 and ST6GAL1 form heteromers. Moreover, the interaction between these two enzymes in GA is a prerequisite for their full catalytic activity (212). The *ST6GAL1* gene is located within the 3q26 chromosomal region, a well-known amplicon frequently amplified in epithelial cancers. The expression of *ST6GAL1* is controlled by multiple promoters, enabling tissue- and cell-type-specific regulation (213). Three major ST6GAL1 mRNA species, each with a distinct 5'-UTR, are driven by the promoters P1, P2 and P3. The P1 promoter is liver-specific, P2 is active in B cells, and P3 functions as an ubiquitous promoter (213–215). Upregulation of *ST6GAL1* has been reported in various cancers, including colon, breast, liver, cervix and brain carcinomas (216). ST6GAL1 plays a role in sialylation of key glycoproteins involved in oncogenic signaling networks, thereby promoting tumor cell behaviors such as migration, invasion, EMT and chemoresistance (213,216).

2.2.1.4. *MGAT5* (α -1,6-mannosylglycoprotein 6- β -N-acetylglucosaminyltransferase A)

The *MGAT5* gene encodes a glycosyltransferase that catalyzes transfer of GlcNAc residues from a UDP-GlcNAc donor substrate to an α 1,6-linked Man *via* a β 1,6-linkage, resulting in tri- or tetra-antennary branched *N*-glycans (217). The β 1,6-GlcNAc can be further modified by the addition of β 1,4-Gal, producing the N-acetyllactosamine (LacNAc) structure. Sequential actions of β 3- and β 4-galactosyltransferases can then extend LacNAc into a polylactosamine structure, a high-affinity ligand for galectins (218). *N*-glycan branching catalyzed by MGAT5 is one of the most frequently observed alterations in cancers, with *MGAT5* being upregulated in various human cancer types such as hepatocellular carcinoma, gastric, breast and lung cancer (218). The aberrant expression of *MGAT5* is often driven by the oncogenic Ras-Raf-Ets signaling pathway (219). Elevated levels of β 1-6 GlcNAc branching are

highly correlated with cancer malignancy and a poor prognosis (182). MGAT5 promotes malignant behavior by modifying *N*-glycans on specific glycoproteins such as growth factor receptors, matriptase, integrins, and cadherins. The β 1,6-GlcNAc branching reduces the adhesive properties of adhesion molecules, leading to enhanced cell migration and metastasis (186,217).

2.2.1.5. *MGAT3 (Beta-1,4-mannosyl-glycoprotein 4-beta-N-acetylglucosaminyltransferase)*

MGAT3 catalyzes the transfer of a GlcNAc residue from UDP-GlcNAc to β -Man *via* a β 1-4 linkage, forming a bisecting GlcNAc structure (220). The unique feature of bisecting GlcNAc is that it inhibits the activity of glycosyltransferases involved in producing *N*-glycan branches, such as MGAT4, MGAT5 and FUT8, as well as those modifying *N*-glycan terminals, including fucosyltransferases and sialyltransferases. Bisecting GlcNAc changes an overall structure of *N*-glycans to a back-fold conformation which reduces their affinity for other glycosyltransferases (186,221). MGAT3 expression is tissue-specific, reported in the brain, kidney, liver, placenta and bone marrow (222–225). Due to its involvement in diverse physiological processes, including cell adhesion, fertilization, neuritogenesis and immunity, MGAT3 is implicated in several complex diseases, such as cancer and Alzheimer's disease (225). Bisecting GlcNAc has been shown to suppress cancer growth and aggressiveness. MGAT3 forms a functional feedback loop with E-cadherin, where MGAT3 overexpression prolongs E-cadherin retention on the cell surface, enhancing cell adhesion, while E-cadherin upregulates the *MGAT3* gene (226,227). Given the mutually exclusive action of MGAT3 and MGAT5 on *N*-glycan branching, it is unsurprising that EMT is associated with increased expression of *MGAT5* and decreased expression of *MGAT3* (217,228).

2.2.1.6. *MGAT4A and MGAT4B (Alpha-1,3-mannosyl-glycoprotein 4-beta-N-acetylglucosaminyltransferase A and B)*

The MGAT4 family consists of four homologs, however, only MGAT4A and MGAT4B possess GnT-IV catalytic activity, enabling them to catalyze the transfer of a GlcNAc residue from UDP-GlcNAc to the α 1-3-linked mannose of the *N*-glycan core structure *via* a β 1-4 linkage (229). While MGAT4B is ubiquitously expressed in the human body, MGAT4A expression is restricted to specific tissues including pancreas, colon, small intestine, spleen, thymus, peripheral blood leukocytes, lymph nodes and prostate. The genes encoding *MGAT4A* and *MGAT4B* are located on chromosomes 2q12 and 5q35, respectively (183,186). In MGAT4B-deficient mice, genetic compensation with the induction of *MGAT4A* expression leads to a normal GnT-IV activity. Nevertheless, a double knockout of both *MGAT4A* and

MGAT4B abolishes GnT-IV activity, leading to the complete loss of β 1-4-GlcNAc branches on *N*-glycans (230). Studies indicate that *MGAT4A* and *MGAT4B* share similar donor and acceptor specificities, with *MGAT4A* showing higher affinity (231). However, recent research by Osada et al. reveals that *MGAT4A* and *MGAT4B* exhibit different glycoprotein selectivity, partially regulated by their C-terminal lectin domains (229). *MGAT4A* is crucial for insulin secretion and glucose metabolism in the pancreas (232). Human pancreatic β -cells from type 2 diabetes patients show downregulated *MGAT4A* and impaired glucose-stimulated insulin secretion (233). It seems that *MGAT4A* regulates the function of the glucose transporter GLUT2 by modifying its *N*-glycans (232). Both *MGAT4A* and *MGAT4B* exhibit aberrant regulation in certain cancers, including choriocarcinoma, pancreatic cancer, and hepatocarcinoma, although their detailed functions in cancer cells remain poorly understood (234–236).

2.2.2. Genetic and epigenetic regulation of protein *N*-glycosylation

The regulation of protein glycosylation is complex and still stays insufficiently understood. Complex glycans decorating around 60% of the human proteins are influenced by a combination of genetic network and environmental factors mediated by epigenetic mechanisms (40). Approximately 800 genes are involved in protein glycosylation. Around 500 of them are directly participating in glycan assembly, remodeling, and degradation (237). As genome-wide association studies (GWAS) continue to emerge, the list of the genes associated with protein glycosylation expands. GWAS studies also discovered that glyco-genes constitute only a small portion of the genetic network associated with *N*-glycome composition (238–240). One of the first GWAS on plasma glycome identified three significant loci: two of them were glyco-genes, *FUT6* and *FUT8*, but a third one was *HNFI1A*, a transcription factor not previously linked to protein glycosylation. *HNFI1A* knockdown leads to upregulation of *FUT8* and downregulation of *FUT* genes involved in antennary fucosylation, suggesting *HNFI1A* to act as a master transcriptional regulator of fucosylation (43). Subsequent GWAS studies associated *HNFI1A* with glycan branching and identified three additional genes—*MGAT5*, *B3GAT1*, and *SLC9A9*—linked to plasma glycome (241). One of the largest GWA studies of IgG glycosylation identified 27 loci associated with this process. By using a data-driven network approach authors proposed a functional network formed by identified loci. They suggest that transcription factors RUNX1 and RUNX3, along with the chromatin remodeling protein SMARCB1, regulate *MGAT3* expression. Additionally, by using short hairpin RNA, authors confirmed that transcription factor IKZF1 regulates *FUT8* expression, with its knockdown resulting in increased *FUT8* expression and higher IgG fucosylation (240).

The majority of the research focused on epigenetic regulation of protein glycosylation was performed on cancer cells/models, given the fact that aberrant glycosylation and epigenetic patterns are both characteristic of cancer cells. MicroRNAs (miRNAs) have emerged as important regulators of glyco-genes, with over 80 identified as miRNA targets, many of which include glycosyltransferases (237,242). For instance, *FUT8* is regulated by several miRNAs in different cancer cells, including its downregulation by miR-122, miR-34a, miR-26a, miR-146a, and miR-455-3p in liver cancer cells and by miR-198 in colorectal cancer (51,52,243). In cervical cancer cells, binding of miR-27a to the 3' UTR region of *B4GALT1* leads to its upregulation (244). Additionally, several miRNAs, including miR-199a, miR-214-3p, and miR-200, have been found to regulate *ST6GAL1* in cancer (50,245,246). Moreover, glycosyltransferases involved in glycan branching, *MGT4A* and *MGAT5*, are regulated by miR-424 and miR-124-3p, respectively (48,49).

Although many glyco-genes seem to be regulated by miRNAs, other publications demonstrate regulation by promoter methylation. For instance, multiple studies showed that the *MGAT3* gene is downregulated by promoter methylation. Klasić et al. demonstrated that 5-aza-2'-deoxycytidine (5-Aza-dC) treatment of HepG2 cells reduced highly branched glycans and core fucose-bearing structures, linked to *MGAT3* upregulation due to decreased CpG methylation in its promoter/first intron (45). Similarly, in ovarian cells BG1, 5-Azacytidine (5-Aza-C) increased *MGAT3* expression and level of bisecting GlcNAc (247). Targeted CpG methylation in the *MGAT3* CpG island downregulated its transcription and reduced quantity of *N*-glycans with bisecting GlcNAc in ovarian adenocarcinoma (62). In CD19⁺ B cells of IBD (Inflammatory Bowel Disease) patients, the *MGAT3* promoter hypermethylation was associated with specific IgG glycosylation patterns, including galactosylated, sialylated, and bisecting GlcNAc-containing glycans (42).

In colorectal carcinoma (CRC), *B4GALT1* hypermethylation and subsequent reduced transcriptional activity was correlated with poor prognosis and diminished cetuximab response (53,248). Additionally, hypermethylated *B4GALT1* demonstrates a highly discriminative ROC curve, effectively distinguishing metastatic CRC patients from healthy controls (248). Hypermethylation of *ST6GAL1* has also been reported in several cancers, including glioblastoma, breast, and bladder cancer (249–251). During differentiation of preadipocytes into adipocytes, downregulation of *ST6GAL1* is regulated through P3 promoter methylation (252). Both *MGT4A* and *MGAT4B* are shown to be regulated by DNA methylation in pancreatic cancer (235). Moreover, the expression of *MGAT5* has also been associated with changes in

DNA methylation. Specifically, treatment of ovarian cancer cells with 5-Aza-dC led to an increase in *MGAT5* expression together with increase in highly branched glycans (55).

A large study conducted by Vojta et al. analyzed two groups of publicly available data, DNA methylation and expression, for 86 glyco-genes in several types of tumors such as melanoma, breast, hepatocellular, and cervical cancers. They revealed ten glyco-genes that show different expression patterns in different types of tumors and metastases through CpG methylation, including *GALNT3*, *GALNT6*, *GALNT7*, *GALNT14*, *MGAT3*, *MAN1A1*, *MAN1C1*, *ST3GAL2*, *ST6GAL1*, and *ST8SIA3*. Furthermore, the *MGAT5B* gene emerged as a novel candidate gene that is epigenetically dysregulated in different cancers (44). The list of genes regulated by DNA methylation is continuously growing with new studies and it encompasses genes involved in both *N*-glycosylation and *O*-glycosylation. These genes include *FUT3*, *B4GALNT2*, *ST6GalNAc6*, *A3GALNT*, *B4GALNT1*, and many others (253,254).

Even though there are some data showing that glyco-genes are also regulated by histone modifications this stays largely unexplored, mostly because of the technical difficulties related to identification of a certain histone modifications in promoters. *MGAT5B* is one of the glyco-genes whose regulation is well studied, and it exhibits neural cell-specific regulation through histone acetylation, as demonstrated in several studies (255,256). It seems also that histone acetylation is involved in regulation of *ST6GalNAc6* in human colon cancer cells (257). Treatment of HeLa cells with HDAC inhibitors Trichostatin A (TSA) and sodium butyrate resulted in changes in HeLa cell membrane *N*-glycans. Furthermore, TSA treatment of HepG2 cells resulted in altered expression of several glyco-genes (258–260). However, there are a few studies associating epigenetic regulation of glyco-genes by histone modifications with corresponding *N*-glycan structures, therefore the knowledge regarding these interactions remains limited.

2.3. CRISPR/dCas9 systems for epigenome editing

Early epigenetic studies were largely correlative, often relying on genetic knockouts of chromatin regulators or global epigenetic perturbations induced by inhibitors of the main epigenetic writers or erasers making it challenging to establish a definitive causal relationship between epigenetic modifications and their subsequent effects on gene expression (59). The emergence of targeted epigenome-editing technologies has revolutionized the field. By fusing epigenetic effectors to DNA-binding domains, researchers can directly interrogate the link between chromatin modifications and gene expression. Initial targeting systems utilized zinc

finger proteins (ZNFs) and transcription activator-like effectors (TALEs), but both required complex protein engineering, thus limiting their scalability (56). The advent of the CRISPR/Cas9 system has significantly streamlined this process. CRISPR/Cas9, guided by small single-guide RNA (sgRNA) molecules complementary to the target sequence, allows for flexible and efficient targeting of specific genomic loci, making it a powerful tool for both genomic and epigenomic studies (56,261). Despite the CRISPR/Cas system's diversity, the components from the type II CRISPR system, especially Cas9 from *Streptococcus pyogenes* (SpCas9), became most commonly used in human genome and epigenome editing (262). The CRISPR/Cas9 system includes the Cas9 endonuclease, CRISPR RNA (crRNA) for target guidance, and trans-activating CRISPR RNA (tracrRNA) for crRNA maturation and Cas9 assembly, with proper Cas9 function requiring a protospacer adjacent motif (PAM) immediately downstream of the target sequence (263,264). This system was simplified by combining crRNA and tracrRNA into a single-guided RNA, with the first 20 nucleotides at the 5' end specifying the target (261). While native CRISPR-Cas9 has been effective in many genome-editing applications, emergence of catalytically inactive Cas9 (dCas9) marked a breakthrough in targeted epigenetic editing (Figure 7). Mutations including D10A in the RuvC domain and H840A in the HNH domain abolished its catalytic activity, allowing dCas9 to be fused to various effectors, including transcriptional repressors or activators and epigenetic modifiers (Figure 8) (57,58).

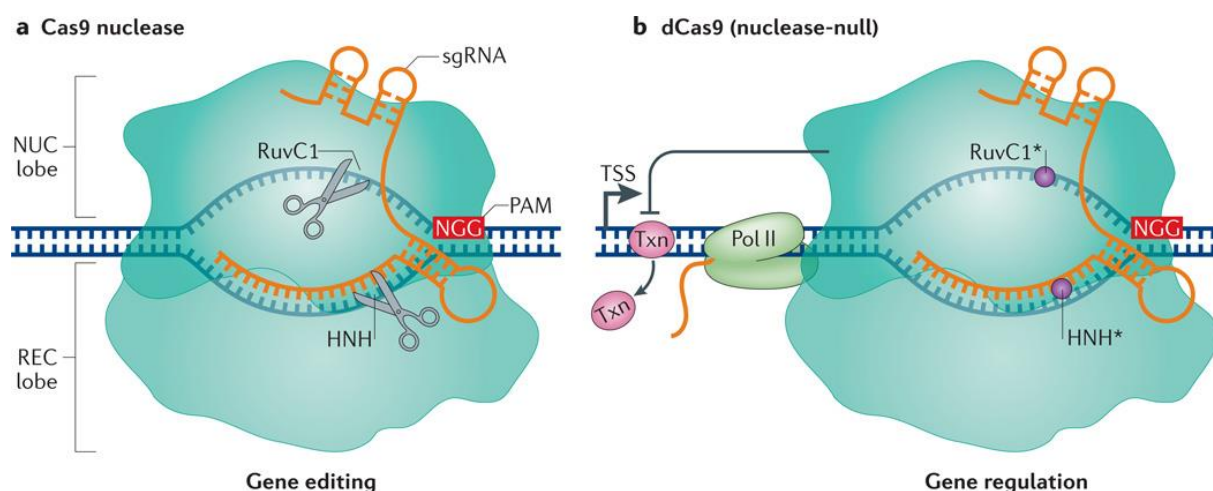


Figure 7. The comparison between CRISPR/Cas9 system used for gene editing and CRISPR/dCas9 used for gene regulation and epigenome editing. (a) The *S. pyogenes* Cas9 (SpCas9) protein consists of two lobes: the nuclease (NUC) lobe and the recognition (REC) lobe. SpCas9 is directed to a specific DNA sequence through complementary base pairing between the sgRNA and the target sequence, requiring the presence of a 5' protospacer-adjacent

motif (PAM) immediately downstream of the target. Cleavage of the target sequence is mediated by the RuvC1 and HNH nuclease domains. (b) Mutations in the RuvC1 (D10A) and HNH (H841A) domains generate a catalytically inactive dCas9. While dCas9 retains the ability to bind to the target DNA sequence *via* sgRNA and PAM recognition, it lacks the ability to cleave DNA. The binding of dCas9 downstream of a transcription start site (TSS) can interfere with transcription elongation by blocking either RNA polymerase II or transcription factors. Additionally, various transcriptional repressors, activators, or epigenetic modifiers can be fused to dCas9 to enable targeted gene regulation and epigenome editing. Adapted from (265).

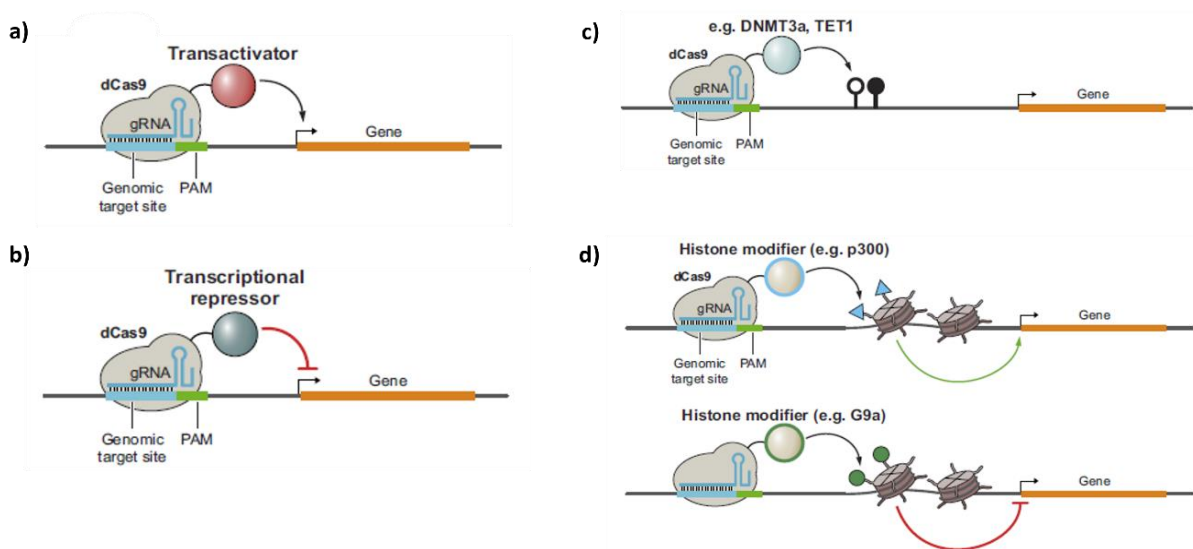


Figure 8. Diverse applications of the CRISPR/dCas9 system. The development of catalytically inactive dCas9 has enabled targeted genetic and epigenetic regulation of specific genomic loci. Fusions of dCas9 to different epigenetic effector domains enabled targeting to any desired genomic location using a single-guide RNA (sgRNA) in a presence of the protospacer-adjacent motif (PAM) sequence (shown as a green rectangle on the DNA sequence in all panels). (a) dCas9 fused to transcriptional activators enables precise upregulation of target gene expression; (b) dCas9 tethered to transcriptional repressors allows targeted silencing of specific genes; (c) dCas9 can be fused to epigenetic effectors that modify DNA methylation, thus enabling precise methylation change in a single or multiple cytosine sites; (d) dCas9 can be linked to histone modifying enzymes to impose or remove histone modifications. Adapted from (266).

Initial studies utilized dCas9 fused to known functional domains for transcriptional downregulation, termed CRISPRi (CRISPR interference), and upregulation, termed CRISPRa

(CRISPR activation) (56). The Krüppel-associated box (KRAB) domain is a widely used repression domain that promotes heterochromatin formation. It interacts with KAP1/TRIM28, hindering RNA polymerase II recruitment. Additionally, KAP1 recruits HP1, leading to increased H3K9me3 levels and chromatin condensation (56,267). An enhanced repression system was developed by fusing dCas9 with a bipartite repressor combining KRAB and MeCP2 domains, achieving stronger gene downregulation than either domain alone (268). CRISPRa was achieved by fusing dCas9 with various transcriptional activators, including p65, HSF1, MyoD, and viral transactivators Rta, VP16 and VP64 (56). These fusion proteins recruit chromatin modifiers that induce chromatin decondensation, introduce activating histone marks (H3K27ac, H3K4me3), and facilitate RNA polymerase II binding, increasing mRNA transcription (56,269). The VPR system, a chimeric protein combining VP64, p65, and Rta activation domains, further enhances gene activation (270).

Several groups have developed dCas9 fusions with catalytic domains of different DNMTs, achieving efficient site-specific DNA methylation at promoters and enhancers in primary cells, cancer cell lines, and embryonic stem cells (ESCs) (56,61,271,272). The catalytic domain of DNMT3A is the most used for such purposes. Studies have shown that utilizing the catalytic domain alone, rather than the full-length protein, can enhance efficiency for DNMTs and other epigenetic effectors (61,273,274). The transcriptional effects of targeted DNA methylation vary, with introduced CpG methylation causing strong silencing, moderate to low downregulation, or even mild upregulation (275–277). Targeted methylation efficiency was enhanced using the SunTag system which involves an array of GCN4 peptide epitopes attached to the dCas9 (277). These epitopes recruit multiple single-chain antibodies (scFv) linked to effector domains, delivering numerous effectors to the target site (278). Further enhancement of targeted DNA methylation was achieved by combining DNMT3A with DNMT3L or KRAB domains (279,280). Apart from targeted methylation, several groups have designed dCas9-based molecular tools for targeted DNA demethylation, primarily using the catalytic domain of TET1 (60,273,281,282). The effects of targeted demethylation on transcriptional function have been diverse, with most studies reporting moderate effects (273,281). However, some studies have reported strong gene reactivation, even leading to phenotypic changes (60,273,282). For instance, targeted demethylation of the *BRCA1* gene not only increased its expression but also inhibited cell proliferation in a cancer cell line (273). Targeted demethylation of the CGG-expansion mutation in the *FMRI* gene, a single gene

epimutation cause of fragile X chromosome syndrome, rescued disease-associated phenotypes of affected neurons both *in vitro* and *in vivo* (60) .

The CRISPR/dCas9 system has been successfully employed to target specific histone modifications at defined genomic loci in ESCs and cancer cell lines. This includes the use of histone H3K methyltransferases such as SMYD3, DOT1L and PRDM9 (64,274). Targeting with dCas9-PRDM9 fusion proteins led to a 60% increase in H3K4me3 and up to an eightfold increase in mRNA levels. Furthermore, it was found that the presence of H3K79 methylation is required for the stable maintenance of H3K4me3 and combining dCas9-PRDM9 and dCas9-DOT1L resulted in prolonged periods of active transcription (64). One of the most commonly used epigenome editing tools involves the catalytic domain of p300. Multiple studies have used dCas9-p300 fusions leading to increased levels of H3K27ac (66,283–285). These studies report that targeted H3K27ac can induce transcriptional activation ranging from 10- to 100-fold (283,284), with one study demonstrating transcriptional induction of up to 10,000-fold at both proximal promoter elements and distal enhancers (66).

The dCas9 fusions have also been designed to induce histone modifications associated with repressed gene state. For instance, genomic loci have been targeted with EZH2, an effector domain that induces H3K27me3, and with G9a or SUV39H1, both of which introduce H3K9me2. The effects of these domains on gene expression were context- and gene-specific. While no detectable changes in H3K9me3 levels were observed with SUV39H1, G9a was able to increase H3K9me3 levels by 13-fold (63). Furthermore, dCas9 has been fused to effectors that catalyze removal of histone modifications. This includes histone deacetylases HDAC3 and HDAC8 (65,286). Targeting promoter regions of *Smn1*, *Mecp2*, and *Isl1* genes in murine N2a cells with dCas9-HDAC3 fusion led to decreased levels of H3K27ac and moderate downregulation of gene's transcription. The study also showed that dCas9-HDAC3 efficiency depends on sgRNA location, with optimal performance observed when a sgRNA is adjacent to H3K27ac marks (65). Successful gene repression has also been achieved using dCas9 fused to the LSD1 demethylase, resulting in up to 85% loss of H3K4 methylation marks at target sites (287).

In addition to using only the catalytic domain of effector proteins, epigenetic editing tools commonly employ amino acid linkers to fuse the effector domain with dCas9. The structure and length of these linkers are critical for ensuring robust and precise epigenetic modifications (281,288). The CRISPR/dCas9 system offers several advantages, including the ability to amplify the desired epigenetic effect. Various strategies have been employed to

achieve this. One such strategy is the aforementioned SunTag system (276–278). Another approach involves the use of multiple sgRNAs, which not only amplifies the effect but also promotes the spreading of the targeted epigenetic modification to adjacent chromatin (271,274,282). Due to their short length, multiple sgRNA cassettes can be incorporated into a single vector and transcribed as a single precursor transcript using tissue-specific Pol II promoters. These transcripts can then be processed into individual sgRNAs through various mechanisms (266). The CRISPR/dCas9 system also offers the advantage of simultaneously editing multiple epigenetic marks at the same or different loci within a single cell by using different Cas9 orthologs. These orthologs, such as *Staphylococcus aureus* Cas9 (SaCas9), often recognize more complex PAM sequences while maintaining efficiency similar to SpCas9 (289). This specificity allows for a design of sgRNAs that recruit distinct Cas9 orthologs to targeted sites, enabling concurrent manipulation of multiple epigenetic marks and genomic loci (62,290). In a study conducted by Josipović et al., dual epigenetic editing of the *HNFL1A* gene with TET1-dSaCas9 and the *MGAT3* gene with DNMT3A-dSpCas9 led to altered glycan phenotype in the BG1 cell line. Moreover, the group created a modular CRISPR/dCas9 toolbox allowing for the expression of orthogonal dCas9 proteins fused to different effectors. This system utilizes a multi-sgRNA strategy to concurrently target up to six different genomic sites (Figure 9) (62).

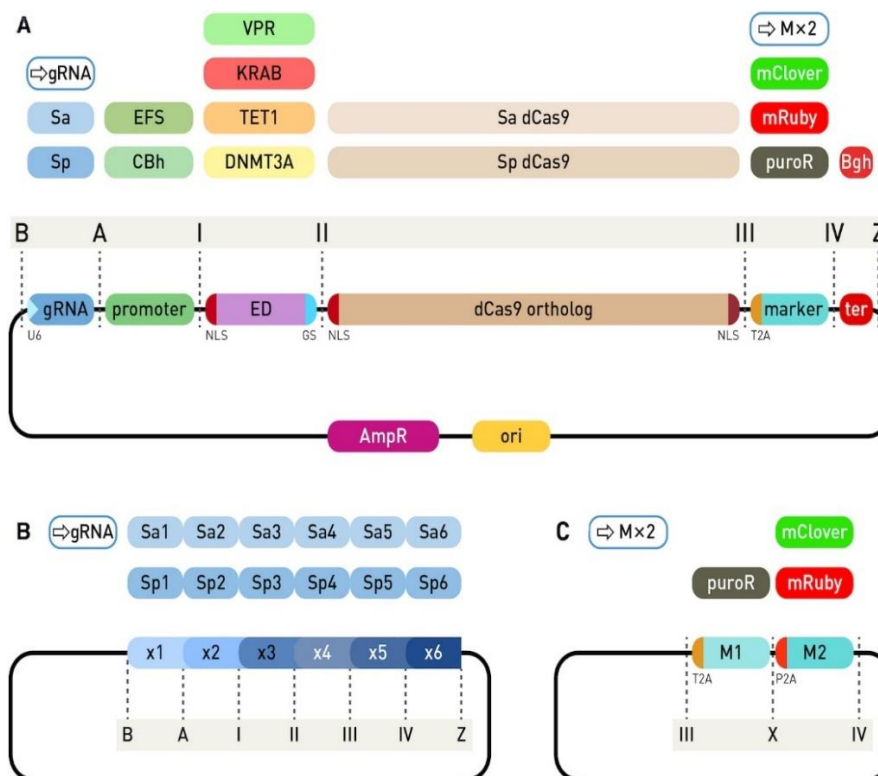


Figure 9. Figure is described on the following page.

Figure 9. Modular CRISPR/dCas9 toolbox for epigenetic editing and direct gene regulation. (A) The N-terminal dCas9 expression cassette is assembled from individual modules using Golden Gate cloning with the BsaI type IIS restriction enzyme. Backbone plasmids have compatible ends designated as 'B' and 'Z'. The sgRNA expression module is inserted between positions 'B' and 'A.' This module contains either the SpCas9 or SaCas9 scaffold with a pre-inserted variable gRNA region, an empty module for gRNA cloning using red-white selection, or a multi-guide module enabling insertion of up to six sgRNAs. A eukaryotic promoter is inserted at the 'A' to 'I' position, followed by an effector domain at the 'I' to 'II' position. The effector domain includes an N-terminal nuclear localization signal (NLS) and short G4S linker linked to dCas9 ortholog inserted at the 'II' to 'III' position. The position from 'III' to 'IV' receives a selection marker linked to a self-cleaving T2A peptide, which can be replaced with a dual-marker system. Finally, a eukaryotic transcription terminator is inserted between the ends 'IV' and 'Z'. (B) The multi-guide system, that allows for the insertion of up to six gRNA modules for either dSpCas9 or dSaCas9 orthologs. Each gRNA module requires pre-cloned variable regions, inserted in a second step using the type IIS restriction enzyme Esp3I, with selection facilitated by red-white screening. (C) The dual marker system enables the addition of both antibiotic resistance and fluorescent protein. Dual modules include T2A and P2A self-cleaving peptides to ensure equimolar expression with dCas9. Adapted from (62).

Despite the widespread use of the CRISPR/Cas9 system in epigenetic and genetic studies, a major issue that still needs to be resolved is the off-target effect. Many studies reported increased CpG methylation at untargeted sites across the genome when using dCas9-DNMT3A. However, the extent of these off-target effects varies between studies (62,271,272,276,280). It has been shown that the off-target effect is dependent on the sgRNA sequence (291). While the complete elimination of off-target activity has not yet been achieved, certain strategies have been employed to minimize it and optimize the balance between on- and off-target effects. These strategies include transfecting with lower amounts of plasmids encoding dCas9 and sgRNAs, using weaker RNA polymerase II promoters to reduce sgRNA transcription levels, and applying temporal control of dCas9 expression through inducible systems, such as a doxycycline-inducible Cas9 system (292–295).

3. MATERIALS AND METHODS

3.1. Materials

3.1.1. Cell lines and bacterial strains

HepG2 (ACC 180) (DSMZ, Braunschweig, Germany), Escherichia coli XL10-Gold (Agilent, Santa Clara, CA, USA), NEB Stable Competent Escherichia coli (New England BioLabs, Ipswich, MA, USA)

3.1.2. Single-guide RNA sequences, pyrosequencing primers and assays, and qPCR primers

Six sgRNAs complementary to the regulatory region of the *B4GALT1*, *ST6GAL1*, *MGT4A*, *MGAT4B* and *MGAT5* gene and five sgRNAs complementary to the regulatory region of the *FUT8* gene were used for targeting with the DNMT3A-dSpCas9 fusion protein. Same sgRNAs were employed to target the regulatory regions of the *B4GALT1* and *FUT8* with the G9a-dSpCas9 and RIOX1-dSpCas9 fusion proteins. Six sgRNAs were also used to target *MGAT3* gene with TET1-dSaCas9. Sequences of these sgRNAs are listed in Table 1.

Table 1. sgRNA sequences targeting *B4GALT1*, *ST6GAL1*, *FUT8*, *MGAT4A*, *MGAT4B*, *MGAT5*, and *MGAT3* regulatory regions, and the corresponding fusion proteins.

Target	Name	Sequence (5'-3'), including PAM (underlined)	Fusion protein
<i>B4GALT1</i>	B4GALT1_sgRNA01	GTGGACCCCGCTGCTTAACGGGGG	DNMT3A-dSpCas9, G9a-dSpCas9, RIOX1-dSpCas9
	B4GALT1_sgRNA02	GCGACCGAAGCTCCGCCGCAAAGG	
	B4GALT1_sgRNA03	GACCCCTTCTTAAAGCGGCGCGGG	
	B4GALT1_sgRNA04	GCAGGGCCAGAATCCACGACTGGG	
	B4GALT1_sgRNA05	GTCACCTGGCCCAAACGATCAGG	
	B4GALT1_sgRNA06	GTACCCAAAACCTAGGTGAGCAGG	
<i>ST6GAL1</i>	ST6GAL1_sgRNA01	GTAGCGACCTCCAGGCCGGTTTGG	DNMT3A-dSpCas9
	ST6GAL1_sgRNA02	GCACTGCCCGGCGTTAAACAAAGG	
	ST6GAL1_sgRNA03	GACACTCCTCCCGGGATAGCCCGG	
	ST6GAL1_sgRNA04	GACCCATACTGACGGTGCCGTGG	
	ST6GAL1_sgRNA05	GAATGTACGAGTCGCCAGTGCGG	
	ST6GAL1_sgRNA06	GAGATGGTTTCGCGGTGAATTGG	
<i>FUT8</i>	FUT8_sgRNA01	GCTGCTCTGCATCGCGGGCGCCGG	DNMT3A-dSpCas9, G9a-dSpCas9, RIOX1-dSpCas9
	FUT8_sgRNA02	GAGCGGGTAGGACGCATCCTAGGG	
	FUT8_sgRNA03	GATGCCATTGTAGGATCGCGCTGG	
	FUT8_sgRNA04	GTCCGGCTCGCACACAGGCGTAGG	
	FUT8_sgRNA05	GCATGCCAGGGTCGCCGTAGGTGG	
<i>MGAT4A</i>	MGAT4A_sgRNA01	GCGGGAGTCGGCGCTTTCGCGGGG	DNMT3A-dSpCas9
	MGAT4A_sgRNA02	GAGATAATGACAGTCGTTCTGG	
	MGAT4A_sgRNA03	GCGGCAAAGTGTTCTCAGCCGTGG	
	MGAT4A_sgRNA04	GGCTCATCGGTGTCACGGCGAGG	
	MGAT4A_sgRNA05	GCGATTCGCGGGGTTCTCACCGGG	
	MGAT4A_sgRNA06	GATAGCAGGCAACCGTATAGCAGG	

<i>MGAT4B</i>	MGAT4B_sgRNA01	GTGCTGGCAGAGCTCGGCGT <u>GGG</u>	DNMT3A-dSpCas9
	MGAT4B_sgRNA02	GATCGCCAAGACCGGCCAGCGGGG	
	MGAT4B_sgRNA03	GCGACGCGTTCTGGGCGCCGA <u>AGG</u>	
	MGAT4B_sgRNA04	GGGCCTTTCTAGGCGGTATC <u>AGG</u>	
	MGAT4B_sgRNA05	GATCGGGAGCTTCGAGGGGTCT <u>GG</u>	
	MGAT4B_sgRNA06	GTCATCTCCTCGGGTGCGCGG <u>CGG</u>	
<i>MGAT5</i>	MGAT5_sgRNA01	GTGTAATGCGTTCTACGAAAGAGG	DNMT3A-dSpCas9
	MGAT5_sgRNA02	GTATTTATGGCCGCGATCAGA <u>AGG</u>	
	MGAT5_sgRNA03	GCCGGATCCGGGTGATCGCGT <u>CGG</u>	
	MGAT5_sgRNA04	GCAACAAGCCCCCTCGTCACG <u>GGG</u>	
	MGAT5_sgRNA05	GCGGCCCTCAGCTCGCAAAGTT <u>GG</u>	
	MGAT5_sgRNA06	GCGCGGCGGCTACAAAACCG <u>CGG</u>	
<i>MGAT3</i>	MGAT3_sgRNA01	GCCGGCTGGCGGGGGAGGGGAGGGGGT	TET1-dSaCas9
	MGAT3_sgRNA02	GGAGCACATTTCGCTGGGATATAGA <u>AT</u>	
	MGAT3_sgRNA03	GGTGCAGGCACAAGGCATTGTG <u>GGT</u>	
	MGAT3_sgRNA04	GGACGCCTCTGAGCCCTGAGAGGA <u>AT</u>	
	MGAT3_sgRNA05	GTCTGTGTGTCTGCTTGGGGCGTG <u>GGT</u>	
	MGAT3_sgRNA06	GTGGCAGGAGAGTAGGCTCAAGAG <u>GGT</u>	

Only one sgRNA was used for targeting regulatory regions of *B4GALT1* and *FUT8* with HDAC3-dSpCas9 as well as for targeting the regulatory region of *MGAT3* with PRDM9-dSaCas9 and p300-dSaCas9. These sgRNAs are listed in Table 2.

Table 2. The sgRNA sequences used with HDAC3-dSpCas9, PRDM9-dSaCas9, and p300-dSaCas9, along with their corresponding target regions.

Target	Name	Sequence (5'-3'), including PAM (underlined)	Fusion protein
<i>B4GALT1</i>	B4GALT1_H3_sgRNA	GCGTCCAGAAAACCCCGCGCC <u>CGG</u>	HDAC3-dSpCas9
<i>FUT8</i>	FUT8_H3_sgRNA	GGGCAAAACATTCCTAGGAC <u>AGG</u>	HDAC3-dSpCas9
<i>MGAT3</i>	MGAT3_hist_sgRNA	GGTGCAGCCGAGCGGCCGCGCC <u>GGT</u>	PRDM9-dSaCas9, p300-dSaCas9

Table 3 lists all primers used for cloning the new N-terminal dSpCas9 fusion with full-length histone deacetylase HDAC3. This includes primers for amplifying the full coding sequence of HDAC3, as well as primers for site-specific mutagenesis used to mutate BsaI restriction sites in the HDAC3 sequence and introduce mutations to generate a catalytically inactive form of HDAC3.

Table 3. Primer sequences used for cloning of the HDAC3-dSpCas9 construct. S indicates the sense strand, and A indicates the antisense strand of the DNA molecule.

Name	Sequence (5' – 3')	Purpose
HDAC3_Fw	TTCGTCTCTGGAGGAGGATCTATGGCC AAGACCGTCGCCTATTTCTACG	PCR amplification of HDAC3 coding sequence
HDAC3_Rev	TTCGTCTCTCGAAAATCTCCACATCGC TTTCCTTGTCATTGTCATGATCTCCATC	
HDAC3_mut_R 265P_S	CTGTGATCCATTGGGCTGCTTTAACCTCAGC	Site-directed mutagenesis for generating catalytically inactive HDAC3
HDAC3_mut_R 265P_A	GCTGAGGTAAAGCAGCCCAATGGATCACAG	
HDAC3_noBsaI S	ATTACGGTCTGTATAAGAAGATGATCGTCTTC	Site-directed mutagenesis of BsaI restriction site
HDAC3_noBsaI A	GCAGGACCAGGCTATGGG	
pUX21_seq_Fw	GTAAAACGACGGCCAGT	Primers used for sequencing of HDAC3 full length domain prior and after site-directed mutagenesis.
pUX21_seq_Re	CCTGTGTGAAATTGTTATCCGCT	

To analyze DNA methylation using bisulfite pyrosequencing, target regions were amplified using primers specific to bisulfite-converted DNA. One of the primers (depending on the DNA strand sequenced) included a biotin (Btn) attached to its 5' end. These amplified regions were subsequently sequenced using pyrosequencing, either with a separate sequencing primer or with one of the PCR primers. The specific primers and pyrosequencing assays used are listed in Tables 4 and 5, respectively. In Table 4, sequencing-specific primers are labeled with "seq" in their name. If no separate sequencing primer is indicated, the PCR primer lacking the Btn at its 5' end was used for sequencing.

Table 4. Primers used for amplification of specific genomic regions on a bisulfite converted DNA and pyrosequencing primers with appropriate annealing temperature (Ta) together with assay according to which amplified regions are sequenced.

Primer name	Sequence (5'-3')	Ta (°C)	Assay
B4GALT1_F1	[Btn]ATAGTTTAGGTTATTTGATG	48	B4GALT1-1
B4GALT1_R1	CTCCCTAACTCAACC		

B4GALT1_F2	TGGAGGAGGAAGAGGAGG	48	B4GALT1-2
B4GALT1_R2	[Btn]AAATATAACTACAACCTC		
FUT8_F1	[Btn]GGTTATAGGGAAGAGTTTG	48	FUT8-1
FUT8_R1	AAACCAATCAAACTAC		
FUT8_F2	GGTTTGGGTTGTTTTGG	57	FUT8-2
FUT8_R2	[Btn]CTTAATACTACTTCCAAC		
FUT8_seq2	GTTTTAGAGGGGTTGT	/	
FUT8_F3	[Btn]AGGGAGTATAGTATTTTTTGGAGG	50	FUT8-3
FUT8_R3	ACCCTAACATATACCAAAAATTCT		
FUT8_seq3	CCACCCCCTAACAAAACC	/	
ST6GAL1_F1	GGAGGAGTGTGATGTAA	52	ST6GAL-1
ST6GAL1_R1	[Btn]TTGTAGAGTTTGGGTTTA		
ST6GAL1_seq1	GAGTGTGATGTAAAGGGG	/	
MGAT3_F1	GTTTTTGAGTTTTGAGAGGAATGG	60	MGAT3-1
MGAT3-R1	[Btn]ACCCTCTTAAACCTACTCTCCTAC		
MGAT4A_F1	GAGAGAGTTGAGGTTTG	45	MGAT4A-1
MGAT4A_R1	[Btn]CAACTACCTATAAAACCC		
MGAT4A_seq1	TATTTTGTGTGAAAATTTTTTG	/	
MGAT4B_F1	TAGGAGTTTTTTTTTGGGTTTTTGGA	52	MGAT4B-1
MGAT4B_R1	[Btn]TACCATTCTAACTAATCACTACTCTACAT		
MGAT5_F1	GATTTAGTTTAGGTAGT	40	MGAT5-1
MGAT5_R1	[Btn]CTCTTACCTCCTTATTA		

Table 5. Sequences of assays used for CpG methylation analysis in selected genomic regions. The table provides sequences of unconverted DNA with the analyzed CpG sites highlighted in red.

Assay name	Sequence (5' – 3')
B4GALT1-1	GGGAGGCACAGAAGTGGCAACCCGTCCTCACTTTCTTTGCGCAGG ACCCCCCGTTAAGCAGCGGGGTCCAGCCG
B4GALT1-2	CGCGGCTCAACGCGACCGAAGCTC
FUT8-1	GGGAAGCTCATCTTCGGGCCCTCTGATTGGCCGGCTCGCACTCCA CTCAGCGGCGCG
FUT8-2	CGCAGCCGCGGGTGGGAGAGG
FUT8-3	GCCGGCGTGCGCAGCCGCTGCCCTGCTGGAAGTGTGCCGTCCCG CTGTGGCCCGC
ST6GAL-1	CGCGGGAGGATAGCGGAGGCGCGGGGCCCGCGGCGCGCGTAGG GCGCAG
MGAT3-1	CCTAGAGCAAGGCCACGAGGAGCCAGGGCACGACACGGTGGGC CCTCGGAGAACCCTG
MGAT4A-1	CGAAGGCTGCACGGCCGGTCCCCT
MGAT4B-1	CGGAGGCGCGCAGGGGCCCGGGAGGCGGGAACGATG
MGAT5-1	CGCGCCGAGGCTCGGGGCGTCGCGACCTCGCGCCTCGGGCCCG GTGGGCACGGCGGGCCGGCGGGTGCTCCCG

To analyze the enrichment with H3K4me3, H3K9me2 or H3K27ac in selected genomic regions after Chromatin immunoprecipitation (ChIP) and CUT&RUN method, quantitative polymerase chain reaction (qPCR) with SYBR green technology was used. For this purpose, three to four different sets of primers were used for *FUT8*, *B4GALT1* and *MGAT3*. Primers are listed in Table 6.

Table 6. qPCR primers used for analyzing H3K27ac, H3K9me2 or H3K4me3 enrichment in *B4GALT1*, *FUT8* and *MGAT3* after ChIP and CUT&RUN.

Primer Name	Sequence	Target Region
B4GALT1_qChIP_F1	CGGCTGATCTCCTGCACGCT	B4GALT_qChIP_1
B4GALT1_qChIP_R1	GTGTGTGGCGGGAGTCCTGT	
B4GALT1_qChIP_F2	CTGAGCCGCCTGCCCCAACTGG	B4GALT_qChIP_2

B4GALT1 qChIP R2	CCCGATGGCGGGCGGCACTGTTC	qChIP_2
B4GALT1 qChIP F3	GCCTCCTCCTGGTATGGGTA	B4GALT_ qChIP_3
B4GALT1 qChIP R3	CAGAAATGGGCAACGTGGTG	
FUT8 qChIP F1	TGGGATGGCAGCTAAATCCTGAGCCTG	FUT8_ qChIP_1
FUT8 qChIP R1	GTCTGCTTTGTTGAATCAATGTGCTTCTCCACC	
FUT8 qChIP F2	GCACCAAATCCTGGGCAAAACATTCC	FUT8_ qChIP_2
FUT8 qChIP R2	GCACTTATTTTCCCTACCTCCTTCCAACCTG	
FUT8 qChIP F3	TCCGAGCGGGTAGGACGCAT	FUT8_ qChIP_3
FUT8 qChIP R3	AGCCCCTCTGAGGCGGAAGT	
FUT8 qChIP F4	GTCAAGCGGCCAAATGCGGG	FUT8_ qChIP_4
FUT8 qChIP R4	GGGGCACCCGCACTAGAGGT	
MGAT3 qChIP F1	GGAAACACGTGGGGGACGCC	MGAT3_ qChIP_1
MGAT3 qChIP R1	GAGGGCCCACCGTGTCGTG	
MGAT3 qChIP F2	GCATGTGAGGGACGGAGGGG	MGAT3_ qChIP_2
MGAT3 qChIP R2	GGCCTGGGCCTGTGATGTGT	
MGAT3 qChIP F3	AACGCACCCGTCCACGCATA	MGAT3_ qChIP_3
MGAT3 qChIP R3	GTGCGGGGAATGCGGGTAGT	

3.1.3. Derived glycan traits

To assess the effect of targeted DNA methylation manipulation on protein *N*-glycosylation, total cell *N*-glycome of HepG2 cells was analyzed. The total *N*-glycome from HepG2 cells contained 31 glycan peaks (GP1-GP31). Instead of analyzing the changes in each peak separately, derived glycan traits were calculated, and all statistical analyses were performed on them. Table 7 lists all derived traits with appropriate glycan peaks they include.

Table 7. Derived glycosylation traits with corresponding glycan peaks included in their calculation.

Derived trait	Description	Glycan peaks
PM	Paucimannose glycans	GP1, GP3, GP4
OM	Oligomannose glycans	GP5, GP9, GP13, GP16, GP18, GP20
LB	Low branched glycans	GP14, GP17, GP19, GP21
HB	High branched glycans	GP23, GP24, GP25, GP26, GP27, GP28, GP29, GP30, GP31
G0	Agalactosylated glycans	GP10, GP12
G2	Digalactosylated glycans	GP14, GP17, GP19, GP21
G3	Trigalactosylated glycans	GP23, GP24, GP26, GP28

G4	Tetragalactosylated glycans	GP29, GP30, GP31
GN	Total galactosylated glycans	GP14, GP17, GP19, GP21, GP23, GP24, GP25, GP26, GP27, GP28, GP29, GP30, GP31
S0	Asialylated glycans	GP10, GP12, GP14
S1	Monosialylated glycans	GP17, GP19, GP29
S2	Disialylated glycans	GP21, GP23
S3	Trisialylated glycans	GP28
SN	Total sialylated glycans	GP17, GP19, GP21, GP23, GP24, GP25, GP26, GP27, GP28, GP29, GP30, GP31
FC	Glycans containing core fucose	GP2, GP4, GP7, GP10, GP12, GP19, GP21, GP23, GP25, GP26, GP27, GP28, GP29, GP30, GP31
FA	Glycans containing antennary fucose	GP27, GP29, GP30, GP31
SR	Sialylated to asialylated ratio	SN/S0
GR	Galactosylated to agalactosylated ratio	GN/G0

3.2. Methods

3.2.1. Cell culture conditions and transfection

Human hepatocellular carcinoma cell line HepG2 was maintained in RPMI-1640 Medium (Sigma-Aldrich, St. Louis, MO, USA) supplemented with 10% heat-inactivated fetal bovine serum (FBS, Sigma-Aldrich). Cells were incubated at 37 °C in a humidified 5% carbon dioxide (CO₂)-containing atmosphere. They were cultured and passaged using 1x Phosphate-saline buffer (PBS) (137 mM NaCl, 2.7 mM KCl, 4.3 mM Na₂HPO₄, 1.47 mM KH₂PO₄, pH 7.4) and 0.25% trypsin-EDTA solution (Sigma-Aldrich). All transfections were performed in the same manner. Twenty-four hours prior transfection, cells were seeded in 10 cm petri dishes in the number of 4.2 million cells per dish. Cells were transfected the next day at around 80% confluency using PEI MAX (Polyethyleneimine hydrochloride, MW 40 000, Polysciences Inc., Warrington, PA, SAD), according to the manufacturer's protocol. Briefly, 8 µg of each plasmid was mixed with three times more PEI max reagent (mass ratio 1:3) in RPMI-1640 media without serum. The mixture of PEI max and plasmid in RPMI-1640 without serum was incubated for 30 min. Fresh RPMI-1640 media with 10% heat-inactivated FBS was added to cells and 1 ml of PEI max and plasmid mixture was added in each petri dish. The next day, cells were either screened for the expression of red fluorescent protein mRuby (Em λ 605 nm) or the

expression of green fluorescent protein mClover (Em λ 518 nm for mClover) using the Olympus IX73 inverted microscope. Furthermore, 24 hours post-transfection, cells were selected with 4 μ g/ml of Puromycin (10 mg/mL, Gibco, Grand Island, NY, USA) for 48 hours. After selection, cells were washed in 5 ml of 1xPBS and fresh RPMI media with 10% FBS was added. Cells transfected with constructs for targeted DNA methylation and demethylation as well as with construct for targeted introduction of H3K9me2 and H3K4me3 were collected 8th and 12th day post-transfection for subsequent analyses. Cells transfected with constructs for targeted introduction or removal of other histone modifications were collected on the 5th and 8th day post-transfection.

3.2.2. Cloning of DNMT3A-dSpCas9 and TET1-dSaCas9 constructs for targeted cytosine methylation and demethylation

The CpG islands of the genes *B4GALT1*, *ST6GAL1*, *FUT8*, *MGAT4A*, *MGAT4B*, and *MGAT5* are hypomethylated in HepG2 cell line and were therefore selected for targeting with the DNMT3A-dSpCas9 construct. For each gene, six sgRNAs spanning the CpG island and surrounding regions were designed, except for *FUT8*, for which five sgRNAs were designed. The sgRNAs were designed according to reference sequences from hg19 version of human genome using the web tool CRISPOR (296). The sgRNAs were designed to be 20 bp in length and to target sequences followed by an NGG PAM motif at the 3' end. sgRNAs with the highest scores and minimal potential off-target effects were selected (Table 1). In sgRNAs lacking base G at the beginning of their 20 bp target sequence, one G nucleotide was added to make the sequences compatible with the U6 promoter that drives their expression from the final expression plasmid. *MGAT3*, the only candidate gene with hypermethylated CpG island in the HepG2 cell line, was selected for targeting with the TET1-dSaCas9 construct. Six sgRNAs spanning its CpG island were previously designed by the research group (62). For each designed guide (sense sgRNA), a complementary antisense sgRNA was designed. Both sense and antisense sgRNAs were extended by four nucleotides at the 5' end to include a BbsI restriction site required for cloning the sgRNA molecules into the destination vector. Sense and antisense sgRNAs were annealed and ligated into BbsI-digested pSgMx-G (x = 1-6) vectors for genes targeted by DNMT3A-dSpCas9, while sgRNAs for *MGAT3* were pre-cloned into pSgMx-A (x = 1-6) vectors. The 'x' denotes the cloning order within the multi-guide module in the final expression plasmid.

Constructs containing either DNMT3A-dSpCas9 or TET1-dSaCas9, along with sgRNAs targeting each gene, were assembled using a modular system developed by Josipović

et al. (62) This system combines an N-terminal dCas9 expression cassette (encoding DNMT3A-dSpCas9 or TET1-dSaCas9 fusion proteins) with a multi-guide module capable of accommodating up to six sgRNAs, using a single Golden Gate reaction with the type IIs restriction enzyme BsaI. Restriction with BsaI generates non-palindromic overhangs, enabling precise assembly of modules in a defined order (Figure 9). In a single Golden Gate reaction, the following modules were assembled into a secondary backbone containing a puromycin resistance cassette: a pSgx6 or pSgx5 multi-guide module (accommodating six or five sgRNAs, respectively), a pPro-EFS promoter, an effector domain (DNMT3A or TET1), a dCas9 variant (dSpCas9 or dSaCas9), a fluorescent marker (mRuby or mClover), and a pTer-H terminator. Apart from the secondary backbone and modules, the 20 µl reaction mix contained: 1× CutSmart buffer (New England Biolabs, Ipswich, MA, USA), 1 U/µl BsaI-HF®v2 (New England Biolabs), 1 mM ATP, and 17.5 U/µl T4 DNA ligase (Takara, Tokyo, Japan). A second Golden Gate assembly step using Esp3I was performed to integrate sgRNAs from pSgMx-G or pSgMx-A into the multi-guide module cassette. This second Golden Gate reaction also included 1× Buffer Tango (Thermo Fisher Scientific, Waltham, MA, USA), 0.5 U/µl Esp3I (Thermo Fisher Scientific), 1 mM ATP, 1 mM DTT, and 17.5 U/µl T4 DNA ligase in a 20 µl reaction. Two control plasmids were generated: an "Inactive" control (IN) with catalytically inactive DNMT3A or TET1 fused to dCas9, and a "Non-target" (NT) control with a non-targeting sgRNA (NT-gRNA). NT-gRNA is not complementary to any sequence in the human genome. Expression plasmids for both controls were cloned as described, with the NT control using a module containing NT-gRNA instead of pSgx6 or pSgx5, and the inactive control using a catalytically inactive effector domain instead of the active one. Plasmids expressing DNMT3A-dSpCas9 fusions and corresponding controls contained red fluorescent marker (mRuby), while plasmids expressing TET1-dSaCas9 fusions and corresponding controls contained green fluorescent marker (mClover). All expression plasmids were amplified in a NEB Stable Competent Escherichia coli bacterial strain and isolated using NucleoBond Xtra Maxi Plus Kit (Macherey-Nagel, Düren, Germany) according to manufacturer's protocol. To ensure correct assembly, restriction analysis was performed on all constructs.

3.2.3. Cloning of a full-length HDAC3 catalytic domain

The HDAC3 effector domain, which was not available in the epi-toolbox developed by the research group, was cloned as part of this research. The full-length HDAC3 domain was amplified using Herculase II Fusion Polymerase (Agilent Technologies, Santa Clara, CA, USA) with primers HDAC3_Fw and HDAC3_Rev (Table 3) according to manufacturer's protocol. In

addition to containing bases complementary to the start and end of the HDAC3 cDNA sequence, the primers included additional sequences at their 5' ends for restriction enzyme recognition and subsequent ligation into a destination vector. The cDNA isolated from FreeStyle™ 293-F cells served as the template. PCR amplification was performed under the following conditions: initial denaturation at 95 °C for 1 minute; 35 cycles of 20 seconds at 95 °C, 20 seconds at 59 °C and 1.5 min at 68 °C; followed by a final elongation at 68 °C for 4 min. The PCR product was resolved on a 1% agarose gel (Sigma-Aldrich) alongside the GeneRuler DNA Ladder Mix (Thermo Fisher Scientific). The gel was stained with GelGreen Nucleic Acid Gel Stain (Biotium, Fremont, CA, USA) and visualized under UVBlue light using the Uvitec Cambridge Transilluminator (Cambridge, England, UK). The band corresponding to the full-length HDAC3 fragment was excised and purified using the QIAquick Gel Extraction Kit (Qiagen, Hilden, Germany). The purified fragment was digested with Esp3I, followed by further purification using the QIAquick PCR Purification Kit (Qiagen). The digested HDAC3 fragment was ligated into a BbsI-digested N-FD_empty backbone vector in a 3:1 molar ratio. This N-FD_empty backbone included a nuclear localization signal (NLS) fused to HDAC3 after ligation and an expression cassette for kanamycin resistance. Ligation was performed using T4 DNA Ligase in T4 DNA Ligase Buffer (Takara) at 16 °C for 30 minutes. *E. coli* XL10-Gold bacteria were transformed with the ligation mixture and plated on LB agar containing 50 µg/mL kanamycin (Sigma-Aldrich). Colony PCR was performed with primers pUX21_seq_Fw and pUX21_seq_Re (Table 3) using EmeraldAmp MAX HS PCR Master Mix (Takara) to confirm the presence of the plasmid containing HDAC3. Positive colonies were cultured in liquid LB media, and the plasmid was isolated using ZymoPURE Plasmid Miniprep Kit (Zymo Research, Irvine, CA, USA). The final construct was named tNS-pN-FD_HDAC3.

The HDAC3 coding sequence (CDS) contained two BsaI restriction sites, which needed to be mutated to enable cloning into the destination vector. One BsaI site was located at the end of the HDAC3 CDS, and the HDAC3_Rev primer was designed to introduce a c1251t substitution during the initial amplification of the HDAC3 sequence. The second BsaI site was mutated using the Q5® Site-Directed Mutagenesis Kit (New England Biolabs), according to the manufacturer's protocol. Mutagenesis primers, designed with NEBaseChanger™ v1.3.3 (New England Biolabs) to introduce a c123g substitution, are listed in Table 3. Following mutagenesis, the plasmids were amplified in *E. coli* XL10-Gold cells and isolated using ZymoPURE Plasmid Miniprep Kit. The resulting construct was named tNS-pN-FD_HDAC3_noBsaI and was used for all subsequent cloning steps involving HDAC3.

To generate a catalytically inactive form of HDAC3, an arginine-to-proline substitution was introduced at position 265. This R265P substitution was also created via site-directed mutagenesis, using the QuikChange Lightning Site-Directed Mutagenesis Kit (Agilent Technologies) according to the manufacturer's protocol. Mutagenesis primers were designed manually (Table 3). After mutagenesis, plasmids were amplified in *E. coli* XL10-Gold bacteria and isolated using a ZymoPURE Plasmid Miniprep Kit. The catalytically inactive construct was named tNS-pN-FD_HDAC3_IN. All plasmids (tNS-pN-FD_HDAC3, tNS-pN-FD_HDAC3_noBsaI, tNS-pN-FD_HDAC3_IN) were verified by Sanger sequencing to confirm the integrity of the sequences and the successful introduction of the desired mutations. For sequencing, primers pUX21_seq_Fw and pUX21_seq_Re were used (Table 3).

3.2.4. Cloning of dCas9 fusions with histone modifying enzymes

To further investigate the epigenetic regulation of *B4GALT1*, *FUT8*, and *MGAT3*, these genes were targeted with dCas9 fusions with histone modifiers. Given that *B4GALT1* and *FUT8* are enriched in positive histone marks (H3K4me3 and H3K27ac) and lack negative histone marks (H3K9me2) in HepG2 cell line (Figure 11a and 11b), they were targeted with RIOX1-dSpCas9, G9a-dSpCas9, and HDAC3-dSpCas9 fusion proteins. RIOX1 removes H3K4me3, H3K4me2, and H3K4me1, while HDAC3 removes H3K27ac. The histone methyltransferase G9a introduces H3K9me2. In contrast, *MGAT3*, which is transcriptionally silenced in HepG2 cells, exhibits low density of positive histone marks such as H3K4me3 and H3K27ac (Figure 11g). Therefore, *MGAT3* was targeted with PRDM9-dSaCas9 and p300-dSaCas9 fusions. Histone methyltransferase PRDM9 catalyzes the introduction of trimethylation on Lys4 of histone H3, while acetyltransferase p300 introduces acetylation on Lys27 in histone H3. All effector domains, except HDAC3, were previously cloned in our research group (unpublished results). The cloning of constructs containing fusion proteins and sgRNAs targeting specific regions in *B4GALT1*, *FUT8*, and *MGAT3* was performed as described in chapter 3.2.1. The same controls were applied: an “Inactive” (IN) control containing catalytically inactive histone modifiers fused to dCas9 and a “Non-targeting” (NT) control. To target RIOX1-dSpCas9 and G9a-dSpCas9 to the *FUT8* and *B4GALT1* promoters the same sgRNAs used for DNMT3A-dSpCas9 targeting to these genes were employed (Table 1). However, for targeting HDAC3-dSpCas9 to these genes, only one newly designed sgRNA was used (Table 2). This sgRNA targets the region upstream of the *FUT8*'s and *B4GALT1*'s TSS adjacent to the H3K27ac-enriched region and was designed following the same principles as the sgRNAs described in chapter 3.2.1. For targeting *MGAT3* with PRDM9-dSaCas9 and p300-dSaCas9, a single

previously designed sgRNA was used (Table 2). The only difference in cloning constructs containing a single sgRNA is the use of the pSgx1 plasmid, which can accommodate only one sgRNA, instead of the multi-guide module in the first Golden Gate assembly. All plasmids were amplified in *E. coli* NEB Stable and isolated using the NucleoBond Xtra Maxi Plus Kit. To ensure correct assembly, restriction analysis was performed on all constructs.

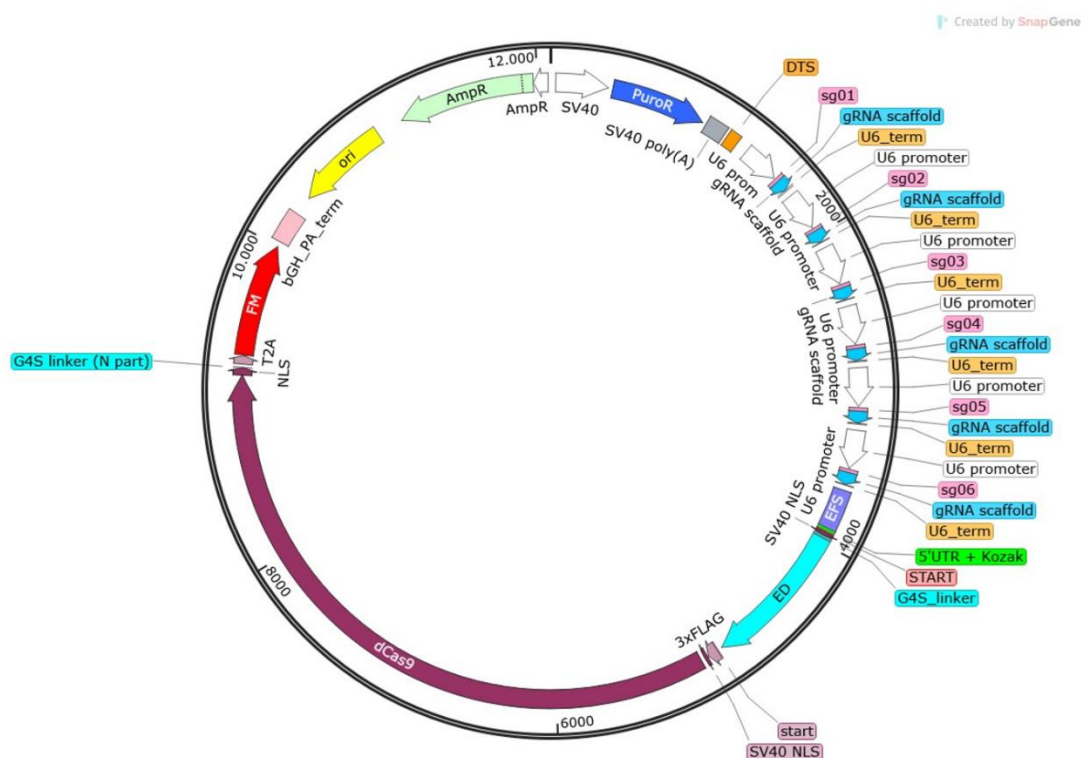


Figure 10. Scheme of expression plasmid used for transfection of HepG2 cells. The scheme shows plasmid from which dCas9 fused to appropriate effector domain and sgRNAs for targeting glycosyltransferases of interest were expressed. EFS - Elongation Factor 1-alpha Short promoter; SV40 NLS - nuclear localization signal from SV40 large T antigen; ED – effector domain (DNMT3A, TET1, HDAC3, RIOX1, G9a, PRDM9 or p300 or their inactive counterparts for IN control); dCas9 - inactive form of Cas9 nuclease (dSpCas9 or dSaCas9); NLS - bipartite nuclear localization signal from nucleoplasmin; G4S linker - Gly-Gly-Gly-Gly-Ser linker; T2A - self-cleaving peptide 2A from *Thosea asigna* virus; FM – encoding for fluorescence marker (mClover or mRuby); bGH_PA_term - termination sequence of the bovine growth hormone gene; ori – origin of replication; AmpR - ampicillin resistance expression cassette followed by its promoter; SV40 – promoter of Simian virus 40 large T antigen; PuroR- Puromycin resistance expression cassette; SV40 poly(A) – polyadenylation signal derived from SV40; DTS - TF binding region from SV40 for nuclear import of the plasmid; U6 promoter - RNA polymerase III promoter for human U6 snRNA; sg01- sg06 – encodes for sgRNAs

targeting the genomic region of interest; gRNA scaffold - guide RNA scaffold for the *S. pyogenes* or *S. aureus* CRISPR/Cas9 system; U6_term - human U6 snRNA termination sequence (in experiments where one sgRNA was used as well for NT control expression plasmids contained one copy of U6 promoter, terminator and gRNA scaffold and appropriate one sgRNA or non-targeting sgRNA respectively).

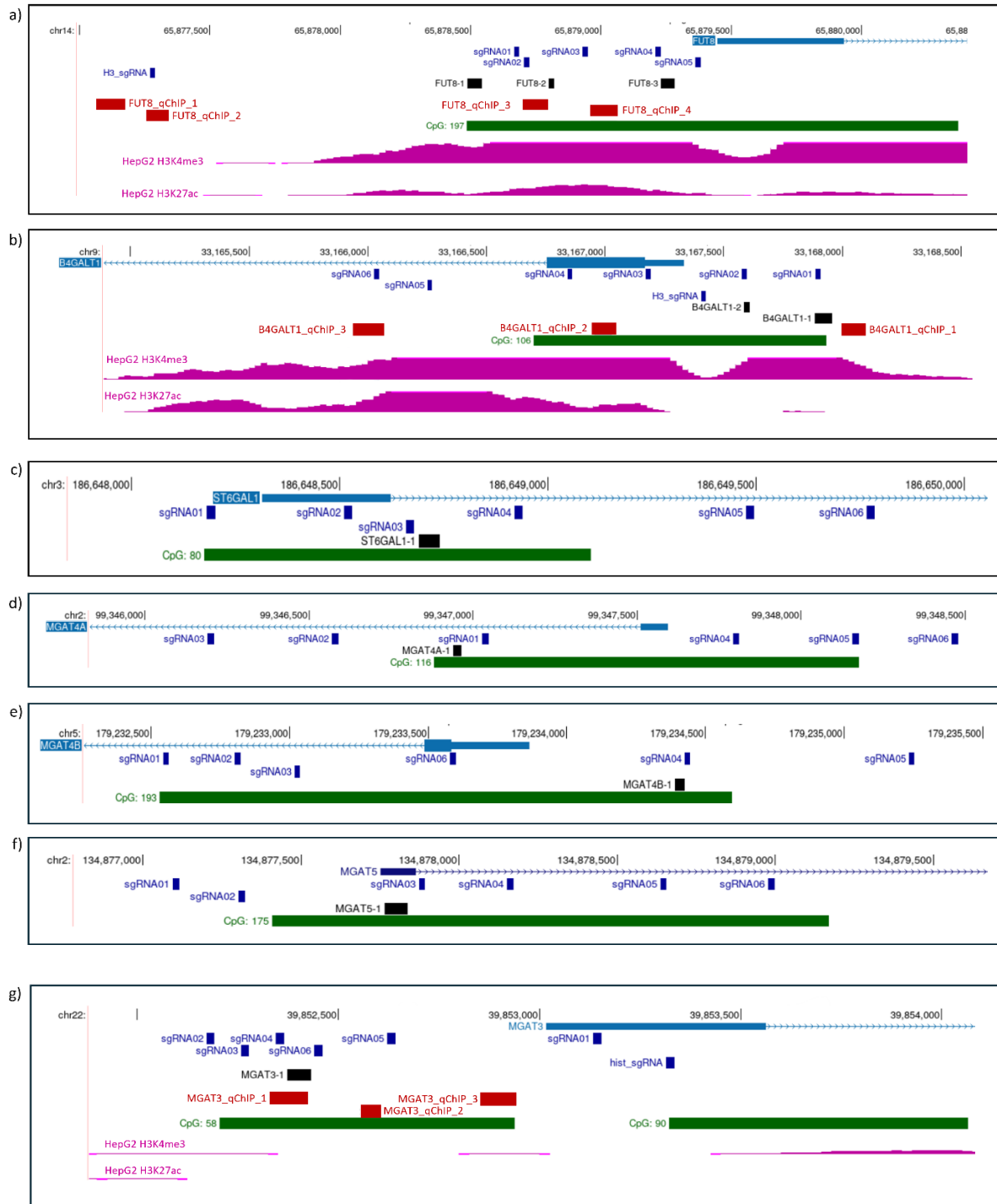


Figure 11. Figure is described on the following page.

Figure 11. Schematic representation of positions of sgRNAs, pyrosequencing assays and qPCR primers (used for analyses of histone quantity levels) relative to CpG islands, together with the distribution of histone marks in promoters of the candidate glyco-genes.

This figure illustrates the layout of sgRNAs used for targeting DNMT3A-dSpCas9 and TET1-dSaCas9 to candidate gene CpG islands, as well as pyrosequencing assays for each analyzed gene: *FUT8* (a), *B4GALT1* (b), *ST6GAL1* (c), *MGAT4A* (d), *MGAT4B* (e), *MGAT5* (f), and *MGAT3* (g). In addition, for *FUT8* (a), *B4GALT1* (b), and *MGAT3* (g), figure displays the location of sgRNAs used for targeting dCas9 fusions with histone modifiers to genes promoters as well as the enrichment with H3K4me3 and H3K27ac in the targeted regions in HepG2 cells and qPCR primers used in histone levels analyzes. The chromosome location and genomic coordinates (in bp) for each gene promoter are shown at the top of each panel. This schematic was generated using the UCSC Genome Browser with the hg19 version of the human genome. The ENCODE/Broad Institute track was utilized to illustrate histone modification enrichment in HepG2 cells.

3.2.5. Determination of CpG methylation levels using bisulfite pyrosequencing

CpG methylation analysis for all transfections was performed using bisulfite pyrosequencing. This method necessitates the design of specific assays targeting the CpG sites of interest. Assays for *B4GALT1*, *ST6GAL1*, *MGAT5* (unpublished results), and *MGAT3* (45) were adapted from previous research within the group, while novel assays were designed for *FUT8*, *MGAT4A* and *MGAT4B*. These assays were designed based on the hg19 human genome assembly. The CpG islands of *FUT8*, *MGAT4A* and *MGAT4B* along with 1000 bp upstream and downstream flanking regions were "*in silico*" converted by replacing cytosines within CpG dinucleotides with "Y" and other cytosines with "T". Primers for bisulfite-specific PCR and pyrosequencing, as well as the pyrosequencing assays themselves, were designed based on these converted sequences. Primer design was conducted either manually or using PyroMark Assay Design Software 2.0.2. (Qiagen). Primer selection adhered to the previously described instructions (297). All designed primers and assays were tested and optimized. To gain more detailed insight into CpG methylation changes in *FUT8* and *B4GALT1* three and two bisulfite pyrosequencing assays were respectively employed to analyze methylation within their CpG islands, whereas a single assay was used for all other genes. Depending on the assay, either the PCR primer or an additional sequencing-specific primer was used for sequencing. Details for all PCR primer pairs, their annealing temperatures (T_a), and sequencing primers are provided in Table 4, while Table 5 provides details on the pyrosequencing assays.

For analyses of DNA methylation following epigenetic manipulation with DNMT3A-dSpCas9, TET1-dSaCas9, G9a-dSpCas9 and PRDM9-dSaCas9, cells were collected 8- and 12-days post-transfection. Cells transfected with HDAC3-dSpCas9 and p300-dSaCas9 were collected 5- and 8-days post-transfection. DNA was isolated by overnight incubation at 65°C with 1 µl of proteinase K (20 mg/ml) (Invitrogen, Austin, Tx, USA) in 50 µl of digestion buffer (50 mM Tris pH 8.5, 1 mM EDTA, 0.5% Tween 20) with shaking at 500 rpm. Proteinase K was inactivated at 98°C for 8 minutes. Bisulfite conversion of isolated DNA was performed using the EZ DNA Methylation-Gold Kit (Zymo Research Europe, Freiburg, Germany) following the manufacturer's protocol. During bisulfite conversion, unmethylated cytosines are converted to uracil, while methylated cytosines remain unchanged. Specific regions of interest were amplified using the PyroMark PCR Kit (Qiagen). PCR reactions were prepared according to the manufacturer's protocol and performed under the following conditions: initial denaturation at 95 °C for 15 minutes; 50 cycles of 30 seconds at 95 °C, 30 seconds at the annealing temperature (Ta) specific to each primer pair (Table 4), and 30 seconds at 72 °C; followed by a final elongation at 72 °C for 10 minutes. Amplified fragments were then sequenced using the PyroMark Q24 Advanced System (Qiagen) according to the assays listed in Table 5. Pyrosequencing reactions were prepared with PyroMark Q24 Advanced Reagents (Qiagen) following the manufacturer's protocol.

3.2.6. Analysis of gene expression on mRNA level

To assess the impact of targeted epigenetic manipulation on gene transcriptional activity, real-time quantitative polymerase chain reaction (RT-qPCR) was employed. Cells designated for RNA isolation were harvested on the 8th and 12th day after transfection with DNMT3A-dSpCas9, TET1-dSaCas9, G9a-dSpCas9, and PRDM9-dSaCas9 and on the 5th and 8th day following transfection with RIOX1-dSpCas9, HDAC3-dSpCas9, and p300-dSaCas9 fusion constructs. RNA was isolated using either the RNeasy Mini Kit (Qiagen) or Quick-RNA Miniprep Kit (Zymo Research) according to the manufacturer's protocols.

For all samples, reverse transcription was performed immediately after RNA isolation, except for those originating from cells where *MGAT3* was targeted with dCas9 fusions. These specific samples were treated with DNase using the TURBO DNA-free Kit (Invitrogen, Waltham, MA, USA) to eliminate genomic DNA, as the *MGAT3* probe can detect both genomic DNA and cDNA. All RNA samples were reverse transcribed into cDNA using PrimeScript Reverse Transcriptase (200 U/µL, Takara). Briefly, 500–1000 ng of RNA was combined with 1 µL of Random Hexamers (50 µM, Thermo Fisher Scientific) and 1 µL of dNTPs (10 mM,

Sigma-Aldrich) in a final volume of 15 μ L. This mixture was incubated for 5 minutes at 65 °C and then placed on ice for 5 minutes. To the cooled mixture, 0.5 μ L of PrimeScript Reverse Transcriptase, 0.5 μ L of Recombinant RNase Inhibitor (40 U/ μ L, Takara), and 4 μ L of 5X PrimeScript Buffer (Takara) were added. Reverse transcription was performed under the following conditions: 60 minutes at 42 °C, followed by 15 minutes at 70 °C.

Quantitative real-time PCR (RT-qPCR) was carried out in the IntelliQube automated PCR instrument (LGC Biosearch Technologies, Hoddeson, UK) using TaqMan® Gene Expression Master Mix (Applied Biosystems) and following TaqMan® Gene Expression Assays: Hs00189535_m1 (*FUT8*), Hs00155245_m1 (*B4GALT1*), Hs00949382_m1 (*ST6GAL1*), Hs00923405_m1 (*MGAT4A*), Hs00365001_m1 (*MGAT4B*), Hs00159136_m1 (*MGAT5*) and Hs00609297_m1 (*HMBS*). For *MGAT3* gene, RT-qPCR was performed in 7500 Fast Real-Time PCR System (Applied Biosystems) using TaqMan® Gene Expression Master Mix and TaqMan® Gene expression assay specific for *MGAT3* (Hs02379589_s1) and *HMBS*. The relative expression of all analyzed genes was calculated using the comparative cycle threshold (Ct) method (298) with *HMBS* as the endogenous control. Results were expressed as fold change (FC) relative to the NT control.

3.2.7. Analysis of gene expression on protein level

After checking if the epigenetic manipulation resulted in change in mRNA levels of the candidate glyco-genes, Western blot was performed to see if the observed changes of *FUT8*, *B4GALT1* and *MGAT3* transcriptional activity was followed by change on protein level. Cell pellets, collected at 8 and 12 days post-transfection, were lysed in RIPA buffer (150 mM NaCl, 1% Triton X-100, 0.5% Na-deoxycholate, 0.1% SDS, 50 mM Tris pH 8.0, 1x cOmplete EDTA-free Protease Inhibitor Cocktail (Roche, Basel, Switzerland)). The lysis was performed for 30 minutes at 4 °C on a rocker, followed by sonication for four cycles (8 seconds of sonication, 8 seconds on ice). Samples were centrifuged at 12,000 rpm for 20 minutes at 4 °C to remove cell debris. Protein concentration was determined using the Pierce™ BCA Protein Assay Kit (Thermo Fisher Scientific) according to the manufacturer's instructions.

The amount of protein loaded onto the gel varied depending on the target protein: 20 μ g for *MGAT3*, 20 μ g for *B4GALT1*, and 7.5 μ g for *FUT8*. Prior to gel loading, the appropriate amount of protein was mixed with RIPA buffer, Roti-Load 2 (Carl Roth, Mannheim, Germany), and DTT (DL-Dithiothreitol solution, 1 M, Sigma-Aldrich), and denatured at 99°C for 8 minutes. Proteins were separated on a 10% SDS-PAGE gel with a 4% stacking gel on top. The PageRuler Plus Prestained Protein Ladder (Thermo Fisher Scientific) was used as a molecular

weight marker. Electrophoresis was performed at 100 V for 120 minutes in cold running buffer (25 mM Tris, 190 mM Glycine, 0.1% SDS). Separated proteins were transferred to an Amersham Protran Premium 0.45 µm NC Nitrocellulose Blotting Membrane (Cytiva, Marlborough, MA, USA) in transfer buffer (25 mM Tris, 190 mM Glycine, 20% methanol) at 100 V for 90 minutes at 4°C. Successful protein transfer was confirmed by Ponceau S solution (Sigma-Aldrich) staining. Membranes were blocked with 5% milk (Blotting Grade, Carl Roth) prepared in TBST (20 mM Tris, 150 mM NaCl, 0.1% Tween 20) for 1 hour with gentle rocking, followed by three washes with TBST. Membranes were then cut into two parts. The upper part was incubated with a primary antibody specific to the protein of interest, while the lower part was incubated with an antibody against the endogenous control (β-actin or H3).

Primary antibody incubations were performed overnight at 4°C with gentle rocking. The following primary antibodies were used at the indicated dilutions: anti-B4GALT1 (1:2000; ab121326, Abcam, Cambridge, UK), anti-FUT8 (1:10000; ab191571, Abcam), anti-MGAT3 (1:1000; ab103427, Abcam), anti-β-actin (1:1000; sc-69879, Santa Cruz Biotechnology, Texas, USA), and anti-H3 (1:5000; ab1791, Abcam). After incubation, membranes were washed three times with TBST for 10 minutes each, followed by a 1-hour incubation with the appropriate secondary antibody at room temperature with gentle rocking. The secondary antibody Goat Anti-Rabbit IgG H&L (HRP) (ab6721, Abcam) diluted in 0.5% milk was used at 1:10000 dilution for B4GALT1, at 1:2000 dilution for FUT8, 1:5000 dilution for MGAT3 and 1:100000 for H3. For β-actin, Goat Anti-Mouse IgG H&L (HRP) (ab205719, Abcam) was used at 1:200000 dilution in 5% milk. Membranes were then washed three times with TBST for 10 minutes each. Protein signals were developed using the SuperSignal West Dura Extended Duration Substrate Kit (Thermo Scientific, Rockford, IL, USA) and visualized using the Uvitec Q9 Alliance imaging system.

3.2.8. Analyses of histone modification levels

3.2.8.1. Native chromatin immunoprecipitation (N-ChIP)

Native chromatin immunoprecipitation (N-ChIP) was performed to analyze the levels of H3K27ac following targeted manipulation of the *B4GALT1* and *FUT8* genes using HDAC3-dSpCas9, as well as the *MGAT3* gene using p300-dSaCas9. For this analysis, two million cells were collected 5 and 8 days after transfection with the respective constructs. The cell pellets were resuspended in 57.2 µl of RSB buffer (10 mM Tris-HCl pH 8.0, 10 mM NaCl, 3 mM MgCl₂). Subsequently, 1.6 mL of buffer B (RSB buffer + 0.1% IGEPAL and 5 mM sodium butyrate) was added, and the mixture was gently inverted 10 times. The cells were centrifuged

at $1,500 \times g$ for 5 minutes at 4 °C, after which the supernatant was removed, and the nuclei were resuspended in 286 μ l of buffer RSC (RSB buffer + 0.25 M sucrose and 3 mM CaCl_2). Another round of centrifugation at $1,500 \times g$ for 5 minutes at 4 °C was performed. The nuclear pellet was then resuspended in buffer D (RSC buffer + 5 mM sodium butyrate supplemented with 1x protease inhibitors (PI)) and transferred to a 1.5 mL tube.

Chromatin digestion was carried out using 25 U of Micrococcal Nuclease (MNase; Thermo Scientific), and the samples were incubated for 5 minutes at 37 °C with inversion every minute. MNase was inactivated with 8 μ l of 0.5 M EDTA. The samples were centrifuged at 5,000 rpm for 5 minutes at 4 °C. The supernatant (fraction S1) was collected, and the remaining pellet was resuspended in 120 μ l of buffer E (10 mM Tris-HCl pH 7.5, 10 mM NaCl, 0.2 mM EDTA, 1x protease inhibitors) and rotated for 1 hour at 4 °C. This suspension was then passed through a 26G needle five times using a 2 mL syringe and centrifuged again at 5,000 rpm for 5 minutes at 4 °C. The resulting supernatant (S2) was combined with fraction S1, and a 100 μ l aliquot of the combined sample was set aside for DNA purification. The remaining sample was stored at -80 °C. To purify the chromatin, 150 μ l of molecular biology grade water was added to the 100 μ l aliquot, and the sample was purified using a QIAquick PCR purification kit following the manufacturer's protocol. The DNA concentration was measured using a NanoDrop spectrophotometer (Thermo Fisher Scientific), and the purified chromatin was analyzed on a 1% agarose gel to assess the degree of digestion. Successful digestion resulted in ~80-90% mono-nucleosomes and a small fraction of di- and tri-nucleosomes.

The optimal amount of chromatin and anti-H3K27ac antibody (ab4729, Abcam) for immunoprecipitation was determined beforehand during optimization experiments. For immunoprecipitation, the digested chromatin was thawed on ice and diluted 10x with Native ChIP Incubation Buffer (10 mM Tris-HCl pH 7.5, 70 mM NaCl, 2 mM EDTA, 2 mM MgCl_2 , 0.1% Triton, 1x protease inhibitors). After a 5-minute centrifugation at 3,000 rpm at 4 °C, three aliquots were prepared. Two contained 400 ng of chromatin each: one was incubated with 0.2 μ g of anti-H3K27ac antibody, while the other was incubated with 0.2 μ g of Rabbit IgG antibody (ab6709, Abcam) as a negative control. A third aliquot, containing 100 ng of chromatin (4x less than the amount of chromatin used for immunoprecipitation), was saved as an INPUT sample and stored at -20 °C until further analysis. Chromatin samples with antibodies were incubated overnight at 4 °C on a rotator. The following day, Protein G Dynabeads (Invitrogen) were prepared by washing them three times with 500 μ l of PBS + BSA and diluting them 2x in Native ChIP Incubation Buffer. The amount of Protein G required to bind the antibodies was

determined per the manufacturer's instructions. For each sample, 1.66 µl of diluted Dynabeads was added and incubated for 4 hours at 4 °C on a rotator. The beads were then washed four times with RIPA buffer (50 mM HEPES pH 7.6, 1 mM EDTA, 0.7% Na-deoxycholate, 1% NP-40, 0.5 M LiCl) and twice with TE buffer (10 mM Tris-HCl pH 8.0, 1 mM EDTA pH 8.0) using a magnetic rack to immobilize the beads on the tube wall. The immunoprecipitated chromatin was eluted from the beads using 200 µl of elution buffer (1% SDS, 0.1 M NaHCO₃ pH 8.0) by rotating the tubes for 10 minutes at room temperature. The eluate was transferred to a new tube. Both the eluted chromatin and INPUT samples were purified using the QIAquick PCR purification kit. The purified DNA was analyzed using qPCR to assess the relative enrichment of DNA fragments of interest. Normalization was performed against the INPUT sample to calculate the relative levels of H3K27ac enrichment at the regions of interest.

3.2.8.2. CUT&RUN

The CUT&RUN assay was utilized to analyze changes in H3K4me3 levels following targeted manipulation of the *FUT8* and *B4GALT1* with RIOX1-dSpCas9 and *MGAT3* with PRDM9-dSaCas9. A total of 100,000 cells were collected 5 and 8 days after transfection with the RIOX1-dSpCas9 construct and 8 and 12 days after transfection with the PRDM9-dSaCas9 construct. The assay was performed using the CUT&RUN Assay Kit (Cell Signaling Technology, Danvers, MA, USA) following the manufacturer's protocol. Briefly, cells designated for INPUT samples were washed and frozen at -20 °C for processing the following day. For the immunoprecipitation samples, cells were immobilized on activated concanavalin A-coated magnetic beads. The cell-bead complexes were then resuspended in Antibody Binding Buffer, supplemented with spermidine, protease inhibitor cocktail (PIC), and digitonin and incubated overnight at 4 °C with gentle rotation in the presence of the following antibodies: 2 µl of rabbit monoclonal anti-trimethyl-Histone H3 (#9751, Cell Signaling Technology) or 5 µl of rabbit monoclonal Antibody IgG XP® Isotype Control (#66362, Cell Signaling Technology). Digitonin permeabilizes the cell membrane, allowing the antibodies to penetrate and bind their respective targets.

The following day, pAG-MNase pre-mix, containing pAG-MNase enzyme, was added and incubated at 4°C for 1 hour. Subsequently, CaCl₂ was added to activate MNase. pAG-MNase binds to the IgG of the primary antibody, targeting MNase to the antibody-bound chromatin. The enzyme activity was stopped by adding 1xSTOP buffer, and chromatin fragments bound to the primary antibodies were released into the solution by incubating the samples for 10 minutes at 37 °C. Immunoprecipitated samples were purified using the

QIAquick PCR Purification Kit (Qiagen) in accordance with the manufacturer's instructions. INPUT samples were thawed and incubated in DNA extraction buffer at 55°C with shaking. DNA was isolated using the phenol/chloroform extraction and ethanol precipitation method as described in the CUT&RUN Assay Kit protocol. The purified DNA was analyzed by qPCR to assess the relative enrichment of DNA fragments of interest. Normalization against the INPUT sample was performed to calculate the relative levels of H3K4me3 enrichment at the regions of interest.

3.2.8.3. Cross linking chromatin immunoprecipitation (X-ChIP)

Cross linking chromatin immunoprecipitation (X-ChIP) was used to analyze levels of H3K9me2 after epigenetic manipulation of *FUT8* and *B4GALT1* with G9a-dSpCas9. Approximately 4 million cells were collected 8 and 12 days post-transfection. Cells were cross-linked in a 1% formaldehyde solution (formaldehyde solution 37 wt. % in H₂O, Sigma–Aldrich) for 8 minutes on a rotator. To quench the formaldehyde, 2.5 M glycine was added, and the mixture was incubated for 5 minutes at room temperature, followed by centrifugation at 500 g for 5 minutes. The cells were then washed in 1 ml of cold PBS, centrifuged again for 5 minutes at 500 g, and the resulting pellet was resuspended in 1 ml of cold cell lysis buffer (10 mM Tris-HCl pH 7.5, 10 mM NaCl, 0.5% IGEPAL). After a 15-minute incubation on ice, the lysate was centrifuged at 3000 rpm for 5 minutes at 4 °C. The pellet was resuspended in 2 ml of MNase digestion buffer (20 mM Tris-HCl pH 7.5, 15 mM NaCl, 60 mM KCl, 1 mM CaCl₂, 1x protease inhibitors) and centrifuged for 2.5 minutes at 12,000 rpm at 4 °C. The resulting pellet was resuspended in 250 µl of MNase digestion buffer, and 25 U of MNase was added to the samples, which were then incubated for 20 minutes at 37 °C with shaking at 1000 rpm. MNase activity was stopped by adding 250 µl of 2x STOP/ChIP buffer (100 mM Tris-HCl pH 8.1, 20 mM EDTA, 200 mM NaCl, 2% Triton X-100, 0.2% sodium deoxycholate). Subsequently, 500 µl of the sample was transferred to bioruptor sonication tubes and sonicated for 20 cycles (30 seconds ON, 30 seconds OFF at 4 °C) using the Bioruptor Plus Sonication System (Diagenode, Belgium). Samples were then centrifuged for 5 minutes at 13,200 rpm at 4 °C, and the supernatant was transferred to a new tube. The total amount of soluble chromatin was estimated using the Qubit dsDNA HS (High Sensitivity) Assay Kit (Thermo Fisher Scientific). Aliquots of the chromatin were stored at -80 °C for future processing, while a small portion was taken for reverse cross-linking. This involved overnight incubation with proteinase K at 65 °C with shaking at 500 rpm, followed by analysis on a 1% agarose gel to confirm that most of the chromatin was sonicated to mono-nucleosome fragments of approximately 150 bp.

Frozen chromatin was thawed on ice, and 0.2 µg of chromatin was aliquoted and stored at -20 °C as the INPUT sample. Meanwhile, 2 µg of chromatin was aliquoted and incubated overnight at 4 °C on a rotator with the following antibodies: 0.63 µg of mouse monoclonal anti-dimethyl-Histone H3 (ab1220, Abcam) or 0.63 µg of IgG. Protein G Dynabeads were washed and diluted in 1xChIP buffer and added to samples in amount determined according to manufacturer's instructions. The samples were then incubated for 4 hours at 4 °C on a rotator. After incubation, Dynabeads were washed at room temperature using the following protocol: twice in 1 ml of 1x ChIP buffer with rotation for 5 minutes, twice in 1 ml of high-salt buffer (1x STOP/ChIP buffer with 0.5 M NaCl) with rotation for 5 minutes, twice in 1 ml of Tris/LiCl buffer (10 mM Tris-HCl pH 8.0, 0.25 M LiCl₂, 0.5% NP-40, 0.5% sodium deoxycholate, 1 mM EDTA) with rotation for 5 minutes, and finally, twice in 1xTE buffer (diluted from 2x TE buffer: 10 mM Tris-HCl pH 8.0, 20 mM EDTA) using a magnetic rack to immobilize the beads. To elute the immunoprecipitated fragments from the beads, 50 µl of 1x ChIP elution buffer (10 mM Tris-HCl pH 8.0, 10 mM EDTA, 150 mM NaCl, 1% SDS) was added, and the samples were incubated at 65 °C for 7 minutes with shaking at 500 rpm. The eluate was transferred to a new 1.5 ml microcentrifuge tube, and an additional 50 µl of 1x ChIP elution buffer was added to the Dynabeads, followed by another incubation under the same conditions. The eluates were then combined. To reverse the cross-linking, both the immunoprecipitated samples and INPUT samples were incubated overnight at 65 °C with 1 µl of proteinase K. The DNA was subsequently purified using the QIAquick PCR purification kit (Qiagen). qPCR was performed to assess the relative enrichment of DNA fragments of interest. Normalization against the INPUT sample was performed to calculate the relative levels of H3K9me2 enrichment at the regions of interest.

3.2.8.4 Analysis of immunoprecipitated fragments via qPCR

Immunoprecipitated fragments generated by N-ChIP, CUT&RUN, and X-ChIP were analyzed using qPCR with SYBR Green technology. For each gene (*FUT8*, *B4GALT1*, and *MGAT3*), multiple primer pairs encompassing their regulatory regions were designed based on the hg19 human genome assembly, either manually or using the NCBI Primer-BLAST tool (299). During primer design, careful attention was given to ensure that the PCR product did not exceed 146 base pairs, that primers did not form stable homo- or heterodimers, and that they exhibited an annealing temperature of approximately 60 °C. Additionally, care was taken to ensure that primers did not bind non-specifically to other regions in the human genome. Primer efficacy and specificity were assessed using both standard PCR and qPCR. Primer efficiency

was determined by amplifying serial dilutions of genomic DNA and MNase-digested DNA using qPCR. The DNA used for these tests was derived from HepG2 cells. Efficiency was calculated from the slope of the standard curve, with optimal values ranging from 90% to 110%. Three to four primer pairs encompassing distinct regulatory regions for each gene were selected (Figure 11, Table 6).

The qPCR reactions were performed in a 20 µl volume containing 1x SYBR® Green PCR Master Mix (Applied Biosystems), 0.1 µM forward primer, 0.1 µM reverse primer, and 1 µl of template. All reactions were performed in technical triplicates. qPCR was performed in 7500 Fast Real-Time PCR System. Relative enrichment was calculated using the % INPUT method. For N-ChIP and X-ChIP samples, the Ct values of INPUT samples had to be corrected to account for the smaller amount of chromatin used for INPUT compared to the immunoprecipitated samples. This correction was made using the formula: $Ct(\text{corrected}) = Ct - (\ln(D)/\ln(2))$, where D represents the dilution factor and Ct is the average Ct value of INPUT sample (averaged across technical replicates). In this study, D = 4 for N-ChIP samples and D = 10 for X-ChIP samples. For CUT&RUN samples, no correction was necessary because equal amounts of cells were used for both INPUT and immunoprecipitated samples. Next, the ΔCt value was calculated by subtracting the average Ct of the immunoprecipitated sample (averaged across technical replicates) from the corrected or average uncorrected Ct value of the INPUT samples. Finally, the relative enrichment, expressed as a percentage of INPUT (%INPUT), was calculated using the formula: $2^{\Delta Ct} \times 100\%$.

3.2.9. Analysis of the total N-glycome of HepG2 cells

The total cell N-glycome of HepG2 cells following transfection of HepG2 cells with DNMT3A-dSpCas9 and TET1-dSaCas9 was analyzed in cooperation with Genos d.o.o. Cells were collected on day 8th and day 12th post-transfection. Cells were resuspended in 200 µL of lysis buffer (50 mmol/L Tris, pH 7.4; 0.1% Triton X-100; 1 mmol/L EDTA; 135 mmol/L NaCl) supplemented with a protease inhibitor cocktail (cOmplete™ ULTRA, EDTA-free; Roche) and incubated on ice for 5 minutes. The cell lysates were then sonicated (30 s at 50% amplitude) and centrifuged (2000 g for 30 min). Supernatants were transferred to new tubes, and proteins were precipitated by sequential addition of 400 µL methanol, 100 µL chloroform, and 300 µL of molecular biology grade water (Corning, Somerville, MA, USA), followed by centrifugation at $14,000 \times g$ for 10 minutes at 4 °C. The upper aqueous phase was carefully removed without disturbing the protein-containing interphase. An equal volume of 50% methanol was added, and the samples were vortexed and centrifuged at $14,000 \times g$ for 10 minutes at 4 °C. The entire

supernatant was discarded. The protein pellets were washed with 1 mL of 100% methanol (vortexed and centrifuged at 14000 g for 10 min at 4°C), and the resulting supernatants were discarded. Finally, protein pellets were air-dried to remove residual methanol. The dried protein pellets were resuspended in 30 µl of 1.33% (wt./vol.) SDS (Invitrogen) and incubated at 65°C for 10 min. Following incubation, 10 µl of 4% Igepal-CA630 (Sigma Aldrich) and 1.2 U of PNGase F (Promega, Madison, WI, USA) in 10 µl 5 × PBS were added to samples. Samples were incubated overnight at 37 °C to enable releasement of *N*-glycans. The released *N*-glycans were then labeled using procainamide (Sigma-Aldrich) and purified using hydrophilic interaction liquid chromatography solid-phase extraction (HILIC-SPE).

Purified fluorescently labeled *N*-glycans were separated by HILIC on Waters Acuity ultra-performance liquid chromatography (UPLC) instrument (Waters, Milford, MA, USA) consisting of a quaternary solvent manager, sample manager and a fluorescence detector set with excitation and emission wavelengths of 310 and 370 nm. The instrument was under the control of Empower 2 software, build 2145 (Waters). Plasma *N*-glycans were separated on a Waters bridged ethylene hybrid (BEH) Glycan column, 150 × 2.1 mm, 1.7 µm BEH particles, with 100 mmol/l ammonium formate, pH 4.4, as solvent A and acetonitrile as solvent B. The separation method used a linear gradient of 70–53% acetonitrile (vol./vol.) at flow rate of 0.561 ml/min in a 25 min analytical run. The data was processed using an automated integration method. The chromatograms were all separated in the same manner into 31 separate glycan peaks (GP1-GP31). The content of glycans in each peak was expressed as a percentage of the total integrated area.

All glycan structures were annotated with a tandem mass spectrometry (MS/MS) approach analysis via HILIC-UPLC coupled to Compact ESI-QTOF-MS system using Ion Booster ion source (Bruker Daltonics, Berlin, Germany). The instrument was controlled by Hystar software version 3.2 (Bruker Daltonics) and operated in a positive ion mode, with capillary voltage set to 2250 V and nebulizing gas pressure set to 5.5 Bar. Drying gas (nitrogen) was applied to source at a flow rate of 4 L/min and temperature of 200°C, while vaporizer temperature was set to 200 °C and flow rate was 5 L/min. Nitrogen was used as a source gas and argon was used as a collision gas. Mass spectra were recorded from 100 to 4000 *m/z* at frequency of 0.5 Hz. MS/MS analysis was performed using Auto MS/MS mode, which selects three precursors with the highest intensities for collision-induced dissociation (CID) fragmentation. Glycan compositions and structural features were assigned using

GlycoWorkbench (300) and Glycomode (301) software tools, based on obtained MS and MS/MS spectra.

3.2.10. Statistical analysis

For DNA methylation analysis, three to five biological replicates were analyzed. The average DNA methylation percentage for each CpG site analyzed in the assays was calculated and plotted on a graph. These calculations were performed using Microsoft Excel.

For gene expression analysis, five biological replicates were analyzed in experiments regarding DNA methylation, while four to six biological replicates were analyzed in experiments involving manipulations of histone modifications. To determine the statistical significance of gene expression differences between test samples and controls, a non-parametric Mann-Whitney U test was employed. Average fold change (FC) values of biological replicates were plotted on graphs. Calculations were performed using GraphPad Prism version 5.0.3 for Windows (GraphPad Software, San Diego, California, USA).

For all ChIP samples (N-ChIP, X-ChIP, and CUT&RUN), up to six replicates were analyzed. To assess the statistical significance of relative enrichment differences between samples and controls, the *t*-test was used. Average %INPUT values of replicates were plotted on graphs. Calculations were performed using GraphPad Prism v.5.0.3.

To analyze changes in the total *N*-glycome of HepG2 cells following manipulations of DNA methylation, five biological replicates were examined. The total *N*-glycome was separated into 31 chromatographic peaks. Rather than evaluating changes in each peak individually, derived glycosylation traits were calculated, and all statistical analyses were conducted on these traits. Derived glycosylation traits represent the sum of glycan peaks that contain structures biologically associated with the activity of specific enzymes within the glycosylation pathway. A detailed list of all derived traits, their descriptions, and the glycan peaks used for their calculation are provided in Table 7. To determine whether differences in derived traits between test samples and controls were statistically significant, a non-parametric Mann-Whitney U test was performed. The average amount of each derived glycan trait across biological replicates was plotted on graphs. All calculations and statistical analyses were performed using GraphPad Prism v.5.0.3.

Standard deviations (SD) were calculated between replicates in all experiments and are displayed as error bars on the corresponding graphs. P-values of ≤ 0.05 were considered statistically significant.

4. RESULTS

4.1. Manipulations of promoter methylation of the candidate glyco-genes using CRISPR/dCas9 molecular tools

To investigate the role of DNA methylation in epigenetic regulation of glyco-genes selected in this study, I used dCas9 fusions with DNMT3A (for targeted cytosine methylation) and TET1 (for targeted cytosine demethylation) in HepG2 cell line. Following cell transfections with these fusion constructs DNA methylation levels were analyzed by pyrosequencing and subsequently the gene expression levels were analyzed on both mRNA and protein levels. I used gene expression as the readout of the engineered cytosine methylation to confirm that certain cytosine residues within the promoter region were regulatory.

4.1.1. Targeting DNMT3A-dCas9 and TET1-dCas9 to the candidate glyco-gene promoters induces hyper- and hypomethylation

Given that the CpG islands in the promoter regions of *B4GALT1*, *FUT8*, *ST6GAL1*, *MGAT4A*, *MGAT4B*, and *MGAT5* are hypomethylated in HepG2 cells, these genes were targeted with DNMT3A-dCas9 using specific sgRNAs in order to introduce methyl groups at specific cytosines within the promoter regions. The TET1-dCas9 fusion, able to remove methyl groups from CpG sites, was targeted to the hypermethylated CpG island of *MGAT3*. Cells were collected at both 8- and 12-days post-transfection for isolation of DNA, RNA and proteins. Bisulfite pyrosequencing revealed that epigenetic manipulation with DNMT3A-dCas9 increased cytosine methylation levels in the CpG islands of all six candidate genes at both time points (Figure 12, Figure 13, Figure 14).

Two assays, B4GALT1-1 and B4GALT1-2 (Table 5, Figure 11b), encompassing a total of 10 CpG sites, were used to analyze *B4GALT1* promoter methylation (Figure 12). The first two CpG sites in both assays exhibited the highest increase in methylation level. For B4GALT1-1, methylation differences reached up to 51% and 54%, and for B4GALT1-2 the methylation change was 44% and 50% compared to IN and NT controls, respectively. Minimal increases in methylation levels (5–16%) were observed at CpG sites 3–5 in B4GALT1-1 assay, and CpG 5 in B4GALT1-2 assay, while CpG3 and CpG4 in B4GALT1-2 showed no changes in DNA methylation levels. This could be due to the fact that CpG3 and CpG4 lie within binding site for sg01 in B4GALT1-1 assay while CpG5 is located right next to it. The CpG4 and CpG5 sites in B4GALT1-2 lie within the binding site for sg02 and CpG3 site is located next to it (Figure 11b). Binding of sgRNA within regions that contain CpG sites blocks the availability of these sites to DNMT3A-dCas9 fusion which could explain why their methylation status did not

change. The degree of methylation increase was generally consistent between 8- and 12-days post-transfection (Figure 12).

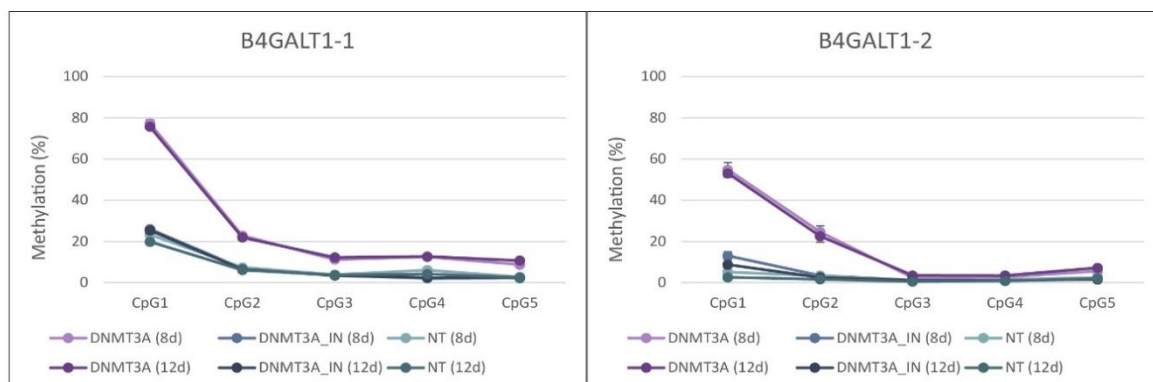


Figure 12. Targeting of DNMT3A-dCas9 to the CpG island of *B4GALT1* increased cytosine methylation. Pyrosequencing encompassing the B4GALT1-1 and B4GALT1-2 assays revealed an increase in methylation level up to 54% at the specific CpG sites targeted with active DNMT3A-dCas9 fusion compared to IN (DNMT3A_IN) and NT control. Error bars are shown as \pm SD ($n = 5$).

For *FUT8*, three assays were designed, covering in total 19 CpG sites (Table 5, Figure 11a). Unlike B4GALT1 assays, no CpG sites overlapped directly with sgRNA binding regions. Nevertheless, CpG1 in FUT8-3 assay, located near sgRNA04, showed no methylation changes (Figure 13). All CpG sites within FUT8-1 and FUT8-2 assays exhibited similar increase in methylation levels with the highest increase observed in CpG1 in both assays (43% in FUT8-1 and 22% in FUT8-2). Targeting CpG sites within FUT8-3 assay with DNMT3A showed more pronounced methylation changes, especially the CpG4 site which showed an increase of 66% and 70% compared to IN and NT control, respectively. The level of methylation change was consistent between 8- and 12-days post-transfection for all *FUT8* assays (Figure 13).

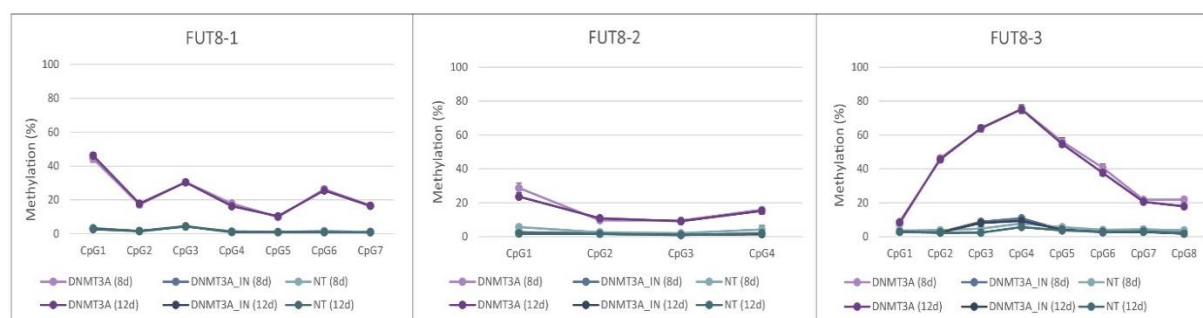


Figure 13. Targeting DNMT3A-dCas9 to the CpG island of *FUT8* increased cytosine methylation level. Pyrosequencing across FUT8-1, FUT8-2 and FUT8-3 assays exhibited an

increase in methylation level up to 70% at the specific CpG sites targeted with active DNMT3A-dCas9 compared to IN (DNMT3A_IN) and NT control. Error bars are shown as \pm SD (n = 5).

A single assay was developed for each of the *ST6GAL1*, *MGAT4A*, *MGAT4B*, and *MGAT5* genes to measure methylation level after targeting with DNMT3A-dCas9 (Table 5, Figure 11). *ST6GAL1* and *MGAT5* showed more prominent methylation increases compared to *MGAT4A* and *MGAT4B* (Figure 14), with CpG1 in *ST6GAL1* and CpG17 in *MGAT5* exhibiting up to 70% of increase (Figure 14a and d). Even though *MGAT4A* and *MGAT4B* showed overall lower increase in methylation level than other genes targeted with DNMT3A, the methylation change was observed in all CpGs analyzed (Figure 14b and 14c), except for CpG6 in *MGAT4B*, located within the sg04 binding region (Figure 11e). The highest methylation level change was detected at CpG3 (up to 28%) in *MGAT4A*, and CpG4 in *MGAT4B* (up to 39%) 8th day post-transfection. The changes in DNA methylation level were more pronounced on day 8 than on day 12 for *MGAT4A*, *MGAT4B*, and *MGAT5*, while the opposite trend was observed for *ST6GAL1*.

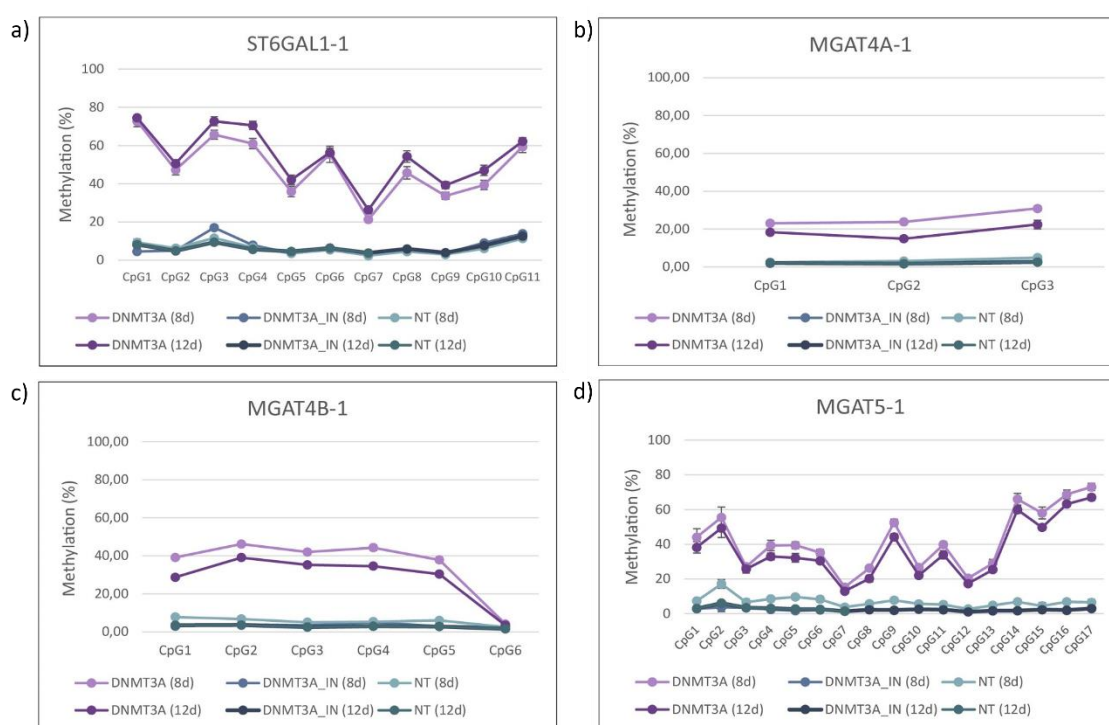


Figure 14. Targeting DNMT3A-dCas9 to the CpG islands of *ST6GAL1*, *MGAT4A*, *MGAT4B* and *MGAT5* increased cytosine methylation level. Pyrosequencing revealed an increase in methylation level in specific CpG sites targeted with active DNMT3A-dCas9 reaching up to 70% increase for *ST6GAL1* (a) and *MGAT5* (d), 28% increase for *MGAT4A* (b)

and 39% increase for *MGAT4B* (c) compared to IN (DNMT3A_IN) and NT control. Error bars are shown as \pm SD (n = 5).

Targeting the TET1-dCas9 fusion to the CpG island of *MGAT3* reduced methylation level across MGAT3-1 assay encompassing five CpG sites (Figure 15). Reductions exceeded 50% at most CpG sites, with CpG4 showing the lowest methylation level (the difference of 60% and 53%, compared to IN and NT control, respectively). These changes were consistent through time.

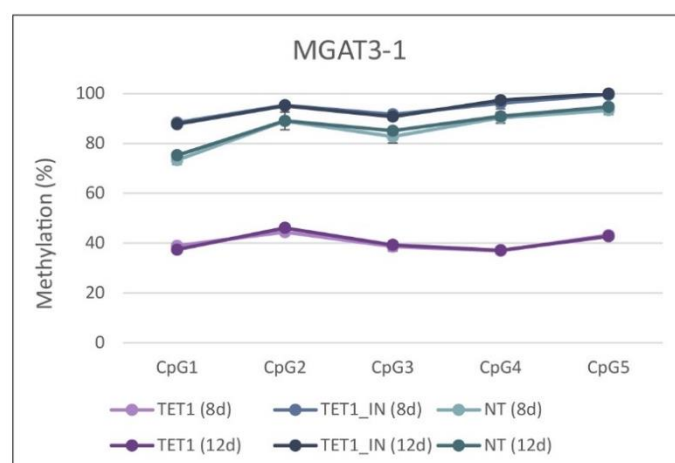


Figure 15. Targeting TET1-dCas9 to the CpG island of *MGAT3* resulted in a decrease of cytosine methylation level. Pyrosequencing using MGAT3-1 assay revealed a decrease in methylation level up to 60% at the specific CpG sites targeted with active TET1-dCas9 fusion compared to IN (TET1_IN) and NT control. Error bars are shown as \pm SD (n = 5).

In conclusion, I was able to induce change in methylation levels in the promoters of all seven candidate glyco-genes using dCas9-based molecular tools underscoring their potential for epigenetic engineering in studies of epigenetic regulation of glyco-genes.

4.1.2. Targeted epigenetic manipulation of DNA methylation affects expression of glyco-genes

Engineered DNA methylation affected gene expression in all genes targeted with DNMT3A-dCas9 either at both or one time point. Targeted methylation in the *B4GALT1* promoter using DNMT3A-dCas9 resulted in significant downregulation at both 8- (FC = 0.47 ± 0.04) and 12-days post-transfection (FC = 0.40 ± 0.04) (Figure 17b). Expression levels were compared to IN control to confirm that the observed downregulation was due to epigenetic manipulation rather than CRISPR interference. No reduction of gene expression was observed in the IN control on either day 8 or day 12 post-transfection, suggesting that downregulation

was a result of increased CpG methylation level. Interestingly, the IN control displayed a significant increase in expression on day 12 compared to NT control suggesting that the binding of the catalytic domain itself may exert some level of transcriptional activation in the *B4GALT1* promoter. This putative effect of the catalytic domain might partially mask the repressive effect of increased DNA methylation. Targeted methylation of the *FUT8* promoter also resulted in transcriptional downregulation compared to both controls at 8- (FC = 0.47 ± 0.11) and 12-days (FC = 0.39 ± 0.04) post-transfection (Figure 18b). The absence of transcriptional change in IN control indicates that observed downregulation was a direct result of the introduced DNA methylation. These findings suggest that *B4GALT1* and *FUT8* are regulated by promoter methylation.

Targeting of the *MGAT4B* promoter with DNMT3A-dCas9 significantly downregulated its transcription on both days 8 (FC = 0.70 ± 0.06) and 12 (FC = 0.69 ± 0.06) post-transfection (Figure 19b). However, on day 8, a significant decrease in transcriptional activity was also observed in the IN control, suggesting on putative CRISPR interference. Nevertheless, by day 12, gene transcription in the IN control was restored, indicating that the observed downregulation of *MGAT4B* in DNMT3A-dCas9-treated cells was largely attributable to increased DNA methylation. *MGAT5* also showed significant gene downregulation compared to both controls at days 8 (FC = 0.49 ± 0.02) and 12 (FC = 0.39 ± 0.12) post-transfection (Figure 20b). While CRISPR interference was observed in the IN control only on day 12, a significant downregulation observed on day 8 suggested that the majority of the downregulation in *MGAT5* expression was due to the targeted increase in DNA methylation. The *MGAT4A* gene was downregulated only on day 12 (FC = 0.71 ± 0.05) compared to both controls (Figure 21c). On day 8 (FC = 0.91 ± 0.05), expression was significantly reduced only compared to IN control. Expression of *ST6GAL1* showed significant downregulation compared to both IN and NT controls on day 8 (FC = 0.68 ± 0.12), but this effect was not sustained till day 12 (FC = 0.94 ± 0.07) (Figure 21b).

Targeted hypomethylation of the *MGAT3* promoter achieved by TET1-dCas9 led to a significant upregulation of gene expression on day 8 compared to both controls (Figure 22b). This suggests that the observed increase in transcription was a direct consequence of the reduced DNA methylation level. On day 12, significant upregulation was observed only relative to NT control, while no significant difference was detected compared to IN control. Notably, the IN control showed a slight increase in *MGAT3* expression on day 12, though this change was not statistically significant.

These findings demonstrate that engineered DNA methylation using dCas9-based molecular tools can significantly impact the expression of glyco-genes indicating a regulatory role of DNA methylation.

4.1.3. Effects of epigenetic manipulations on total *N*-glycome of HepG2 cell line

To assess the functional consequences of altered DNA methylation and subsequent glyco-gene expression, the total cell *N*-glycome of HepG2 cells was analyzed as a final phenotype. The chromatogram showed that total cell *N*-glycome comprised 31 distinct glycan peaks (Figure 16). Dysregulated expression of most candidate glyco-genes resulted in significant changes in the total cell *N*-glycome. However, not all glycan changes were directly associated with the corresponding glycosyltransferase.

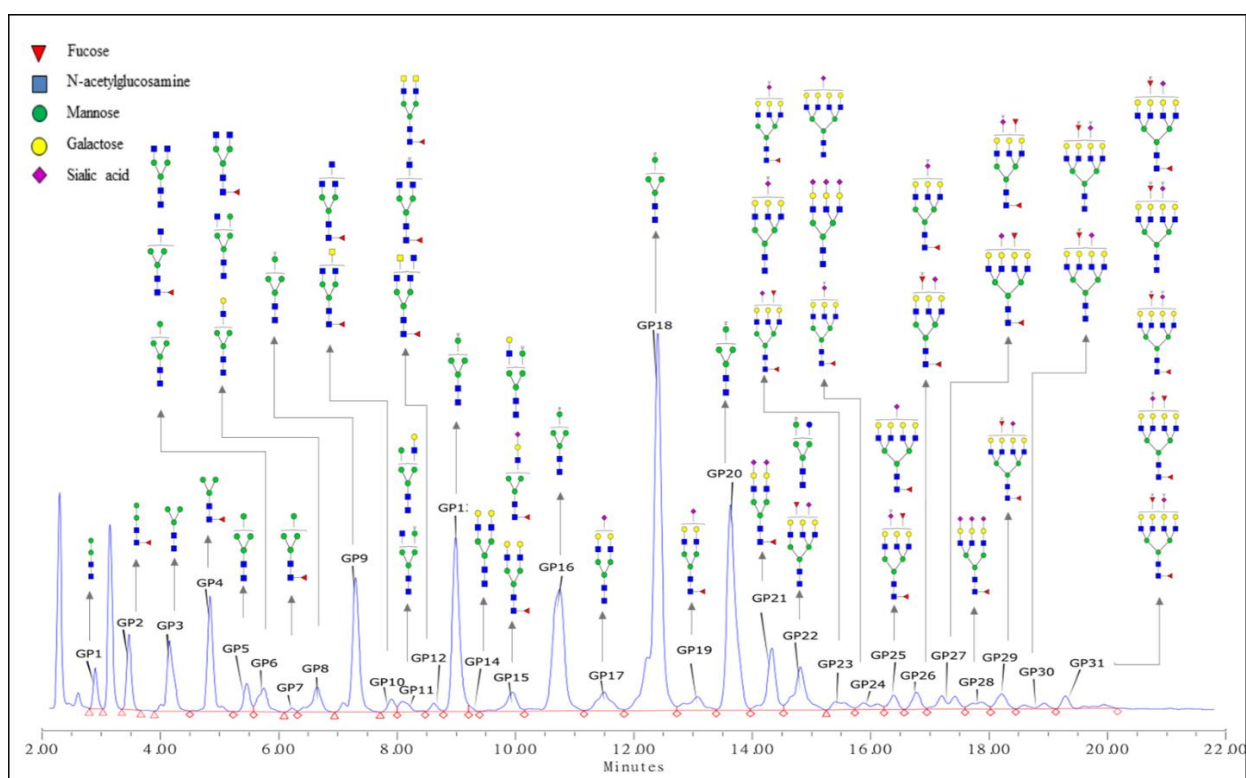


Figure 16. The chromatogram of total HepG2 cell *N*-glycome. Hydrophilic interaction ultra-high performance liquid chromatography (HILIC-UPLC) identified 31 chromatographic peaks in total cell *N*-glycome. The structures of the *N*-glycans present in each peak were characterized by LC-ESI-MS/MS analysis. The figure depicts only major glycan structures for each peak. GP – glycan peak.

B4GALT1 catalyzes the addition of galactose to *N*-acetylglucosamine residues (Figure 17a). Downregulation of *B4GALT1* was followed by an increase in agalactosylated (G0) structures and a decrease in digalactosylated (G2) structures. This led to a decrease in the overall

ratio of galactosylated and agalactosylated structures (GR). Additionally, a significant increase in asialylated (S0) and a decrease in disialylated (S2) structures were observed, leading to a lower sialylation ratio (SR) (Figure 17c). These changes were statistically significant compared to both NT and IN controls on days 8 and 12 post-transfection.

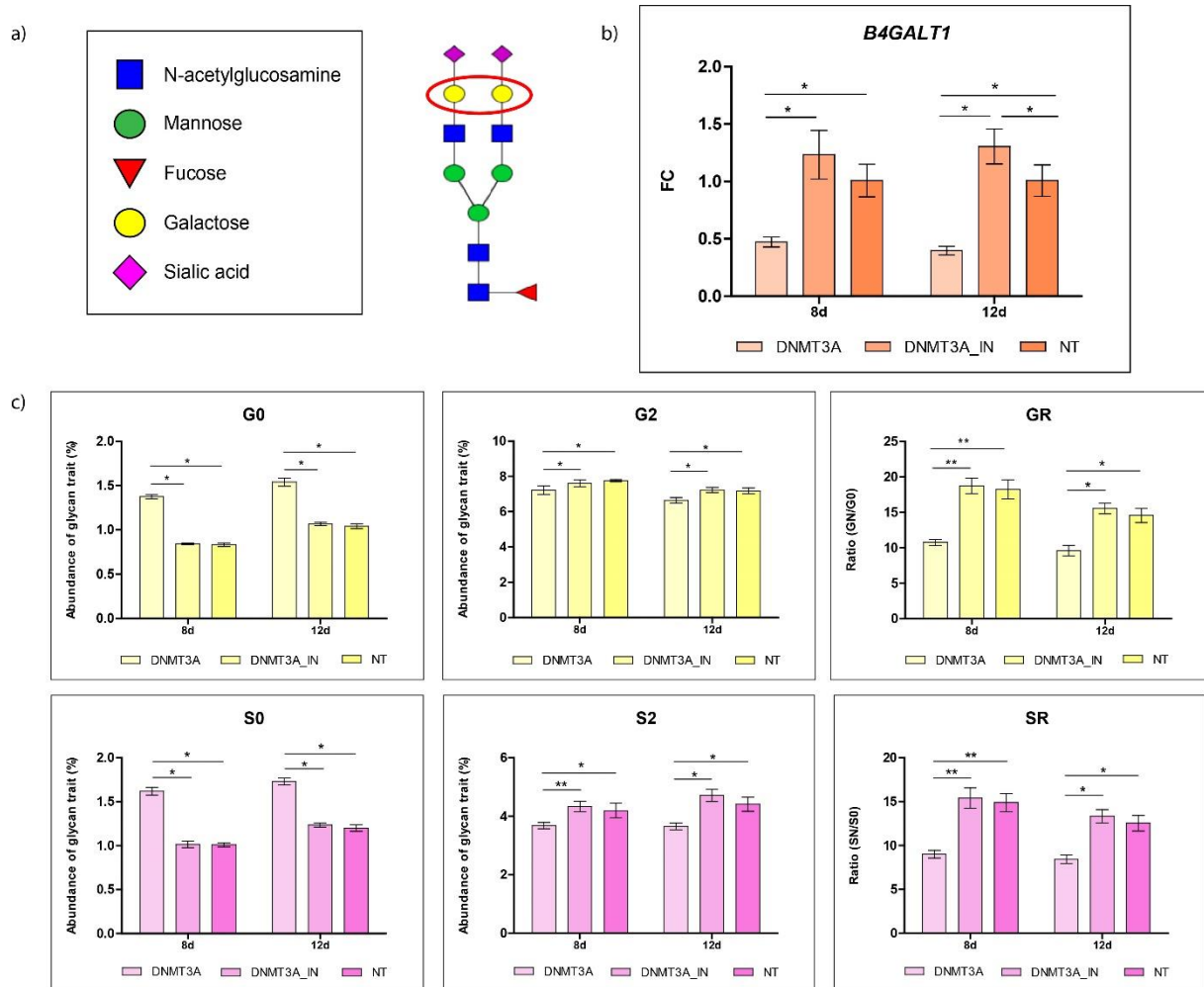


Figure 17. Downregulation of *B4GALT1* induced by targeted hypermethylation leads to significant alterations in galactosylation and sialylation. *B4GALT1* catalyzes the addition of galactose on growing glycans (a). Targeted hypermethylation of the *B4GALT1* CpG island resulted in a significant transcriptional downregulation (b), resulting in changes in the total cell *N*-glycome (c) including a significant increase in agalactosylated (G0) and asialylated (S0) glycans, a significant decrease in digalactosylated (G2) and disialylated (S2) glycans, and a significant reduction in the ratios of galactosylated to agalactosylated (GR) and sialylated to asialylated (SR) glycans. Error bars are shown as \pm SD ($n = 5$). Statistical significance between samples targeted with active DNMT3A and its respective inactive (DNMT3A_IN) and non-target control (NT) was determined using the Mann–Whitney U test (* $P < 0.05$, ** $P < 0.01$).

FUT8 is the only known enzyme catalyzing the addition of fucose to a core of a glycan structure (Figure 18a). Targeted hypermethylation and subsequent downregulation of the *FUT8* gene led to a significant decrease in core fucose-containing glycan structures at both time points (Figure 18c). On day 8, a small but significant increase in core fucose was observed in the IN control, potentially indicating CRISPR interference at off-target sites involving glycosylation-related factors. This effect was not observed on day 12, where the reduction in core fucosylation was more pronounced. Other glycan traits affected by the *FUT8* gene downregulation include reduced agalactosylated (G0) and disialylated (S2) glycans, both of which likely reflect the loss of core fucose since all glycan peaks included in these traits contained core-fucosylated glycans (visible in chromatogram of total cell *N*-glycome). Additional changes included reduced digalactosylated (G2) glycans and low-branched (LB) structures, alongside an increase in oligomannose (OM) glycans on day 12. Asialylated (S0) structures were significantly decreased only on day 8 (Figure 18c). Interestingly, IN control displayed a significant increase in agalactosylated (G0) and asialylated (S0) glycans on day 12 post-transfection, suggesting the effect of off-target CRISPR interference.

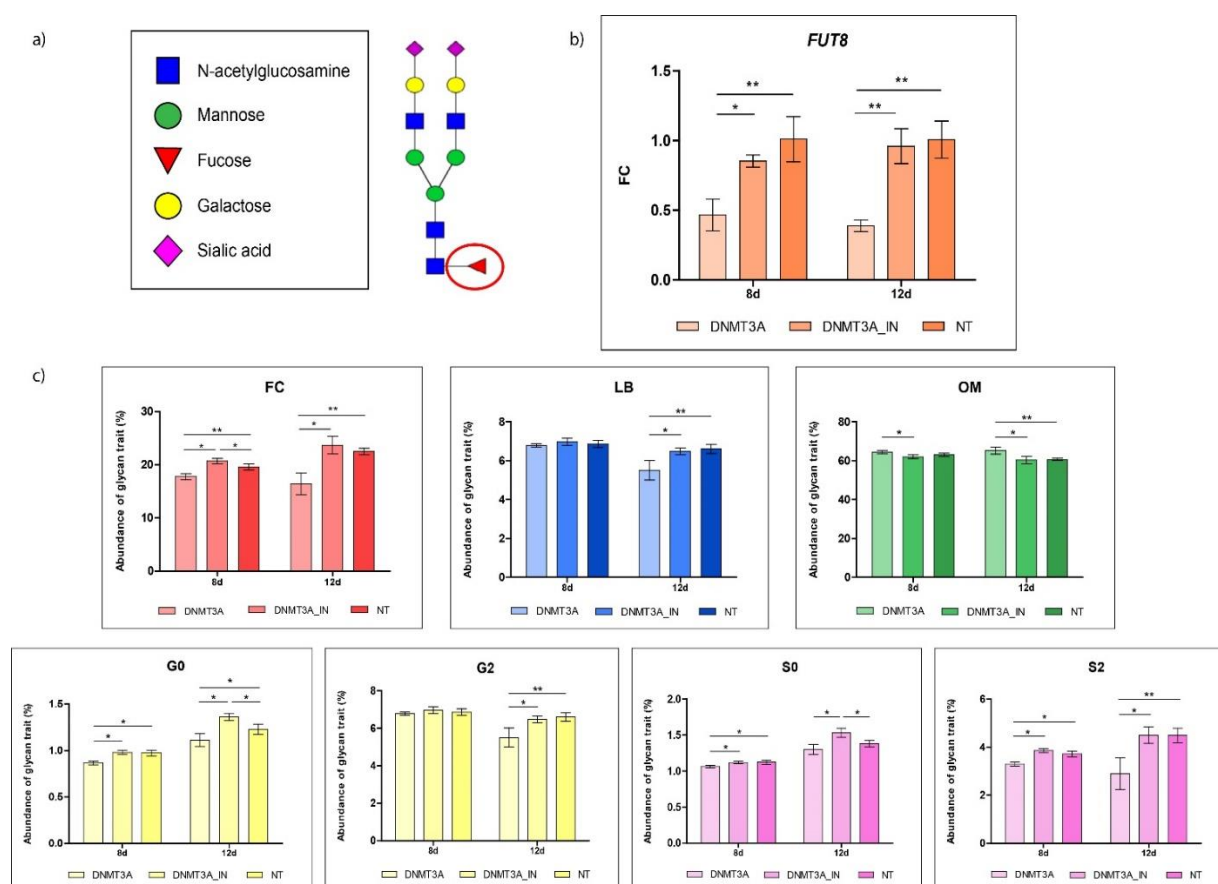


Figure 18. Figure is described on the following page.

Figure 18. Downregulation of *FUT8* following targeted hypermethylation leads to alterations in core fucosylation and additional glycan traits. *FUT8* is responsible for catalyzing the addition of a fucose to a core of a glycan chain (a). Targeted hypermethylation of the *FUT8* CpG island resulted in a significant reduction in its transcriptional activity (b) which was reflected in a decrease in core fucosylation (FC) and significant changes in several other glycan traits (c), including reductions in agalactosylated (G0), digalactosylated (G2), asialylated (S0), disialylated (S2), and low-branched *N*-glycans (LB), along with an increase in oligomannose *N*-glycans (OM). Error bars are shown as \pm SD ($n = 5$). Statistical significance between samples targeted with active DNMT3A and its respective inactive (DNMT3A_IN) and non-target control (NT) was determined using the Mann–Whitney U test (* $P < 0.05$, ** $P < 0.01$).

The *MGAT4B* gene downregulation, encoding for an enzyme involved in glycan branching (Figure 19a), resulted in subtle but significant changes in low-branched (LB) structures on both days 8 and 12. An increase in digalactosylated (G2) structures was also observed at both time points, most likely reflecting alterations in low-branched glycans since these derived traits (LB and G2) are comprised of same glycan peaks as seen in table 7. Additionally, monosialylated (S1) structures increased in quantity significantly only on day 8 (Figure 19c). Downregulation of the *MGAT5* gene, encoding for another key enzyme involved in formation of glycan branches (Figure 20a), resulted in increased quantity of low-branched (LB) structures compared to both NT and IN controls on day 8, while on day 12, the increase in their quantity was significant only relative to NT control. However, on day 8, an increase in highly branched (HB) structures was also observed compared to both controls, but this increase was also evident in the IN control. Increase in IN control persisted until day 12. The *MGAT5* gene downregulation also led to changes in several other glycan traits observed either at one or at both time points (Figure 20c). These changes included decreases in asialylated (S0) and agalactosylated (G0) glycans and increases in core fucosylated (FC), digalactosylated (G2), mono-, di- and trisialylated glycans (S1, S2 and S3), as well as total galactosylated (GN) and total sialylated (SN) glycans leading to increased galactosylation (GR) and sialylation ratios (SR). For many of these glycan traits, the change in quantity was observed also in IN control, suggesting potential CRISPR interference at off-target genomic sites affecting protein *N*-glycosylation.

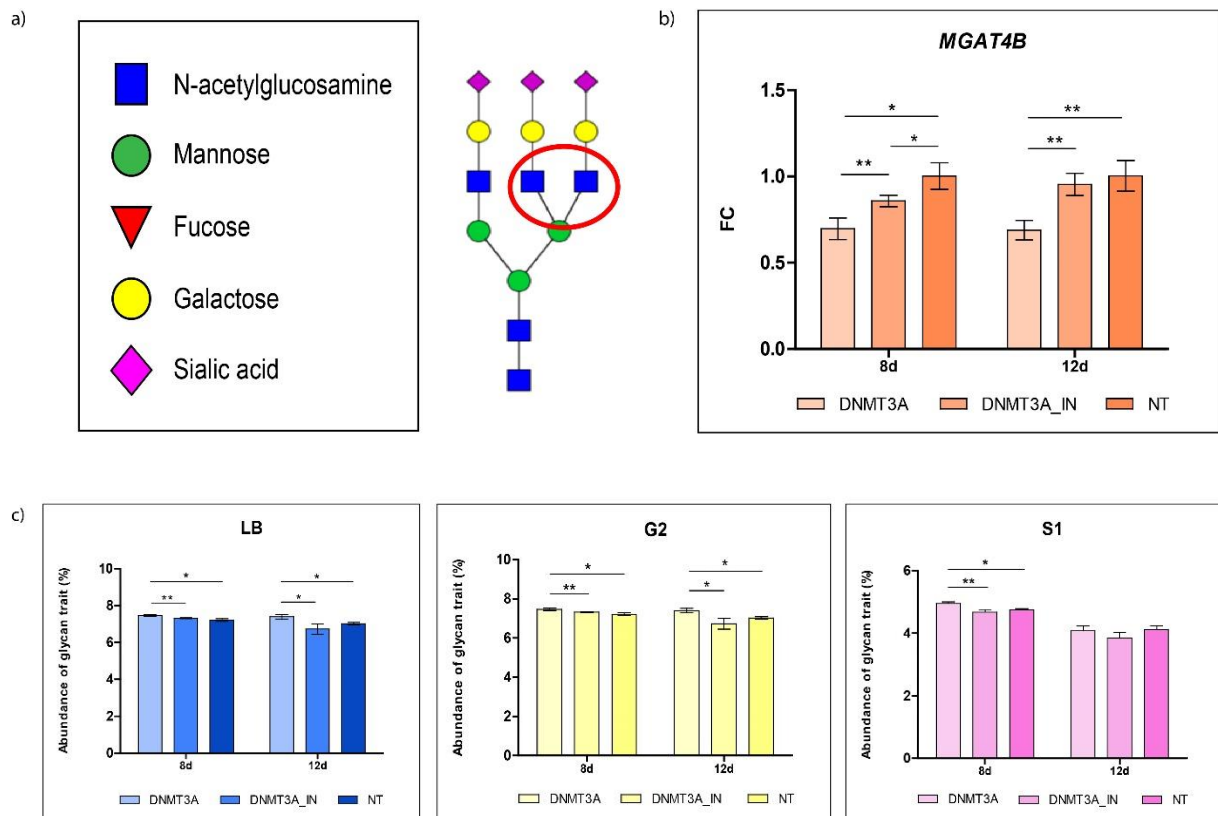


Figure 19. The *MGAT4B* gene downregulation by targeted hypermethylation affects several aspects of HepG2 total cell *N*-glycome. Promoter hypermethylation of the *MGAT4B* gene, encoding for the enzyme involved in glycan branching (a), significantly decreased its transcription (b) which led to a significant increase in low-branched (LB), digalactosylated (G2), and monosialylated *N*-glycans (S1). Error bars are shown as \pm SD ($n = 5$). Statistical significance between samples targeted with active DNMT3A and its respective inactive (DNMT3A_IN) and non-target control (NT) was determined using the Mann–Whitney U test (* $P < 0.05$, ** $P < 0.01$).

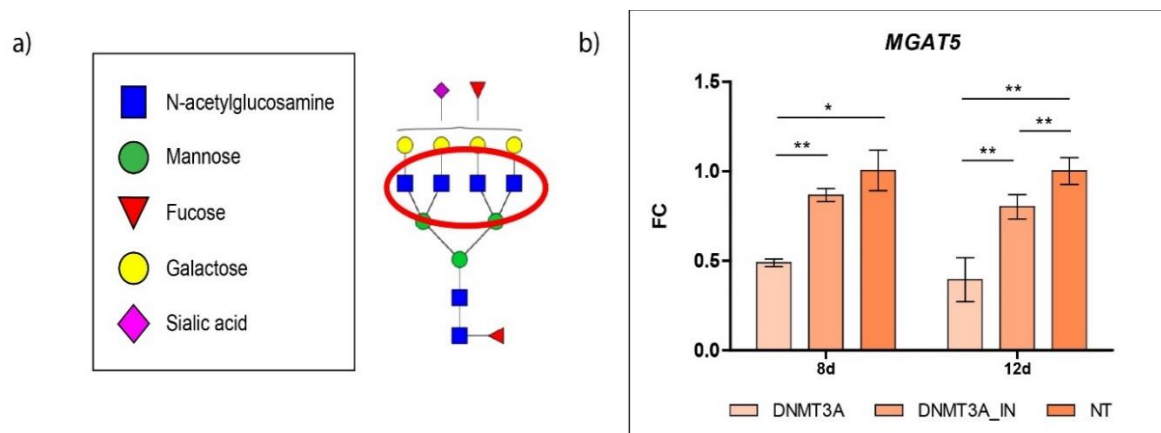


Figure 20. Figure is continued and described on the following page.

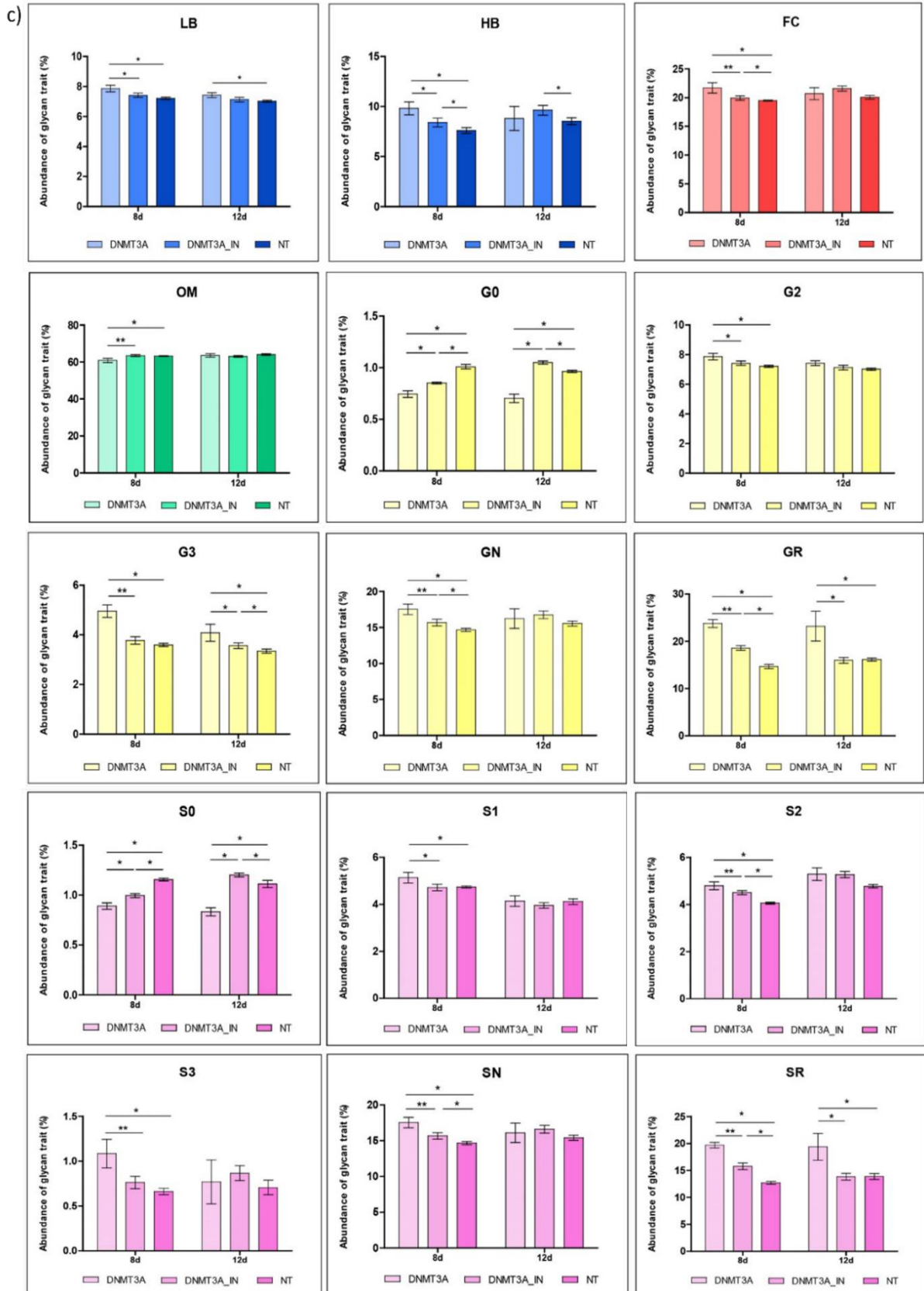


Figure 20. The *MGAT5* gene downregulation by targeted hypermethylation resulted in extensive perturbations in HepG2 total cell *N*-glycome. *MGAT5* is involved in the formation

of glycan branches (a). Targeted hypermethylation significantly reduced *MGAT5* transcriptional activity (b), resulting in significant changes in the majority of derived glycan traits (c). Error bars are shown as \pm SD ($n = 5$). Statistical significance between samples targeted with active DNMT3A and its respective inactive (DNMT3A_IN) and non-target control (NT) was determined using the Mann–Whitney U test (* $P < 0.05$, ** $P < 0.01$).

Despite its known role in formation of glycan branches (Figure 21a), *MGAT4A* downregulation did not result in corresponding changes of complex branched glycans. Instead, significant changes in other glycan traits were observed on day 8, including increased quantity of agalactosylated (G0), total galactosylated (GN), and trigalactosylated (G3) structures, as well as asialylated (S0) and trisialylated (S3) structures, leading to a reduced sialylation ratio (SR) (Figure 21c). As *MGT4A* appeared to be downregulated only on day 12 (and not on day 8) it suggests again that observed glycans changes possibly reflect off-target effects and not decreased gene activity. Only an increase in the agalactosylated (G0) glycans persisted through day 12. Furthermore, many of the changes (e.g., G0, G3, S0, and SR) were also observed in IN control, suggesting CRISPR interference at off target sites. Although *ST6GAL1* was significantly downregulated on day 8 (Figure 21b), no corresponding changes were detected in sialylated glycans or any other glycan traits.

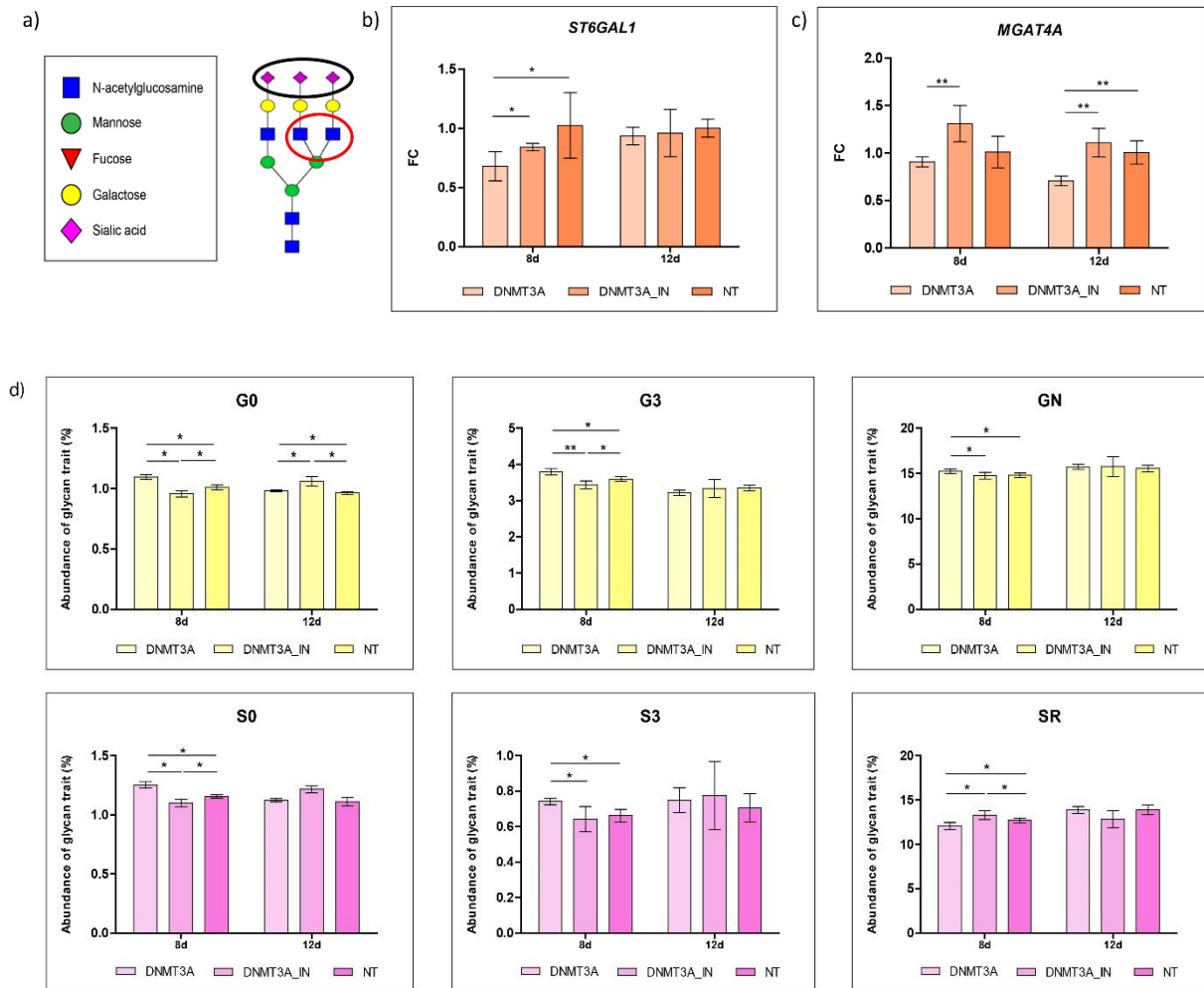


Figure 21. Targeted hypermethylation of *MGAT4A*, but not *ST6GAL1*, led to alterations in several glycan traits. *ST6GAL1* catalyzes the addition of sialic acid to glycans (circled in black), while *MGAT4A* catalyzes glycan branching (circled in red) (a). Targeted hypermethylation resulted in significant downregulation of *ST6GAL1* on the 8th day post-transfection (b) and *MGAT4A* on the 12th day post-transfection (c). However, only targeted hypermethylation of *MGAT4A* led to significant changes in several glycan traits (d). Error bars are shown as \pm SD ($n = 5$). Statistical significance between samples targeted with active DNMT3A and its respective inactive (DNMT3A_IN) and non-target control (NT) was determined using the Mann–Whitney U test (* $P < 0.05$, ** $P < 0.01$).

MGAT3 adds bisecting GlcNAc to *N*-linked glycans (Figure 22a), thus suppressing their further elongation. The glycan profile of HepG2 cells (Figure 16) does not contain glycans with bisecting GlcNAc, and the upregulation of *MGAT3* on day 8 post-transfection by targeted hypomethylation did not result in appearance of the corresponding structures. However, small but significant alterations in the *N*-glycome were detected on day 12 post-transfection (Figure

22c). These included a decrease in highly branched (HB) structures and an increase in agalactosylated (G0) and asialylated (S0) structures. Interestingly, opposite direction of glycan change was observed in IN control (decrease in G0 and S0), suggesting on a potential off-target effect of the TET1-dCas9 fusion binding. Furthermore, decrease in quantity of tetragalactosylated (G4) and antennary fucose-containing (FA) structures was observed exclusively in cells treated with active TET1-dCas9 on day 12, suggesting that the upregulation of *MGAT3* induced by demethylation may have more pronounced effects on *N*-glycome.

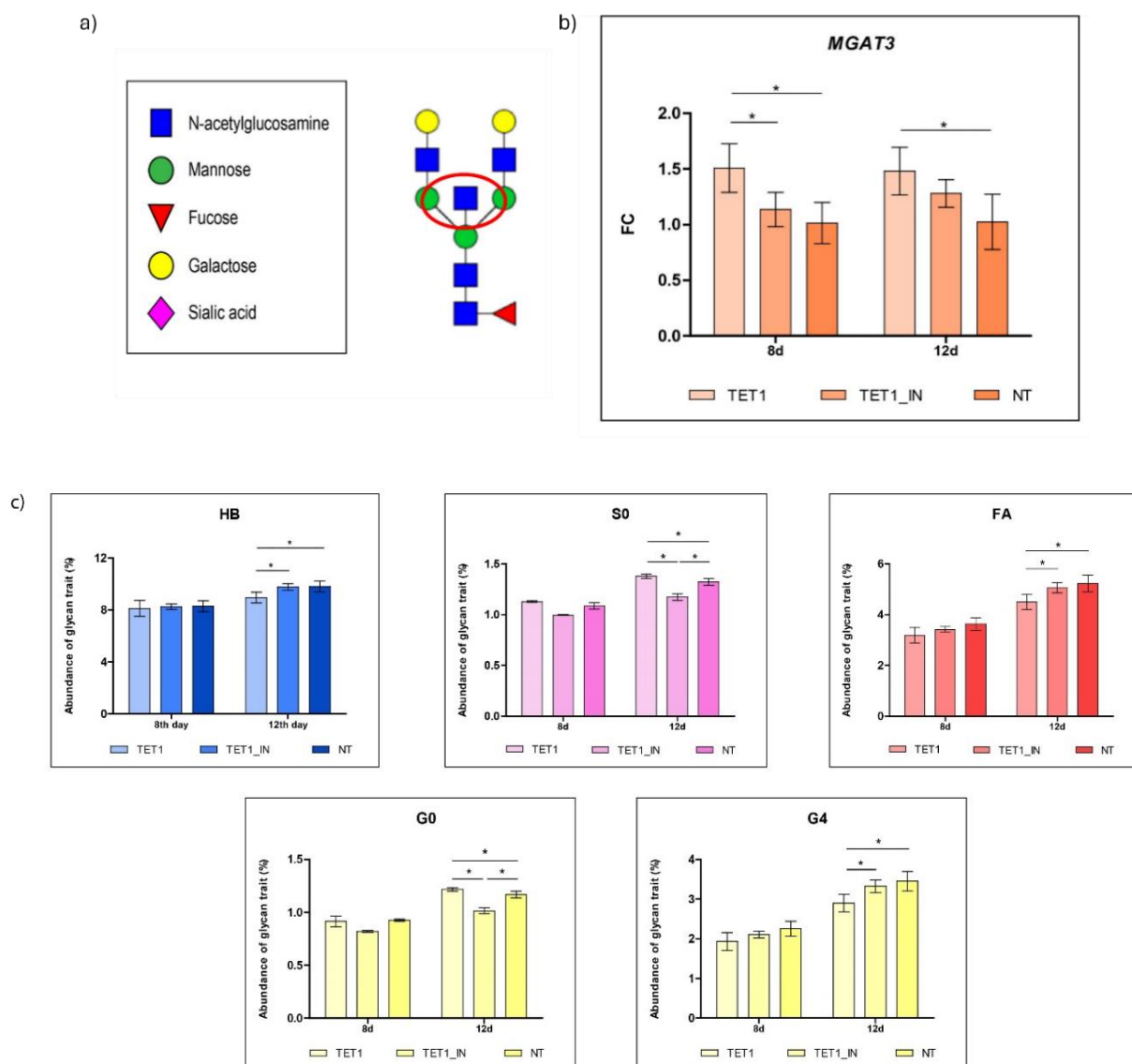


Figure 22. Upregulation of the *MGAT3* gene by targeted hypomethylation induced moderate changes in the HepG2 total cell *N*-glycome. *MGAT3* is a glycosyltransferase responsible for the formation of bisecting GlcNAc (a). Targeted hypomethylation using TET1-dCas9 led to significant upregulation of *MGAT3* on the 8th day post-transfection (b). However,

alterations in the total *N*-glycome were observed only on the 12th day post-transfection, including a decrease in highly branched (HB) glycans, glycans bearing antennary fucose (FA), and tetragalactosylated glycans (G4), as well as an increase in asialylated (S0) and agalactosylated (G0) glycans. Error bars are shown as \pm SD ($n = 5$). Statistical significance between samples targeted with active TET1 and its respective inactive (TET1_IN) and non-target control (NT) was determined using the Mann–Whitney U test (* $P < 0.05$, ** $P < 0.01$).

Overall, dysregulated expression of most of the candidate glyco-genes by targeted hyper- or hypomethylation, using the dCas9-based molecular tools, resulted in significant alterations in the HepG2 total cell *N*-glycome. While not all the glycan changes were attributed to the corresponding glycosyltransferases, the results underscore the role of DNA methylation as a potential epigenetic mechanism regulating protein *N*-glycosylation in HepG2 cells.

4.1.4. The *B4GALT1* and *FUT8* gene downregulation by hypermethylation and the *MGAT3* gene upregulation by hypomethylation resulted in changes at the protein level

To investigate in more detail the epigenetic regulation of glyco-genes, *B4GALT1*, *FUT8*, and *MGAT3* were selected for further experiments. These genes were selected based on several factors. *B4GALT1* and *FUT8* exhibited strong downregulation following targeted hypermethylation, and changes in their transcriptional activity were reflected in corresponding glycan structures. Although the effect of targeted hypomethylation on *MGAT3* transcriptional upregulation and corresponding glycan phenotype was moderate, *MGAT3* was selected because it was the only glyco-gene that was targeted by TET1-dCas9 in this study. Before conducting further epigenetic manipulations, I performed western blot analysis to determine whether changes in gene transcription were also reflected at the protein level. As shown in Figures 23a and 23b, downregulation of both *B4GALT1* and *FUT8* at the mRNA level translated into a corresponding decrease in protein level compared to both IN and NT controls at both time points. Also, the significant upregulation of the *MGAT3* gene on mRNA level was reflected on a protein level only on day 8 (Figure 23c).

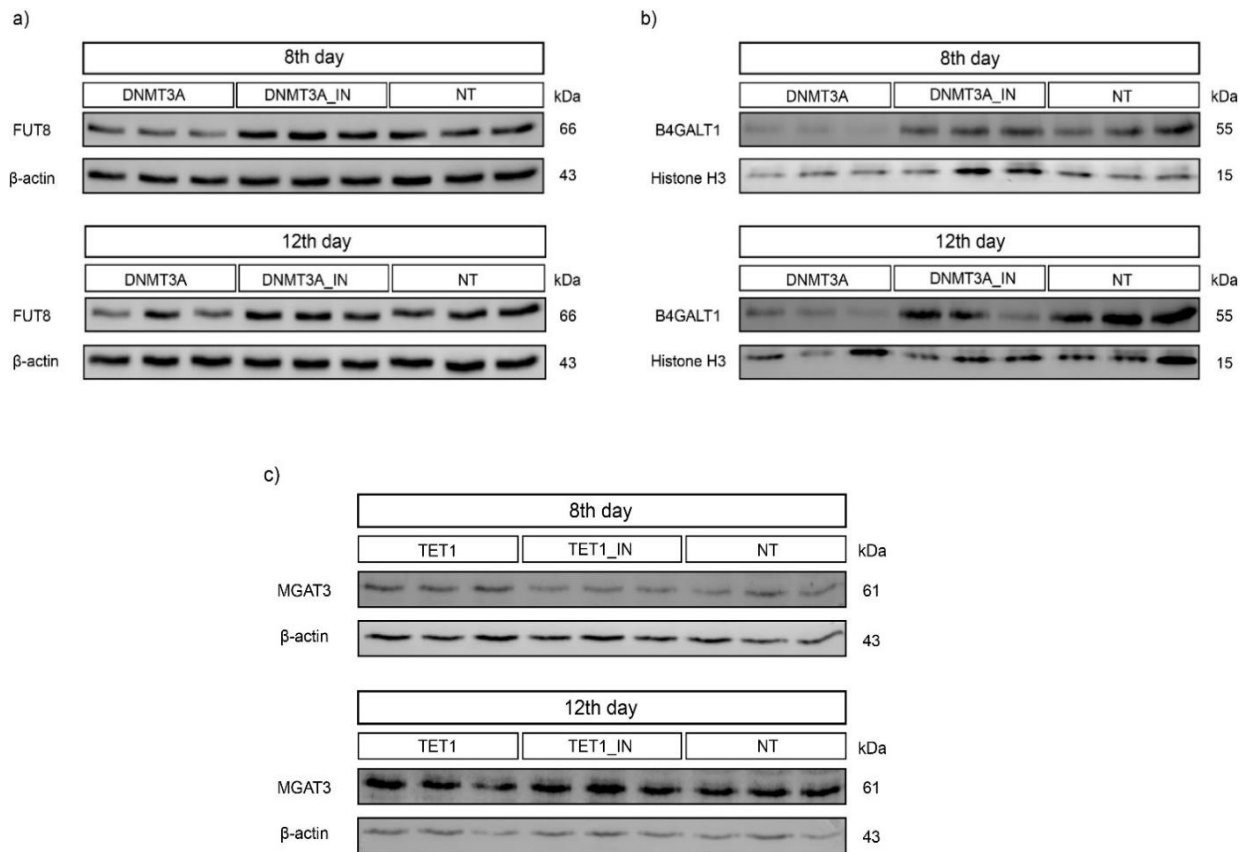


Figure 23. Western blot analysis revealed that down- or upregulation of *FUT8*, *B4GALT1*, and *MGAT3* at mRNA level was followed by changes in protein level. Transcriptional changes induced by targeted hypermethylation of *FUT8* and *B4GALT1*, or targeted hypomethylation of *MGAT3*, were reflected on the protein level as well. Targeting with DNMT3A-dCas9 resulted in decreased expression of FUT8 (a) and B4GALT1 (b) glycosyltransferases on both post-transfection days, while targeting with TET1-dCas9 led to increased MGAT3 expression only on the 8th day post-transfection (c), consistent with gene expression analysis results. β -actin and H3 were used as endogenous controls. Protein size was expressed in kilodaltons (kDa). DNMT3A_IN/TET1_IN – Inactive control; NT – Non-targeting control.

4.2. Targeted manipulation of histone modifications in promoters of *FUT8*, *B4GALT1*, and *MGAT3* genes

Glyco-genes *FUT8*, *B4GALT1* and *MGAT3* were selected for further manipulations with CRISPR/dCas9 tools for targeted engineering of histone modifications in HepG2 cell line. Specifically, to investigate the role of histone methylation and acetylation in epigenetic regulation of these genes, I used dCas9 fusions with HDAC3, RIOX1, G9a, p300 and PRDM9 domains for removing or introducing corresponding histone marks. Following cell transfections

with these fusion constructs, gene expression levels were analyzed on mRNA level while level of engineered histone marks was measured using chromatin immunoprecipitation methods.

4.2.1. Cloning of a full-length HDAC3 histone deacetylase domain

To manipulate H3K27ac levels in the regulatory regions of the *FUT8* and *B4GALT1* genes the HDAC3 histone deacetylase domain was cloned in a way compatible with the CRISPR/dCas9 modular system developed by Josipović et al (62). The full-length HDAC3 sequence was amplified from FreeStyle™ 293-F cDNA using primers designed to specifically amplify HDAC3 while incorporating overhangs required for cloning into the N-FD_empty backbone vector. To ensure compatibility with the CRISPR/dCas9 modular system, two BsaI restriction sites within the HDAC3 sequence were eliminated. The first BsaI site was removed by introducing a c123g substitution through site-directed mutagenesis while a second BsaI site was intentionally introduced during amplification step *via* the reverse primer, which incorporated the c1251t substitution. Additionally, to create a catalytically inactive HDAC3 variant, the R265P substitution was introduced through site-directed mutagenesis. The successful cloning of both active and inactive HDAC3 modules (Figure 24) was confirmed by Sanger sequencing, and these modules were then used in subsequent cloning steps into the modular CRISPR/dCas9 system designed for epigenetic editing.

points (Figure 25a). Although transcription was expected to decrease after deacetylation occurred, counterintuitively in both active ($FC = 1.32 \pm 0.33$) and inactive ($FC = 1.49 \pm 0.21$) HDAC3 samples, I observed an increase in the *B4GALT1* gene transcription on day 8 post-transfection (Figure 25d).

Additionally, the level of H3K27ac was measured in the region targeted with HDAC3-dCas9 by N-ChIP method. For *FUT8*, a significant reduction in H3K27ac level was observed in one of the analyzed regions (FUT8_qChIP_3) on day 5 compared to both controls. However, at this time point, a significant reduction was observed also in the IN control. In this study, the full-length HDAC3 domain was used, and as such it includes protein interaction domains that may mediate H3K27ac removal through interactions with other chromatin regulators endogenously present, even when used as inactive domain. On day 8, a significant H3K27ac reduction persisted in the cells treated with active HDAC3 while in the IN control H3K27ac level was restored (Figure 25b). In the other two analyzed regions, FUT8_qChIP_1 and FUT8_qChIP_2, the level of H3K27ac was consistently low across all samples (including controls) on day 5 post-transfection thus making it impossible to draw any coherent conclusion. On day 8 post-transfection, no significant changes in H3K27ac level was detected in either region (Figure 25c). Interestingly, despite being closer to the sgRNA binding site, FUT8_qChIP_1 and FUT8_qChIP_2 were less affected than FUT8_qChIP_3, which is located over 1000 bp away. This might suggest that the chromatin environment, particularly H3K27ac enrichment, may influence the efficacy of HDAC3-dCas9. Specifically, FUT8_qChIP_1 and FUT8_qChIP_2 are situated in regions with natively low H3K27ac level (Figure 11a), which therefore shows that forcible removal of H3K27ac has had minimal impact in these regions.

For *B4GALT1*, H3K27ac level was analyzed in only one region within its promoter. Interestingly, only the IN control showed significant changes in H3K27ac level, with a notable increase on day 5 compared to samples targeted with active HDAC3 and the NT control. On day 8 post-transfection, the IN control exhibited a significant decrease in H3K27ac level compared to cells targeted with active HDAC3, whereas the NT control showed high variability between biological replicates (Figure 25e). These variable effects of active and inactive HDAC3 on *B4GALT1* suggest that full-length HDAC3 may influence both transcriptional activity and the chromatin environment in a manner that is independent of its catalytic activity.

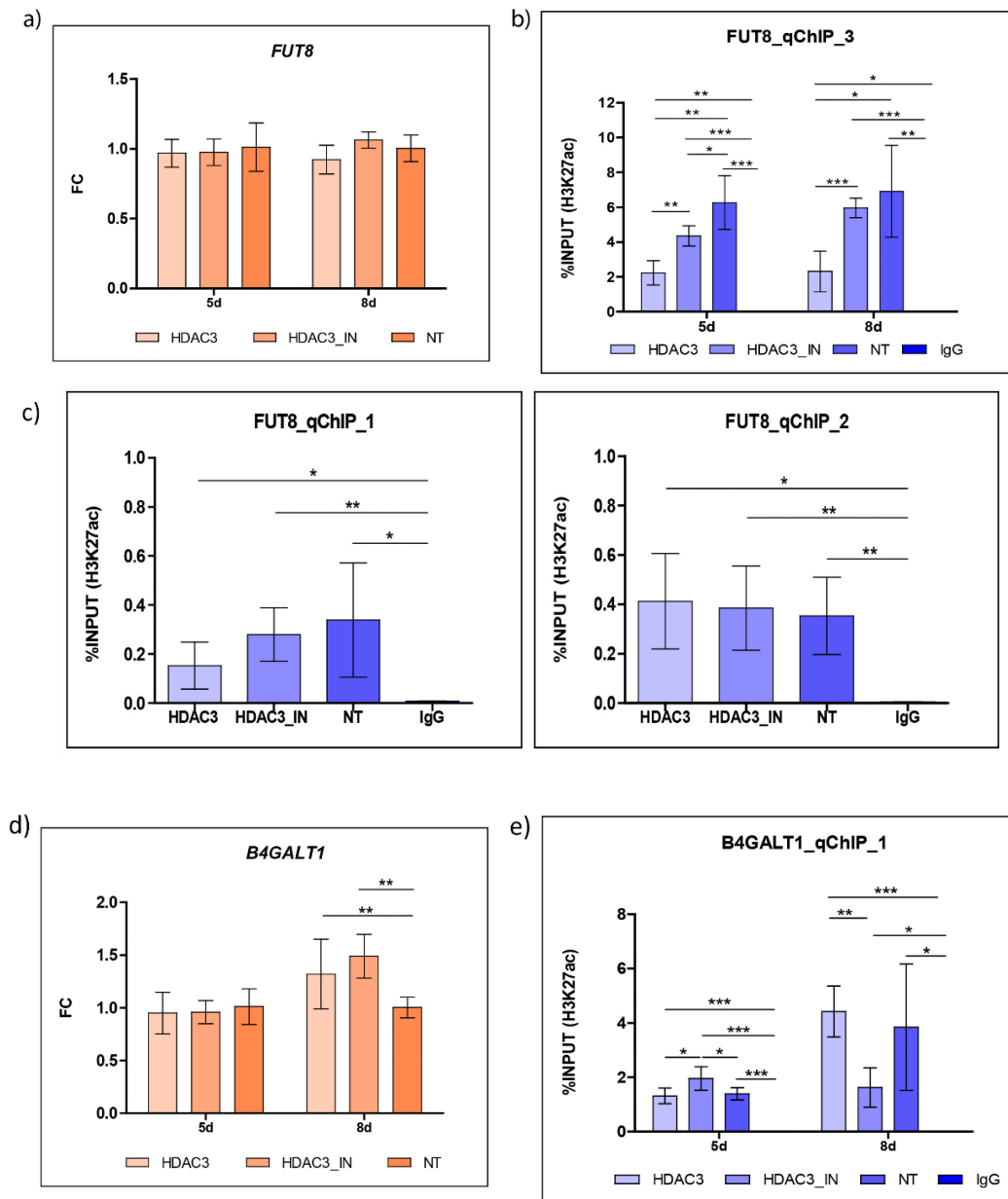


Figure 25. Targeting with HDAC3-dCas9 decreased H3K27ac levels in the promoter region of *FUT8* but not in *B4GALT1*. Although HDAC3-dCas9 did not affect the transcriptional activity of *FUT8* (a), it significantly reduced H3K27ac level in *FUT8_qChIP_3* region (b) on both days post-transfection, but not in *FUT8_qChIP_1* and *FUT8_qChIP_2* regions (c). The *B4GALT1* gene was significantly upregulated following HDAC3-dCas9 targeting, both in active and inactive HDAC3 samples (d), even though there was no significant change of H3K27ac level in analyzed region (e). In all analyzed regions, the negative control (IgG) was mostly undetectable, confirming that the observed H3K27ac enrichment was not due to nonspecific binding of the anti-H3K27ac antibody to chromatin. Error bars are shown as \pm SD (n = 3-6). Statistical significance between samples targeted with active HDAC3 and its

respective inactive (HDAC3_IN) and non-target control (NT) was determined using the t-test (* $P \leq 0.05$, ** $P \leq 0.01$, *** $P \leq 0.001$).

In summary, targeting the *FUT8* promoter with HDAC3-dCas9 effectively reduced H3K27ac level in a specific region but did not lead to a significant gene downregulation, suggesting that H3K27ac may not play a regulatory role in targeted region or the reduction was insufficient to affect transcription. For *B4GALT1*, both active and inactive HDAC3 targeting resulted in upregulation of gene transcriptional activity. This unexpected effect could be attributed to the recruitment of other chromatin regulators by the full-length HDAC3 domain or to off-target binding of either the active or inactive HDAC3 to genomic regions containing factors whose altered expression could result in *B4GALT1* upregulation.

4.2.3. Targeting RIOX1-dCas9 to the *FUT8* and *B4GALT1* promoters and the effects on corresponding histone mark and gene transcriptional activity

The promoters of *B4GALT1* and *FUT8* are also enriched with H3K4me3, another histone mark associated with active transcription. To explore its role in their regulation, both genes were targeted using RIOX1-dCas9. However, no significant changes in transcriptional activity were observed for any of the genes (Figure 26a and 26c).

The CUT&RUN analysis was performed to assess the impact of RIOX1-dCas9 on H3K4me3 level. For *FUT8*, a significant reduction in H3K4me3 level was observed in the FUT8_qChIP_4 region on day 5 compared to NT but not to IN control. By day 8, the reduction did not persist, and instead, a significant increase in H3K4me3 level was detected in this region compared to NT control. Due to these variable results, it was difficult to draw any coherent conclusion. In FUT8_qChIP_3 region there were no significant changes in H3K4me3 level both days post-transfection (Figure 26b). For *B4GALT1*, no significant changes in H3K4me3 level were detected in examined regions (Figure 26d).

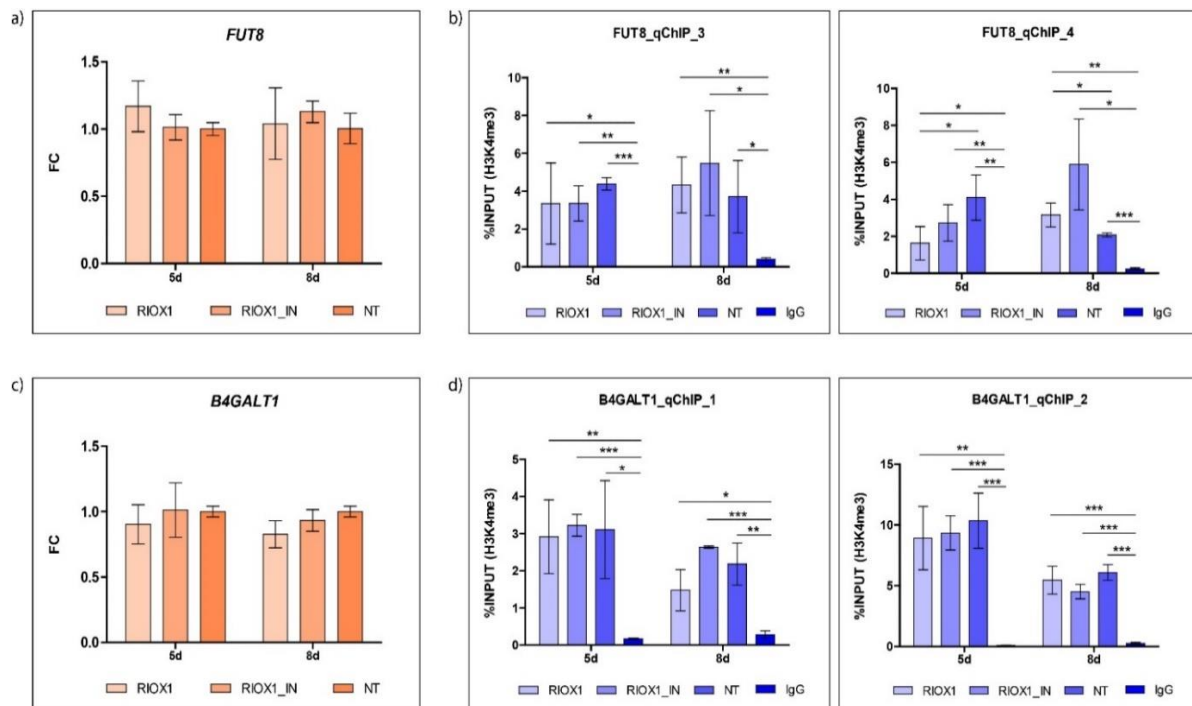


Figure 26. Targeting RIOX1-dCas9 to the promoter regions of *FUT8* and *B4GALT1* did not alter H3K4me3 levels or their transcriptional activity. No significant downregulation was observed in *FUT8* (a) or *B4GALT1* (c) following RIOX1-dCas9 targeting. The CUT&RUN method revealed a significant decrease of H3K4me3 level in the FUT8_qChIP_4 region on day 5 compared to NT but not to IN control, while there was no change of the H3K4me3 level in FUT8_qChIP_3 region (b). H3K4me3 level remained unchanged in both analyzed regions of *B4GALT1* (d). In all analyzed regions, the negative control (IgG) was mostly undetectable, confirming that the observed H3K4me3 enrichment was not due to nonspecific binding of the anti-H3K4me3 antibody to chromatin. Error bars are shown as \pm SD ($n = 3-4$). Statistical significance between samples targeted with active RIOX1 and its respective inactive (RIOX1_IN) and non-target control (NT) was determined using the t-test (* $P \leq 0.05$, ** $P \leq 0.01$, *** $P \leq 0.001$).

Overall, targeting with RIOX1-dCas9 had no effect on the expression of *B4GALT1* or its H3K4me3 levels. Even though targeting RIOX1-dCas9 to the *FUT8* promoter resulted in some H3K4me3 reduction there was no effect on its transcriptional activity. Although RIOX1 was selected for its ability to remove all methyl groups at H3K4 (mono-, di- and trimethylation), an alternative histone demethylase may have been more effective for this purpose.

4.2.4. Targeting G9a-dCas9 to the *FUT8* and *B4GALT1* promoters and the effect on corresponding histone mark and gene transcriptional activity

The G9a-dCas9 fusion was employed to introduce H3K9me2, a repressive histone mark, into the promoters of *FUT8* and *B4GALT1*. While G9a-dCas9 targeting had no effect on the *FUT8* gene transcription (Figure 27a), it resulted in a significant downregulation of *B4GALT1* compared to the NT control on day 8 (FC = 0.67±0.06) and compared to both IN and NT control on day 12 (FC = 0.50±0.09) (Figure 27c). Although a significant gene downregulation was also observed in the IN control on day 12, the stronger gene downregulation in cells treated with active G9a suggests that the observed effect was not solely due to CRISPR interference but also due to introduced H3K9me2 mark.

To confirm this, X-ChIP analysis was performed. Counterintuitively, analyzed regions of *FUT8* showed a decrease and not an increase in quantity of H3K9me2 mark (Figure 27b), although statistically insignificant. For *B4GALT1*, an increase in H3K9me2 level was not observed compared to controls on day 8 after transfection, however, a moderate increase was detected in both analyzed regions on day 12, which were significant only compared to the IN control (Figure 27d). This suggests that elevated H3K9me2 levels may have contributed to the *B4GALT1* gene downregulation.

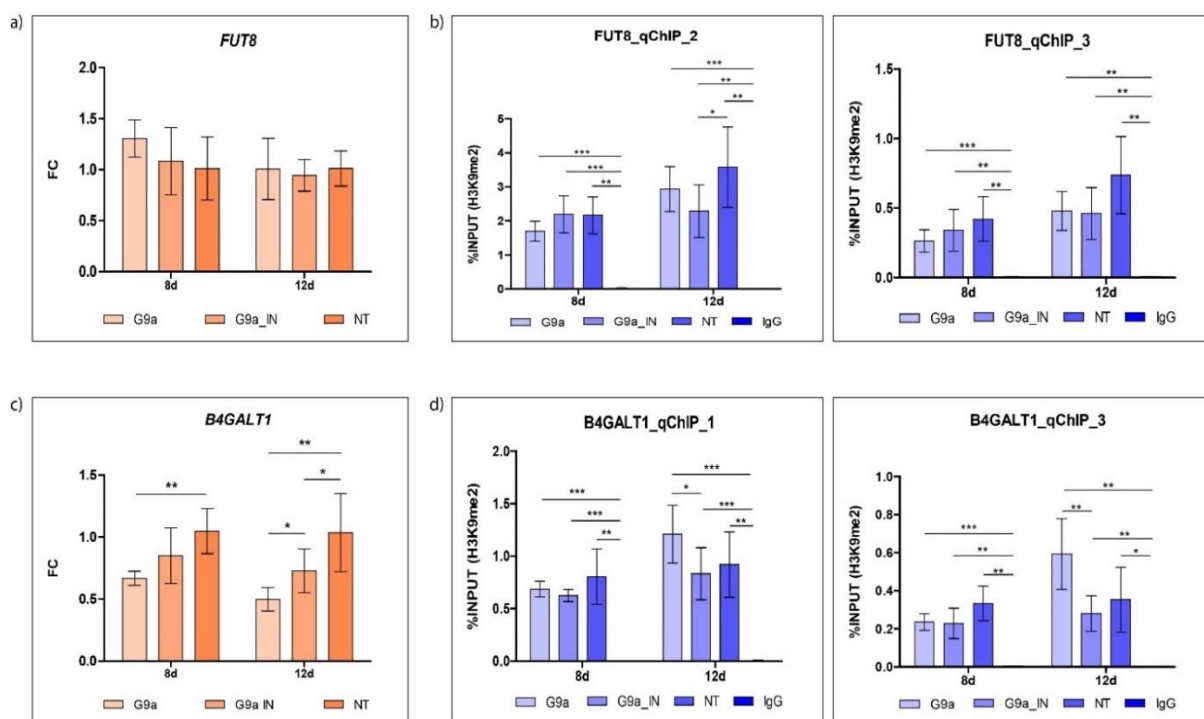


Figure 27. G9a-dCas9 decreased *B4GALT1* but not *FUT8* transcriptional activity. Targeting of the G9a-dCas9 fusion on the *FUT8* promoter resulted in unchanged transcriptional

activity (a) as well as unchanged H3K9me2 level in both analyzed regions (b). In contrast, significant downregulation of *B4GALT1* was detected on the 12th day post-transfection with G9a-dCas9 (c). Samples targeted with active G9a showed a trend toward increased H3K9me2 level in both analyzed regions on the 12th day post-transfection, although statistically insignificant (d). In all analyzed regions, the negative control (IgG) was mostly undetectable, confirming that the observed H3K9me2 enrichments were not due to nonspecific binding of the anti-H3K9me2 antibody to chromatin. Error bars are shown as \pm SD ($n = 3-6$). Statistical significance between samples targeted with active G9a and its respective inactive (G9a_IN) and non-target control (NT) was determined using the t-test (* $P \leq 0.05$, ** $P \leq 0.01$, *** $P \leq 0.001$).

In conclusion, targeting G9a-dCas9 to the *FUT8* promoter region did not significantly alter its transcriptional activity nor H3K9me2 levels. While significant downregulation of *B4GALT1* was observed, the lack of a robust and consistent increase in H3K9me2 level in the analyzed regions makes it difficult to attribute the observed gene downregulation to G9a methyltransferase activity. However, the trend of increased H3K9me2 level in cells treated with active G9a, suggests that G9a-dCas9 may have exerted some degree of activity in this region.

4.2.5. Targeting p300-dCas9 and PRDM9-dCas9 to the *MGAT3* promoter and the effects on corresponding histone marks and gene transcriptional activity

The *MGAT3* promoter, which shows low expression in HepG2 cells, has a natively low H3K27ac or H3K4me3 enrichment (Figure 11g), the histone marks associated with active transcription. To explore whether these marks regulate *MGAT3* expression, its promoter was targeted with p300-dCas9 to introduce H3K27ac and PRDM9-dCas9 to introduce H3K4me3. A moderate upregulation of *MGAT3* was observed on day 8 after transfection with p300-dCas9, but this increase was only significant compared to the IN control (Figure 28a). A trend of a decreased gene transcription was observed in IN control, therefore suggesting that CRISPR interference, as a result of the p300-dCas9 construct binding, could partially obscure the effects of introduced epigenetic modification. Targeting *MGAT3* with PRDM9-dCas9 resulted in a strong upregulation ($FC = 5.34 \pm 3.03$) compared to both IN and NT control on 8th day post-transfection (Figure 28c), though the effect was transient and diminished by day 12, suggesting a rapid turnover of the introduced H3K4me3 mark.

To assess H3K27ac and H3K4me3 levels after epigenetic manipulations, NChIP and CUT&RUN analyses were conducted, respectively. In the *MGAT3*_qChIP_3 region, a significant increase in H3K27ac was observed on the 8th day post-transfection compared to both controls (Figure 28b) confirming that p300-dCas9 effectively introduced acetylation at this

site. Conversely, in the *MGAT3*_qChIP_2 region, a moderate increase in H3K27ac was detected, but it reached significance only when compared to the IN control on the 5th day post-transfection (Figure 28b). Additionally, the IN control showed a significant decrease in H3K27ac relative to the NT control, indicating that the binding of p300-dCas9 itself might influence chromatin modifications. The H3K4me3 level was analyzed in two different regions (*MGAT3*_qChIP_1 and *MGAT3*_qChIP_2), but no significant changes were observed in either region following targeted manipulation with PRDM9-dCas9 (Figure 28d).

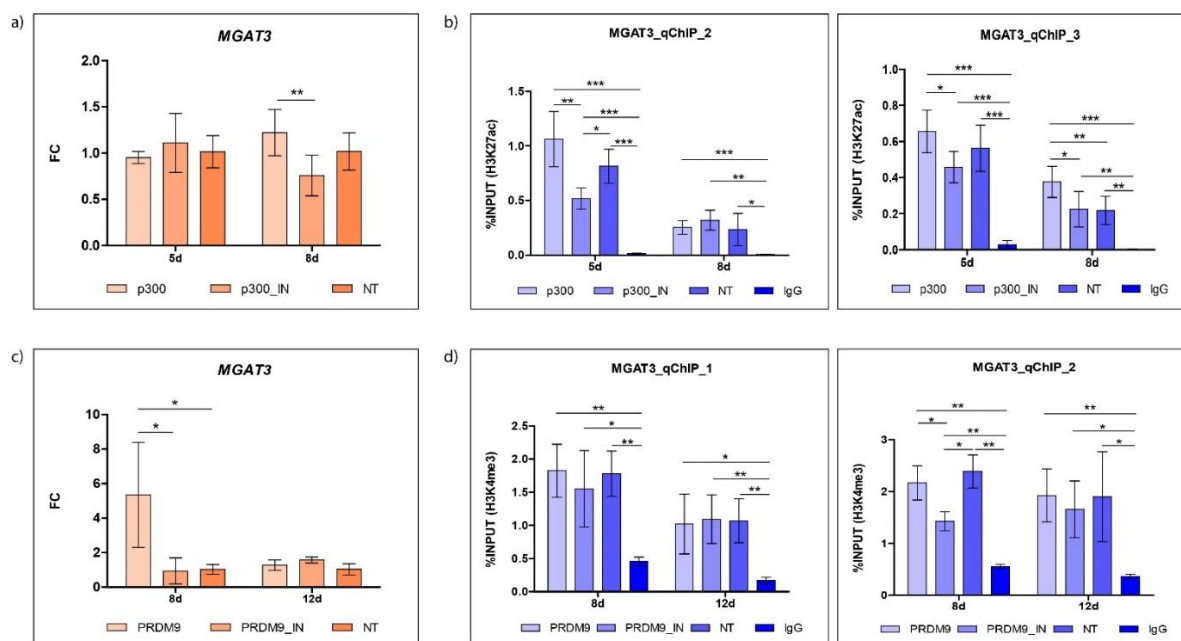


Figure 28. Levels of H3K27ac and H3K4me3 marks at the *MGAT3* promoter region and gene's transcriptional activity after targeting it with p300-dCas9 and PRDM9-dCas9. The *MGAT3* was not significantly upregulated following targeting with p300-dCas9 (a) despite a significant increase in H3K27ac levels observed in one analyzed region (*MGAT3*_qChIP_3) on the 8th day post-transfection (b). Targeting PRDM9-dCas9 to *MGAT3* promoter led to a significant gene upregulation (c) regardless of the unchanged H3K4me3 level in the *MGAT3*_qChIP_1 and *MGAT3*_qChIP_2 regions analyzed by CUT&RUN (d). In all analyzed samples, the negative control (IgG) was mostly undetectable, confirming that the observed enrichments were not due to nonspecific binding of the anti-H3K27ac antibody to chromatin. Although negative control was higher in samples analyzed for H3K4me3, it was still significantly lower compared to all other samples confirming that majority of observed enrichments come from specific binding of anti-H3K4me3 antibody to chromatin. Error bars are shown as \pm SD (n = 3-6) Statistical significance between samples targeted with active p300

or PRDM9 and their respective inactive (p300_IN and PRDM9_IN) and non-target controls (NT) was determined using the t-test (* $P \leq 0.05$, ** $P \leq 0.01$, *** $P \leq 0.001$).

To summarize, p300-dCas9 effectively increased H3K27ac in one of the analyzed regions of the *MGAT3* promoter, however, this change was not sufficient to induce changes in its transcriptional activity. PRDM9-dCas9 treatment led to strong *MGAT3* upregulation, but the lack of consistent H3K4me3 increases suggests either that this histone mark is not involved in the transcriptional regulation or the qPCR assays did not cover the regions where the PRDM9 introduced this histone mark. It cannot be excluded that *MGAT3* upregulation arose from off-target PRDM9-dCas9 binding to other genomic regions or that PRDM9-dCas9 itself exerts effect on transcriptional activity through mechanisms independent of its catalytic activity.

4.2.6. Effects of targeted epigenetic manipulation of histone modifications on DNA methylation

Epigenetic modifications and mechanisms rarely act alone. Instead, multiple epigenetic layers closely cooperate in regulation of gene expression. One of the goals of this study was to examine the interplay of DNA methylation and specific histone modifications.

DNA methylation was assessed only in samples in which I observed significant effect on the engineered histone modification or gene expression. One of these was *FUT8* which showed significant increase in H3K27ac following HDAC3-dCas9 targeting (Figure 25b). However, no changes in DNA methylation level were found at the analyzed CpG sites (Figure 29a). Targeting *B4GALT1* with G9a-dCas9 introduced some levels of H3K9me2 modification which resulted in a significant downregulation of gene expression (Figure 27c), but it did not impact DNA methylation level at the cytosines analyzed with B4GALT1-2 assay (Figure 29b). Successful introduction of H3K27ac by p300-dCas9 at the *MGAT3* promoter region (Figure 28b) did not have an effect on DNA methylation, as observed after pyrosequencing with MGAT3-1 assay (Figure 29c). Finally, substantial upregulation of *MGAT3* was observed following PRDM9-dCas9 targeting (Figure 28c). Since H3K4me3 is known to inhibit DNA methylation, it was hypothesized that PRDM9 activity might influence DNA methylation levels. However, as shown in Figure 29d, PRDM9-dCas9 did not alter methylation levels at the analyzed cytosines in CpG island of the *MGAT3* gene.

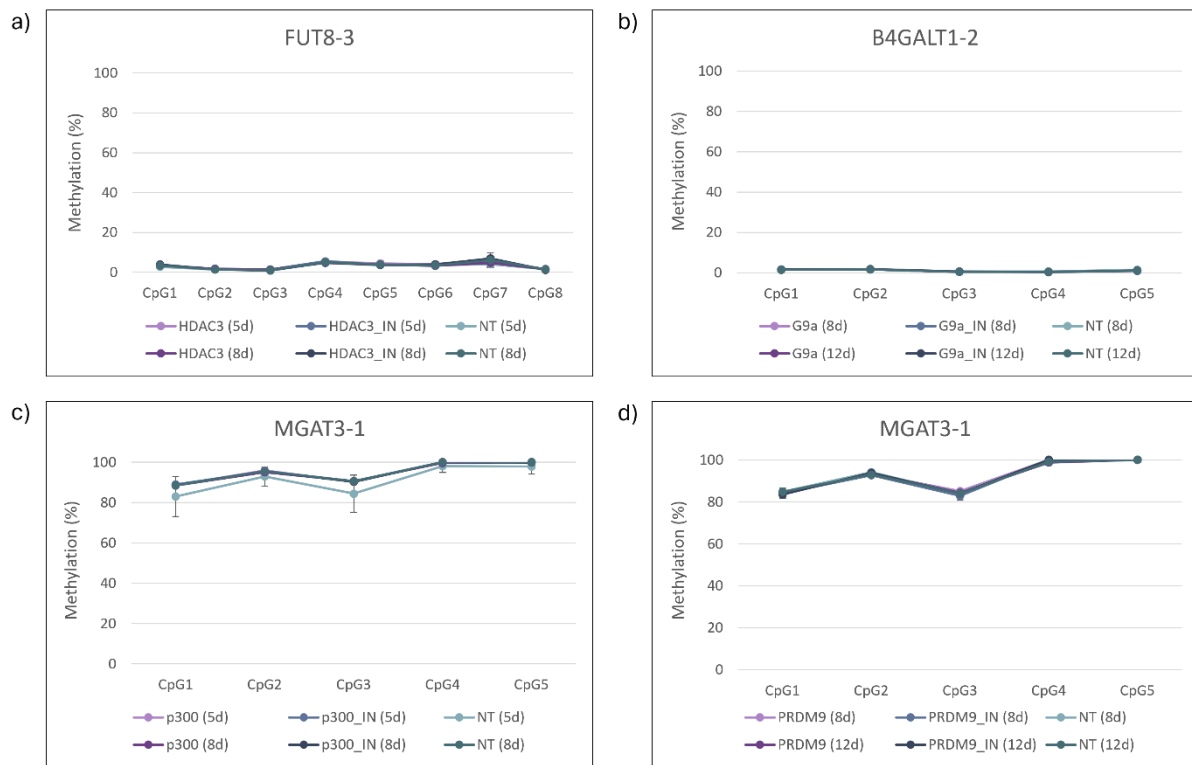


Figure 29. Engineered histone modifications using dCas9 fusions with histone modifiers in the *FUT8*, *B4GALT1* and *MGAT3* promoters did not affect CpG methylation. Removal of H3K27ac histone mark from the *FUT8* promoter region using HDAC3-dCas9 did not affect DNA methylation level in CpG sites analyzed by FUT8-3 assay (a). Despite pronounced *B4GALT1* transcriptional downregulation by the G9a-dCas9 fusion, methylation at the specific CpG sites covered by B4GALT1-2 assay remained unchanged (b). After the successful introduction of H3K27ac by p300-dCas9 at the *MGAT3* promoter region there was no increase in methylation of CpG sites covered by MGAT3-1 assay (c). Targeted manipulation with PRDM9-dCas9 had no effect on CpG methylation in region covered by MGAT3-1 assay (d). Error bars are shown as \pm SD ($n = 3$).

In conclusion, engineered histone modifications did not affect DNA methylation level at least in the analyzed regions of the *MGAT3*, *B4GALT1* and *FUT8* genes. However, it should be considered that the change in quantity of engineered histone modifications may have been insufficient to affect DNA methylation. Alternatively, the pyrosequencing assays might not have encompassed the region containing CpG sites whose methylation status might have consequently changed. Future investigations would benefit from examining wider regions in genes targeted with dCas9 fusions as well as other gene loci in order to further explore interplay between histone modifications and DNA methylation.

5. DISCUSSION

Protein *N*-glycosylation is a complex, non-template-driven process governed by a sophisticated interplay between genetic factors and environment mediated through epigenetic mechanisms. Over 800 genes are implicated in glycosylation, with this number continuously expanding due to advancements in genome-wide association studies (GWAS) (40,237). It is estimated that over 1% of the human genome encodes proteins involved in glycan biosynthesis, recognition, and degradation. Glycosyltransferases are not sole actors in the complex process of protein glycosylation, but many other proteins are involved such as transcriptional factors, ion channels, transporters, chromatin remodelers and others (187,302). The essential role of glycosylation is underscored by the fact that most genetic defects in this process are embryonically lethal. When not lethal, such defects—seen in congenital disorders of glycosylation (CDGs)—lead to severe muscular, developmental, and neurological impairments (37). However, knock-out experiments of glyco-genes encoding for glycosyltransferases have demonstrated compensatory mechanisms in glycosylation. While some glycosyltransferase knockouts can lead to severe phenotypes, many show only mild changes, indicating redundancy and compensation among different glycosyltransferases. These compensatory mechanisms allow cells to maintain essential glycosylation functions despite the loss of a specific glycosyltransferase (303). The ubiquitous change of protein glycosylation observed in virtually every disease more plausibly arises from the strong effect of environment mediated through epigenetic mechanisms (40,302).

Many studies have attempted to link epigenetic changes to the expression of glyco-genes and corresponding glycan alterations; however, most have relied on epigenetic inhibitors or correlations between specific chromatin modifications and glyco-gene transcriptional levels (40,237,253,254). The use of epigenetic inhibitors induces widespread epigenetic changes, complicating the attribution of observed transcriptional and glycan alterations to the effect of an individual gene. A major advancement in epigenetic research came with the development of the CRISPR/dCas9 system, enabling precise epigenetic manipulation of targeted genomic loci (57,58). This dissertation aimed to leverage the precision of the CRISPR/dCas9 system to investigate the role of DNA methylation and histone modifications in the regulation of glyco-genes, encoding for key glycosyltransferases involved in formation of complex *N*-glycans, by observing the effect on the final glycan phenotype. To achieve this, dCas9 was fused to various effector domains that modulate DNA methylation and histone modifications and was targeted to promoters of the *B4GALT1*, *FUT8*, *ST6GAL1*, *MGAT4A*, *MGAT4B*, *MGAT5*, and *MGAT3*

genes using sgRNAs complementary to these regions. The impact of the induced epigenetic changes was assessed at the mRNA, protein, and phenotypic level, i.e. on HepG2 total cell *N*-glycome. An additional objective of this dissertation was to explore the potential influence of induced histone modifications on DNA methylation within the targeted regions, aiming to elucidate the interplay between different epigenetic mechanisms while also dwelling deeper into epigenetic regulation of glyco-genes.

In the first phase of this dissertation, the promoter regions of selected candidate genes underwent targeted manipulation of DNA methylation using either DNMT3A-dCas9 or TET1-dCas9. The choice of the fusion protein for each gene was guided by publicly available data from the UCSC Genome Browser, specifically considering the degree of CpG methylation within CpG islands and the transcriptional activity of these genes in the HepG2 cell line. Genes exhibiting high expression levels and low CpG methylation (*B4GALT1*, *FUT8*, *ST6GAL1*, *MGAT4A*, *MGAT4B*, and *MGAT5*) were targeted with DNMT3A-dCas9 to induce DNA methylation, and the *MGAT3* gene with low expression and high CpG methylation was targeted with TET1-dCas9 to promote demethylation. The dCas9 fusions were guided with five to six distinct sgRNAs to the CpG islands and flanking sequences of each candidate gene, aiming for comprehensive coverage of the CpG island. The dCas9 fusions successfully induced changes in DNA methylation across all seven candidate gene promoters, resulting in significant alterations in gene transcriptional activity at both analyzed time points for most targets. The effect of methylation changes on protein *N*-glycosylation varied depending on the targeted glyco-gene and was not always consistent with change of corresponding glycan structures.

Targeted hypermethylation of the *B4GALT1* gene promoter using DNMT3A-dCas9 resulted in a strong downregulation of both its mRNA and protein levels. This downregulation correlated with changes in corresponding glycans, i.e. in an increase of agalactosylated (G0) and a decrease of digalactosylated (G2) structures, consequently altering the overall G0/GN ratio in the HepG2 total cell *N*-glycome. These findings align with the functional role of B4GALT1, the glycosyltransferase responsible for adding galactose to N-acetylglucosamine residues (205). Given that galactose addition is a prerequisite for addition of sialic acid (185), it was not surprising that *B4GALT1* downregulation also resulted in a significant increase in asialylated (S0) and a decrease in disialylated (S2) structures. The HepG2 cell line serves as a relevant model for HCC, and *B4GALT1* was identified among three candidate genes exhibiting hypermethylation in HCC tumor samples compared to adjacent normal tissue (304). The functional consequences of aberrant *B4GALT1* promoter hypermethylation have been also

investigated in the context of CRC. A study of Poeta et al. has demonstrated that *B4GALT1* hypermethylation leads to its transcriptional repression in tumor tissues relative to normal colonic mucosa and unmethylated tumor samples (53). Subsequent research revealed that promoter hypermethylation and downregulation of *B4GALT1* are associated with a negative prognostic impact in CRC. Notably, this study also highlighted the prognostic potential of *B4GALT1* methylation in plasma, showing that hypermethylated *B4GALT1* effectively distinguished metastatic CRC patients from healthy controls. Furthermore, three specific aberrantly methylated CpG sites (cg13834453, cg14829378, and cg14440947) were found to correlate with reduced disease-free survival (DFS) and overall survival (OS) (248). Importantly, these three CpG sites were also targeted in the present research using DNMT3A-dCas9. While these prior studies have established the clinical relevance of *B4GALT1* methylation in cancer, none have investigated the direct impact of *B4GALT1* hypermethylation on protein glycosylation profiles. Therefore, a key contribution of my dissertation was the demonstration that hypermethylation of the *B4GALT1* CpG island led to a substantial reduction in gene expression, which was directly reflected in alterations of the cellular glycan phenotype, specifically impacting galactosylation and sialylation patterns within the total *N*-glycome of HepG2 cells.

When CpG island of the *FUT8* gene was targeted with DNMT3A-dCas9 its hypermethylation significantly affected gene transcription which resulted in a corresponding decrease in core fucosylation, the specific glycan modification catalyzed by FUT8 fucosyltransferase. Additionally, it induced changes in other glycan traits, including an increase in oligomannose (OM) and a decrease in agalactosylated (G0), digalactosylated (G2), asialylated (S0), disialylated (S2), and low-branched (LB) glycans. These changes likely reflect a reduction in the quantity of core-fucosylated glycans, as LB, G0, S0, G2, and S2 derived traits contain glycan peaks bearing core fucose. While the primary role of *FUT8* is core fucosylation, previous *FUT8* knockout studies have shown its influence on other *N*-glycans. In Chinese hamster ovary (CHO) cells, *FUT8* knock-out led to a decrease in oligomannosylated glycans and an increase in sialylated glycans (305). Similarly, studies in CRC model cell lines demonstrated a significant reduction in oligomannosylated *N*-glycans, and *FUT8*-attenuated clones of SW480 and SW620 cells exhibited increased levels of $\alpha(2,6)$ -sialylation, with decreased *FUT8* expression being significantly associated with a higher degree of glycan branching (306). Consistent with these findings, my research also showed changes in sialylation and glycan branching, further supporting the notion that *FUT8* regulates more than

just core fucosylation. Although one study reported that the *FUT8* promoter is hypomethylated in most cancers (307), the role of promoter methylation in gene regulation and its effect on glycan phenotype remains poorly understood. Notably, the majority of research suggests that *FUT8* expression is predominantly regulated by various microRNAs (miRNAs). Studies in HCC tissues and highly metastatic HCC cell lines have shown that miRNAs miR-26a, miR-34a, and miR-455-3p directly bind to and negatively regulate *FUT8* expression (243). Alongside miR-34a, miR-122 has also been shown to target *FUT8* in hepatocarcinoma cell lines (52). In CRC, miR-198 overexpression has been shown to downregulate *FUT8*, leading to inhibition of cell proliferation, migration, and invasion of CRC cell lines (51). Despite the established role of miRNAs in *FUT8* regulation, my research is among the first to demonstrate that direct manipulation of the *FUT8* CpG island methylation not only strongly downregulates this gene but also significantly impacts core fucosylation in HepG2 total cell *N*-glycome. Another study demonstrated that targeted *FUT8* hypermethylation using dCas9-DNMT3A3L significantly reduces its expression; however, this study was conducted on CHO cell lines and did not analyze the consequences of this epigenetic manipulation on core fucosylation (308). Further research is warranted to comprehensively investigate the association between DNA methylation and the *FUT8* gene regulation, particularly in human tumor samples such as those from HCC (given the HepG2 cell line origin) or colorectal cancer. Ultimately, the sensitivity of *FUT8* expression to both miRNAs and DNA methylation highlights the complexity and cell-specific nature of epigenetic regulation, which cannot be attributed to a single epigenetic mechanism.

Alterations in glycan branching are frequently observed in cancers and can influence tumor growth, invasion, and metastasis (38,178). In this study, DNMT3A-dCas9 was used to target the CpG islands of three key enzymes involved in glycan branching: *MGAT4A*, *MGAT4B* and *MGAT5*. Targeted hypermethylation of *MGAT4B* and *MGAT5* resulted in their downregulation at both analyzed time points, whereas *MGAT4A* showed a significant decrease in expression only on day 12 post-transfection. Downregulation of *MGAT4B* was accompanied by a moderate but significant increase in low-branched (LB) structures, along with changes in digalactosylated (G2) and monosialylated (S1) structures. Nevertheless, given that G2 and S1 share common glycan peaks with the LB-derived trait, these alterations likely reflect the changes in glycan branching, as glycan branches are often extended by the addition of galactose and sialic acid. In contrast, downregulation of *MGAT4A* did not lead to changes in glycan branching but did influence galactosylation and sialylation in a distinctive manner, with

concurrent increases in agalactosylated (G0) and trigalactosylated (G3), as well as asialylated (S0) and trisialylated (S3) structures. However, except for G0, these changes were only observed at day 8 post-transfection, a time point when *MGAT4A* downregulation was not statistically significant, suggesting they might be attributed to non-specific effects of the DNMT3A-dCas9 fusion. The *MGAT5* gene downregulation led to an increase in both low-branched and highly-branched glycans, but interestingly it also caused widespread glycan alterations, affecting more than half of the analyzed derived glycan traits. Since low- and highly-branched glycans are typically sialylated, galactosylated, and often core-fucosylated, the observed increases in sialylated (S1, S2, S3, and SN), galactosylated (G2, G3, and GN), and core-fucosylated traits likely stem from these changes in glycan branching. Accordingly, agalactosylated and asialylated traits were decreased. There are a few other studies showing involvement of DNA methylation in regulation of glycan branching. The *MGAT4A* gene was upregulated after treatment of pancreatic cell lines with epigenetic modulator 5-Aza-C (235). In astrocytes, 5-Aza-dC treatment downregulated *MGAT1-MGAT5*, with a reduction in tri-antennary glycans carrying a β 1,4-GlcNAc branch attributed to *MGAT4B* downregulation (309). Although several studies reported changes in *MGAT5* expression following 5-Aza-dC treatment, the authors suggested that these changes were most probably indirect effects mediated by other genes (55,310). In this research, instead of inducing global epigenetic changes with epigenetic inhibitors, the CpG islands of the *MGAT4A*, *MGAT4B*, and *MGAT5* genes were directly targeted by DNMT3A-dCas9. This approach enabled the establishment of a more causal relationship between methylation of specific cytosine residues and gene expression changes, suggesting a regulatory role for DNA methylation in these glyco-genes and the corresponding glycan structures.

Although *ST6GAL1* was downregulated following targeted hypermethylation using DNMT3A-dCas9, this was the only gene in this research that showed no significant changes in the total cell *N*-glycome of HepG2 cells. Namely, ST6GAL1 catalyzes the transfer of sialic acid to galactose residues on *N*-glycans, forming α 2,6-linked sialic acid (185), yet no significant alteration in the abundance of sialic acid-bearing glycans was detected. A great body of research investigated the relationship between *ST6GAL1* expression and DNA methylation. Hypermethylation of the *ST6GAL1* gene is negatively correlated with the gene expression in breast cancer patients (249). Tumor-specific hypermethylation of *ST6GAL1* was also detected in bladder tumors and was inversely correlated with its expression. Treatment of bladder cancer cell lines with 5-Aza-dC resulted in the upregulation of *ST6GAL1* (251). Another study showed

that epigenetic manipulation of glioma cells using 5-Aza-dC led to the re-expression of *ST6GAL1* which was accompanied by increased expression of cell surface α 2,6 sialoglycoconjugate, enhanced α 2,6 sialylation of β 1 integrin, and reduced adhesion to the fibronectin substrate (250). These findings highlight the role of DNA methylation in the *ST6GAL1* gene regulation, with downstream effects on the glycan phenotype. In CHO cell line reactivation of *ST6GAL1* gene transcription was achieved by targeted demethylation with TET1-dCas9, and the gene was subsequently re-silenced by DNMT3A-dCas9, further demonstrating that cytosine methylation plays regulatory role for this gene (311). In my research, however, the downregulation of *ST6GAL1* caused by targeted hypermethylation did not impact the glycan phenotype, unlike the other targeted genes. This could be attributed to several factors. One possibility is that the transcriptional repression was not strong enough to decrease sialyltransferase activity. As observed in various studies, the efficacy of DNMT3A-mediated methylation is variable and depends on factors such as the targeted genomic region, chromatin context, and the specific cell line. This variability can lead to different levels of gene silencing (275–277). Additionally, ST6GAL1 is not the sole sialyltransferase responsible for adding sialic acid to glycans (185), so some other sialyltransferases may have compensated for the reduced *ST6GAL1* expression.

MGAT3 was the only gene in this study targeted with TET1-dCas9, a molecular tool designed for precise DNA demethylation. The relationship between *MGAT3* expression and DNA methylation has been suggested through correlation studies which used epigenetic inhibitors as well as through targeted methylation/demethylation approaches. In one of the first such studies, ovarian cancer and non-cancerous cell lines were treated with 5-Aza-C, leading to a significant increase in *MGAT3* expression in non-cancerous cell lines. The authors hypothesized that the *MGAT3* promoter hypomethylation is responsible for the presence of bisecting *N*-glycans in ovarian cancer cell lines, although they did not directly assess the methylation status or glycan phenotype following 5-Aza-C treatment (247). In another study, HepG2 cells were treated with two different concentrations of 5-Aza-dC which resulted in changes in expression in 18 out of 84 genes. Correlation analysis suggested *MGAT3* as the gene responsible for the observed glycan changes including highly branched glycans and core fucose-bearing glycans in HepG2 secretome (45). The modular CRISPR/dCas9 system used in my research has previously been employed for targeted methylation and demethylation of *MGAT3* in BG1 and HEK293 cell lines, respectively. Targeted *MGAT3* demethylation using TET1 did not increase its transcriptional activity in HEK293 cells (62). In contrast, in my

research, targeted hypomethylation of *MGAT3* in HepG2 cells led to significant gene upregulation on day 8 post-transfection, indicating that the effect of TET1 on *MGAT3* transcriptional activity could be cell specific. This variability in gene reactivation by TET1-dCas9 has also been observed in other studies (60,273,281,282). Conversely, targeted methylation of *MGAT3* using DNMT3A in BG1 cells resulted in its downregulation, leading to a significant decrease in structures with bisecting GlcNAc (62). Although in my research *MGAT3* upregulation was not followed by corresponding glycan change, i.e. increase of glycans with bisecting GlcNAc, a moderate change in quantity of other derived glycan traits was observed. These included a decrease in highly branched (HB) and tetragalactosylated (G4) structures and structures with antennary fucose (FA), as well as an increase in agalactosylated (G0) and asialylated (S0) structures. Given that highly branched structures are typically galactosylated and sialylated, the observed increase in agalactosylated and asialylated traits is consistent with the decrease in glycan branching. As previously explained, the addition of bisecting GlcNAc inhibits glycan branching (221). Since the HepG2 total *N*-glycome does not contain structures with bisecting GlcNAc, it is possible that the moderate *MGAT3* upregulation induced by TET1-dCas9 was insufficient to produce detectable amounts of these structures. Instead, an indirect effect of *MGAT3* upregulation was observed as a decrease in highly branched structures.

The results of my study demonstrate that CRISPR/dCas9 is an effective tool for studying the role of DNA methylation in the regulation of *N*-glycosylation. With the increasing number of EWAS studies and the identification of new regulators associated with *N*-glycosylation, this tool could be employed to functionally validate emerging EWAS hits. Indeed, dCas9 fused with KRAB or VPR transcriptional regulators has already proven to be an excellent tool for the functional validation of GWAS hits associated with IgG galactosylation (312). Given that several studies, including this one, have demonstrated the impact of DNA methylation on glyco-genes in cancer cell lines, the therapeutic potential of CRISPR/dCas9 should be considered. However, a major hurdle in using CRISPR/dCas9 for therapeutic purposes is the off-target effect and the difficulties with the delivery of the constructs *in vivo*. A challenge with dCas9 fusions is that off-target activity can arise not only from non-specific DNA binding but also from the unguided activity of the effector domains. This was demonstrated in a study where dCas9-DNMT3A fusion induced a global increase in CpG methylation even in the absence of guide RNAs (313). Performing whole-genome DNA methylation analysis to comprehensively assess off-target effects of DNMT3A-dCas9 and TET1-dCas9 exceeds the scope of this study.

Nevertheless, the off-target effects of dCas9 fusions based on the modular system used here have been previously analyzed using Illumina Infinium MethylationEPIC BeadChip arrays by Josipović et al. Their findings indicated that placing the DNMT3A-dCas9 and TET1-dCas9 cassette under the control of a weaker promoter (specifically EFS) reduced off-target activity without compromising on-target activity compared to the constructs with a strong promoter (CbH). However, this approach did not completely abolish the off-target effect (62). Since the same strategy was adopted in my research—placing dCas9 fusions under the control of the EFS promoter—I cannot exclude the possibility that DNMT3A-dCas9 and TET1-dCas9 exerted off-target activity at other genomic loci, potentially contributing to some of the observed changes in the HepG2 glycan phenotype. For most of the targeted glyco-genes, in addition to corresponding changes, alterations in other glycan traits were also observed, some of which are difficult to directly attribute to the targeted enzyme. For instance, in case of *MGAT4A* manipulation, even though gene downregulation was significant on day 12 post-transfection, the glycan changes were observed already on day 8. Furthermore, the observed alterations were contradictory—both agalactosylated and trigalactosylated as well as asialylated and trisialylated structures increased simultaneously. Also, downregulation of *FUT8* resulted in a significant increase in oligomannose glycans, whereas other studies have shown that *FUT8* silencing reduces oligomannosylated glycans (305,306). These discrepancies suggest that some of the observed glycan changes may result from non-specific activity of the DNMT3A-dCas9 fusion at other genomic regions.

The non-specific activity of dCas9 fusions also arises from the off-target binding of sgRNA molecules. The PAM-proximal region exhibits lower tolerance to mismatches, indicating the presence of a "seed region" in the sgRNA. Research has shown that Cas9 binding can tolerate up to 3-5 mismatches in the PAM-distal region (314). However, a study conducted by Kuscu et al. suggests that the total number of mismatches at dCas9 binding sites can reach as high as ten, with as many as nine consecutive mismatches in the PAM-distal region. The same study demonstrated that the number of off-target sites varies depending on the sgRNA used, ranging from 10 to over 1000. Moreover, off-target sites are enriched in open chromatin regions such as gene promoters, 5'-UTR regions, and exons, likely due to higher chromatin accessibility (315). Another factor to consider when using dCas9 fusions is that the binding of dCas9 alone or dCas9 fusions to regulatory regions can sterically hinder or otherwise interfere with the expression of genes under the control of those regions (56,57,266). To confirm that the effects on gene expression in my study were due to the introduced DNA methylation changes,

I employed an inactive control (IN) where candidate genes were targeted using dCas9 fused to inactive DNMT3A or TET1. For the *MGAT4B* and *MGAT5* genes, a significant decrease in expression was observed in the IN controls. However, samples targeted with active DNMT3A showed even stronger downregulation, indicating that in addition to steric interference, the imposed DNA methylation by DNMT3A-dCas9 further suppressed transcription of these genes. Interestingly, for certain candidate genes (*FUT8*, *MGAT4A*, *MGAT5* and *MGAT3*), significant changes in glycan traits were observed also in IN controls that were opposite to those observed in samples targeted with active DNMT3A or TET1. This suggests that these changes cannot be attributed solely to CRISPR interference at the candidate genes. Given the preference of dCas9 for binding to active genomic regions, it is plausible that the changes observed in the IN control resulted from off-target CRISPR interference at other regulatory elements affecting protein glycosylation. Additionally, the IN control for *B4GALT1* showed a significant increase in its expression 12 days post-transfection, further indicating potential off-target CRISPR interference in distal genomic regions that indirectly affect *B4GALT1* expression. Despite these off-target effects, my research clearly demonstrates that targeted introduction or removal of cytosine methylation at regulatory regions of glyco-genes influences their expression and leads to changes in the total cell *N*-glycome of HepG2 cells. These findings strongly suggest that some of glyco-genes and glycan traits are regulated epigenetically by DNA methylation.

Histone modifications represent a major epigenetic mechanism whose role in regulating protein glycosylation is severely understudied. Beyond the established neural-specific regulation of *MGAT5B* via histone acetylation, direct evidence linking histone modifications to the expression of glyco-genes remains limited (255,256). While studies using epigenetic inhibitors—such as HDAC inhibitors—have shown changes in *N*-glycosylation and expression of certain glyco-genes, they still lack direct correlation between a specific histone modification, glyco-gene expression and glycan structure (258–260). To address this gap, this dissertation employed CRISPR/dCas9-based epigenetic editing to target histone modifications at selected glyco-genes. The *FUT8* and *B4GALT1* genes showed the strongest response to targeted hypermethylation with DNMT3A-dCas9, which also led to changes in the gene activity and finally to changes in their corresponding glycans, i.e. core fucosylation and galactosylation, respectively. To investigate their epigenetic regulation in more detail, CRISPR/dCas9 tools were employed to manipulate specific histone modifications within these gene's promoter regions. Both *FUT8* and *B4GALT1* are active in HepG2 cell line, and accordingly, their

promoters are enriched in histone modifications associated with transcriptional activity, including H3K27ac and H3K4me3 marks.

To specifically remove H3K27ac from the *B4GALT1* and *FUT8* promoters full-length HDAC3 was designed and cloned to be compatible with the modular CRISPR/dCas9 fusion system. A study by Kwon et al. demonstrated that proper positioning of sgRNA is crucial for dCas9-HDAC3 optimal function. They observed that dCas9-HDAC3 exerts its repressor activity only when sgRNA is positioned at or near the tail of H3K27ac enrichment. Furthermore, they showed that dCas9-HDAC3 must be directed upstream of the TSS to avoid interference and ensure a catalytic-specific effect on transcription. While many studies have shown that the simultaneous expression of multiple sgRNAs can synergistically enhance the effects of dCas9 fusions, Kwon et al. reported that the use of multiple sgRNAs abrogated the effect observed with one sgRNA for targeting dCas9-HDAC3 (65). Considering these findings, for targeting *FUT8* and *B4GALT1* genes with HDAC3-dCas9 fusion, I used only one sgRNA designed to target a region upstream of their TSS and adjacent to H3K27ac enrichment. However, I did not observe a significant decrease in either *B4GALT1* or *FUT8* transcriptional activity. Instead, both active and inactive HDAC3-dCas9 led to a moderate but significant upregulation of *B4GALT1* on day 8 post-transfection. A similar effect was observed in the DNMT3A-dCas9 IN control, suggesting that off-target binding of HDAC3 fusions indirectly affected *B4GALT1* expression. Furthermore, unlike for DNMT3A-dCas9 fusions, in which only the catalytic domain was used, the HDAC3 constructs utilized the full-length protein, which also contains protein interaction domains that could contribute to this effect by interacting with factors influencing *B4GALT1*'s expression. For instance, targeting the *Mecp2* gene with dCas9-HDAC3 resulted in its upregulation in MC3T3-e1 pre-osteoblasts, while in transiently transfected N2a neuroblastoma cells, dCas9-HDAC3 downregulated *MecP2*, suggesting that the effect of HDAC3-dCas9 is cell-specific and dependent on the chromatin context (65). It has been shown that HDAC3 can be associated with transcriptional activation in certain scenarios, such as at the *Ucp1* locus, where its co-localization with estrogen-related receptor- α (ERR α) is necessary for *Ucp1* activation (316). In this work, NChIP analyses of H3K27ac levels revealed that HDAC3-dCas9 did not decrease H3K27ac levels in the analyzed region of *B4GALT1*, which could explain the absence of *B4GALT1* downregulation. For the *FUT8* promoter, a significant decrease in quantity of H3K27ac mark was observed while gene's transcriptional activity remained unchanged. Two out of three analyzed regions in *FUT8* promoter showed no significant changes in H3K27ac levels, however, these regions already exhibited low H3K27ac enrichment, making

further decrease potentially undetectable by the employed method. Notably, the region showing H3K27ac reduction was over 1000 bp from the sgRNA binding site, aligning with previous findings that dCas9-HDAC3 fusion can induce deacetylation across a 1-kb region from its binding position (65). On day 5 post-transfection, this decrease in H3K27ac level was also observed in the IN control, again indicating that full-length HDAC3 exerts some degree of function independently of its catalytic activity. In conclusion, HDAC3-dCas9 affected H3K27ac levels only in one analyzed region of one of two genes analyzed, with no repressive effect on gene transcriptional activity. Beyond forming a complex with NCoR and SMRT proteins, the catalytic activity of HDAC3 requires interaction with the deacetylase activating domain (DAD) of these proteins (317). Given that HDAC3 activity requires the presence of both NCoR and SMRT, the unchanged levels of H3K27ac in some promoter regions might be due to a lack of interaction between HDAC3-dCas9 and these cofactors. Investigating the extent of HDAC3-dCas9's interaction with NCoR/SMRT and optimizing these interactions may enhance its efficacy. Although it requires further optimization, HDAC3-dCas9 remains a promising molecular tool for exploring the role of histone deacetylation in gene regulation. Other histone deacetylases, such as HDAC8, have also been explored in dCas9 fusions and could provide alternative strategies for studying histone acetylation in glycosyltransferase gene regulation (286,318).

For removing trimethyl group from Lys4 in histone H3 (H3K4me3) from the *FUT8* and *B4GALT1* promoters, the RIOX1-dCas9 fusion was employed. This effector domain was not previously used with CRISPR/dCas9 system. RIOX1 was chosen due to its demonstrated ability to demethylate both H3K4me1 and H3K4me3, and to a lesser extent H3K4me2 (27). To cover a broader region enriched with H3K4me3, six and five sgRNAs were used to target RIOX1-dCas9 to the *B4GALT1* and *FUT8* promoters, respectively. However, there were no discernible effect on the transcriptional activity following epigenetic manipulation. CUT&RUN analyses revealed that H3K4me3 levels stayed unchanged in the analyzed regions. Although, an unexpected effect was observed for one region of the *FUT8* promoter. In cells targeted with active RIOX1, a significant decrease in H3K4me3 was detected on day 5, followed by a significant increase in H3K4me3 on day 8 post-transfection, but only when compared to the NT control. This suggests that RIOX1-dCas9 may exert some effect on histone modifications, although the mechanism remains unclear. Previous work within the research group demonstrated that using multiple sgRNAs to target H3K4me2-enriched and H3K4me3-enriched regions with LSD1-dCas9 and KDM5A-dCas9, respectively, successfully reduced

transcriptional activity of targeted genes (unpublished results). This rationale led me to adopt a similar multi-sgRNA strategy for RIOX1-dCas9 targeting. Although RIOX1 has not been widely used for targeted epigenome editing, results from studies involving other KDMs offer valuable insights. For instance, dCas9-LSD1 was used to target enhancers involved in *Oct4* regulation. Targeting a distal enhancer led to a loss of *Oct4* expression and phenotypic changes, while targeting the proximal promoter had no effect. Similarly, targeting the *Tbx3* enhancer (~10 kb upstream of the gene) reduced *Tbx3* mRNA levels and decreased H3K4me2 levels near the sgRNA binding site (287). Another histone lysine demethylase, KDM5A, was used with the dCas9-SunTag system to target the *SNCA* promoter. This approach reduced both H3K4me3 levels and α -synuclein expression in SH-SY5Y neuronal cells and dopaminergic neurons derived from Parkinson's disease patient iPSCs. Notably, in this study, one sgRNA located approximately 1 kb upstream of the *SNCA* gene's TSS was sufficient to induce these effects (319). The studies involving LSD1 and KDM5A highlight the importance of precise sgRNA positioning for successful effect on histone modification and gene regulation. Given their demonstrated efficacy in modifying H3K4 methylation, these KDMs may be more effective for investigating the epigenetic regulation of glyco-genes than RIOX1. However, before completely dismissing RIOX1, further optimization is warranted. While I used multiple sgRNAs in this study, employing one sgRNA at a strategically chosen position may yield better results, as shown with LSD1 and KDM5A. Additionally, since RIOX1 can also demethylate H3K36me3 (27), future experiments should examine how RIOX1-dCas9 affects this histone modification as well.

To explore potential regulatory role of H3K9me2 mark for *FUT8* and *B4GALT1* genes, the G9a-dCas9 fusion was targeted using multiple sgRNAs to their promoters. This approach was already confirmed within the research group, where this fusion successfully introduced H3K9me2 and reduced transcriptional activity of targeted genes (unpublished results). Some other studies have corroborated this approach, too. For example, simultaneous targeting of the *HER2* promoter with three different sgRNAs using G9a-dCas9 resulted in increased H3K9me3 levels and *HER2* downregulation. Interestingly, this study also demonstrated that G9a only affects transcriptional activity when fused to the N-terminal end of dCas9, and not the C-terminal end (63). The G9a-dCas9 construct used in my research had also G9a fused to N-terminus of the dCas9 protein. However, targeting it to the *FUT8* promoter did not result in either a change in quantity of H3K9me2 or gene transcription. In contrast, strong downregulation was detected on the 12th day post-transfection after targeting the *B4GALT1*

promoter with G9a. Although *B4GALT1* downregulation was also observed in the IN control, suggesting CRISPR interference, the reduction in mRNA levels was more pronounced in the active G9a samples, indicating some G9a activity. Notably, on the 8th day post-transfection, decrease in *B4GALT1* transcription was also significant but only compared to the NT control. These results suggest that G9a-dCas9 influenced the chromatin environment to a certain extent, which was observed in X-ChIP analyses as higher levels of H3K9me2, although this change was not significant. The trend of increased levels of H3K9me2 became significant on the 12th day post transfection when comparing active samples to IN control suggesting that observed gene downregulation cannot be solely attributed to CRISPR interference. Other studies have also shown that catalytic domains fused to dCas9 can repress gene expression without altering histone modification levels. For instance, O’Geen et al. demonstrated that SET domain of SUV HKMT induced gene repression without affecting H3K9me3 levels (63). It is also important to consider in my experiments that qPCR analysis, following immunoprecipitation with specific antibodies for histone modifications, typically examines only a small portion of the target region. This means that potential histone modifications beyond the qPCR amplicon may remain undetected. Since previous studies have shown that dCas9 fusions can influence histone modifications up to 1 kb from the target site, the ChIP-seq rather than ChIP-qPCR analysis could provide a more comprehensive picture of histone modification changes. Also, O’Geen et al. observed that the effects of dCas9 fusions on transcriptional repression are both locus- and cell-type-dependent. G9a-dCas9 targeting resulted in strong downregulation of the *HER2* gene and moderate downregulation of the *MYC* gene but did not affect the *EPCAM* gene expression in the HCT116 cell line, whereas in the HEK293T cell line, it produced a moderate effect on *HER2* gene expression and had no effect on *MYC* gene expression (63). The absence of an effect of G9a-dCas9 targeting on *FUT8* expression and the limited effect on H3K9me2 levels in *B4GALT1* could therefore be cell- and locus-specific, and perhaps other genes in HepG2 cells would be more responsive. An intriguing finding by See et al. revealed that the H3K9-targeted histone methyltransferase activity of G9a is sufficient to reposition the targeted locus to the nuclear periphery (320). It is tempting to investigate whether G9a-dCas9 exerts its effect on the *B4GALT1* gene transcription by its repositioning within the nucleus.

In this study, *MGAT3* was the only gene exhibiting low expression in the HepG2 cell line. Consequently, its promoter region displays low quantities of active histone marks H3K4me3 and H3K27ac. Since removing DNA methylation in this region moderately increased *MGAT3* transcriptional activity, I aimed to investigate whether introducing histone

modifications associated with active transcription would have a more pronounced effect on its expression. To this end, I targeted the *MGAT3* regulatory region using p300-dCas9 and PRDM9-dCas9. Targeting p300-dCas9 to the *MGAT3* promoter had no effect on its transcription, although the level of H3K27ac mark was increased on the 8th day post-transfection in region MGAT3_qChIP_3. Compared to other analyzed region which lacked H3K27ac increase, MGAT3_qChIP_3 is positioned more closely to sgRNA binding site. No effect on H3K27ac level in MGAT3_qChIP_2 region suggests that the activity of p300-dCas9 does not extend beyond 700 bp since this region is located approximately 713 bp away from the sgRNA binding site. Multiple studies have shown that p300-dCas9 is a robust tool for epigenome targeting, resulting in the upregulation of most candidate genes, whether proximal promoters or distal enhancers were targeted (66,283). However, a study by Wu et al. proposed that dCas9-p300 activity is dependent on the chromatin context, as it strongly activated endogenous gene expression in differentiated cell lines but had no effect on gene activation in pluripotent stem cell lines (321). It is possible that the chromatin environment of the *MGAT3* promoter region was not permissive for efficient editing by p300-dCas9. The CpG island of the *MGAT3* gene is highly methylated, which could contribute to its resistance to p300-mediated activation. CpG methylation inhibits the binding of transcription factors and other DNA-binding proteins and recruits MBD proteins, which in turn attract co-repressor complexes that promote chromatin condensation and transcriptional silencing (6,87). Thus, in the context of *MGAT3*, the addition of H3K27ac may be insufficient to overcome the repressive chromatin state. Timing may also be a crucial factor in capturing p300-mediated gene activation. In HepG2 cells, transient transfection with p300-dCas9 led to increased gene expression within 27-32 hours post-transfection, with expression levels returning to baseline after 48 hours (322). Due to the time required for antibiotic selection and cell recovery, the earliest point at which I could assess *MGAT3* expression was the 5th day post-transfection. An increase in *MGAT3* expression may have occurred earlier in the time-course but the effect was gone by the time when gene expression was analyzed. However, since H3K27ac enrichment was not observed on day 5 but became apparent on day 8 post-transfection, it is unlikely that the gene expression changes occurred significantly earlier. It was reported that p300-dCas9 exerts similar effectiveness with either one or multiple sgRNAs (66). Nevertheless, the possibility of enhanced effect on *MAGT3* transcriptional activity with increased number of sgRNAs should be considered. Despite the lack of effect on transcriptional activity, the successful introduction of H3K27ac by p300-dCas9 in the *MGAT3* promoter suggests that further optimization of sgRNA design and experimental

timing is needed before drawing definitive conclusions regarding the role of H3K27ac in the *MGAT3* gene regulation.

Targeting the *MGAT3* promoter with PRDM9-dCas9 resulted in a significant increase in its expression on day 8 post-transfection. However, this upregulation was not accompanied by an increase in H3K4me3 levels in the analyzed regions. While it is possible that the qPCR analysis, which covers only a limited portion of the targeted region, failed to capture H3K4me3 enrichment, other explanations should also be considered. One possibility is that PRDM9 interacts with additional effectors that enhance transcriptional activation regardless of H3K4me3 active mark. Nevertheless, since PRDM9's interactions with other proteins are largely mediated by KRAB domain (323), and only its catalytic domain was used in this study, it is mostly unlikely that the observed upregulation was due to such interactions. PRDM9-mediated H3K4me3 introduction plays a crucial role in meiotic recombination, with PRDM9 binding sites determining sites of recombination. In the absence of PRDM9, double-strand breaks are redirected to other H3K4me3-marked loci (323,324). Research has shown that PRDM9 binding and H3K4 trimethylation reorganize nucleosomes into a symmetrical pattern, creating an extended nucleosome-depleted region (325). Considering this fact, the increased *MGAT3* expression observed in this study may be attributed to nucleosome repositioning around the sgRNA binding site, making the region more accessible to transcriptional machinery. If such repositioning indeed occurred, the introduced H3K4me3 marks may have been relocated farther from the sgRNA binding sites, potentially beyond the regions analyzed by qPCR assays *MGAT3_qChIP_1* and *MGAT3_qChIP_2*. To fully understand the impact of PRDM9 on *MGAT3* expression, it would be necessary to analyze a broader chromatin region using ChIP-seq. Additionally, investigating nucleosome occupancy in the targeted region would provide further insights. A previous study utilizing dCas9-PRDM9 reported both upregulation of the target gene and an increase in quantity of H3K4me3 mark, which preferentially accumulated near the TSS (64). The analyzed regions in my study were located approximately 904 bp and 382 bp from TSS in the *MGAT3* promoter, suggesting that a closer region should also be analyzed. Furthermore, the same study demonstrated that combining H3K4me3 and H3K79me3 introduction by dCas9-PRDM9 and DOT1L, respectively, resulted in prolonged effect on gene reactivation. Moreover, the authors found that hypermethylated CpG islands strongly hinder dCas9 binding (64). Despite hypermethylation of the targeted region in the *MGAT3* promoter, an increase in its expression was still detected. It would be interesting to investigate whether combining targeted DNA demethylation by TET1 with PRDM9-mediated

H3K4me3 deposition would lead to a stronger upregulation of *MGAT3* and a higher increase in H3K4me3 levels. Although the results obtained in this study do not allow a direct attribution of H3K4me3 modifications to *MGAT3* transcriptional activity, PRDM9-dCas9 appears to be a promising molecular tool. With further optimization, it could be effectively used to study the epigenetic regulation of *MGAT3* and other genes involved in protein *N*-glycosylation. Across all experiments, none of the effector domains used were able to impose/remove histone modifications and change gene expression at the same time — either histone modification was introduced/removed without an effect on gene transcriptional activity or a gene changed transcription independently of histone modification change. Because of this, the *N*-glycan phenotype was not analyzed following these epigenetic interventions. Also, these results suggest that further experimental optimization is necessary for studying involvement of histone modifications in glyco-gene regulation.

Since the epigenetic engineering using histone modifiers fused to dCas9 led to either a change in quantity of corresponding histone mark or in a gene transcriptional activity, I aimed to investigate whether the same epigenetic manipulations influenced DNA methylation level at the targeted regions. Common knowledge is that there is a crosstalk between DNA methylation and histone modifications, but its existence and role depend on genomic region/gene loci as well as on chromatin environment (28,142). Many CRISPR/dCas9 studies exploring these interactions have either combined dCas9 fusions with epigenetic inhibitors or genes were targeted simultaneously with different epigenetic effectors. For instance, treating NIH3T3 cells with HDAC and HKMT inhibitors alongside targeted demethylation of *Oct4* by the dCas9-TET1 fusion resulted in significantly stronger gene reactivation compared to using dCas9-TET1 alone (326). Also, several studies suggest that combining different dCas9 fusions enhances effects on gene expression. For example, the simultaneous targeting of Ezh2-dCas9 and DNMT3A-dCas9 led to a long-term repression of *Her2* with an increase in H3K27me3 and DNA methylation levels, along with a reduction in H3K27ac quantity (327). Most studies examining whether changes in one chromatin modification influence another have focused on targeted DNA methylation/demethylation. Some studies have demonstrated that modifying DNA methylation can alter histone modifications at target sites. Targeted demethylation of the CGG expansion in the 5' UTR of the *FMRI* gene by dCas9-TET1 not only reactivated the gene but also shifted the upstream promoter from a heterochromatic to an active chromatin state, as evidenced by increased H3K4me3 and H3K27ac levels and decreased H3K9me3 level (60). A study conducted on CHO cells analyzed levels of histone modifications in the *FUT8* and

ST6GAL1 genes following targeted methylation or demethylation. Specifically, the targeted hypermethylation of *FUT8* with dCas9-DNMT3A3L led to a reduction in H3K27ac and H3K4me3 quantities, while H3K27me3 level increased. Conversely, hypomethylation of *ST6GAL1* with dCas9-TET1 resulted in increased H3K27ac and H3K4me3 levels, accompanied by a decrease in H3K9me3 level (308). In the present study, I analyzed DNA methylation following targeted deacetylation of the *FUT8* promoter region by HDAC3 and observed no changes in cytosine methylation levels, at least at the region covered by pyrosequencing assay spanning an 8 CpG sites. Furthermore, the increased H3K27ac level in *MGAT3* promoter using p300-dCas9 had no effect on cytosine methylation. It has been shown by others that *de novo* CpG methylation relies on the G9a resulting in silencing of specific genes and genomic elements (33,34,135). In this work, targeting the *B4GALT1* promoter with G9a-dCas9 downregulated its transcription but this effect was not accompanied with alterations in DNA methylation level at least in the region covered by B4GALT1-2 assay. The H3K4me3 mark has been shown to be inevitably associated with DNA methylation, and it has also appeared to be responsive to targeted DNA methylation/demethylation (60). Furthermore, it is well established that H3K4me3 inhibits *de novo* DNA methylation (142). To explore this relationship within the promoter of the candidate glyco-genes in this work, cytosine methylation levels were analyzed within the *MGAT3* promoter after PRDM9-dCas9 targeting, yet no alteration in cytosine methylation was observed despite the strong upregulation of *MGAT3*. Given that all dCas9 fusions with histone modifiers used in my work resulted only in moderate changes of the corresponding histone marks it is possible that the change was insufficient to elicit a detectable effect on DNA methylation. Further optimization and analyses of the broader gene regions are required to determine whether there is an interplay of specific histone marks and DNA methylation in the candidate glyco-genes.

In summary, results obtained within this doctoral dissertation demonstrate that selected glyco-genes, encoding for the main glycosyltransferases defining *N*-glycome of HepG2 cells, are sensitive to epigenetic engineering. Also, the effect of DNA methylation change on their expression has been significant enough to alter glycan phenotype what underscores the pivotal role of the epigenetic regulatory network in protein *N*-glycosylation. Although dCas9 fusions with histone modifiers did not produce conclusive or robust changes in glyco-gene expression, they exhibited a significant potential. With further optimization, these tools could be instrumental in advancing our understanding of the epigenetic regulation of protein glycosylation. Furthermore, the present study offers the DNMT3A-dSpCas9 and TET1-

dSaCas9 molecular tools for investigating the epigenetic regulation of other genes involved in the intricate process of protein *N*-glycosylation but also highlights their potential in therapeutic purposes. Targeted manipulation of DNA methylation could be useful in glycoengineering of therapeutic antibodies by transiently changing the expression of desired genes. While CRISPR/Cas9 technology has been employed to modify glycosylation pathways in mammalian cells to enhance the efficacy of therapeutic antibodies (328), studies utilizing dCas9 for these purposes remain scarce. The dCas9 fusions targeting epigenetic modifications could provide an alternative approach in cases where a complete knockout of glyco-genes is not ideal for improving antibody effectiveness.

6. CONCLUSIONS

- DNMT3A-dCas9 targeting to the CpG island of glyco-genes *B4GALT1*, *FUT8*, *ST6GAL1*, *MGAT4A*, *MGAT4B*, and *MGAT5* successfully increased DNA methylation level while TET1-dCas9 targeting to CpG island of *MGAT3* effectively decreased DNA methylation level.
- Promoter hypermethylation resulted in gene repression in all seven targeted glyco-genes, whereas targeted hypomethylation of the *MGAT3* promoter resulted in transcriptional reactivation. These findings indicate that targeted regions are regulated by cytosine methylation.
- CRISPR/dCas9 mediated downregulation of the candidate glyco-genes *via* targeted hypermethylation altered the HepG2 total cell *N*-glycome, except for *ST6GAL1* and *MGAT4A*, for which results were inconclusive. Downregulation of *B4GALT1*, *FUT8*, *MGAT4B* and *MGAT5* led to modifications in glycan structures directly associated with their enzymatic activities, i.e. galactosylation, core-fucosylation, and glycan branching, respectively. However, the downregulation of these genes also impacted other glycan traits, highlighting the complexity of the regulatory gene network involved in *N*-glycan biosynthesis. Upregulation of the *MGAT3* gene by hypomethylation resulted in significant changes in glycan branching, sialylation, galactosylation, and antennary fucosylation. Collectively, these results indicate that HepG2 total cell *N*-glycome is epigenetically regulated by DNA methylation.
- Epigenetic manipulation of promoter methylation in the *B4GALT1*, *FUT8* and *MGAT3* genes resulted in expression change on both mRNA and protein level.
- Catalytically active and inactive forms of full-length HDAC3 were successfully cloned and adapted for use within the CRISPR/dCas9 modular system for targeted epigenome editing.
- Targeting the proximal TSS region of the *B4GALT1* and *FUT8* genes with HDAC3-dCas9 significantly decreased H3K27ac quantity in *FUT8* but not in *B4GALT1* promoter region. Localized epigenetic change in the *FUT8* promoter region was not accompanied by change in gene expression suggesting that either this gene is not regulated by H3K27ac mark or that the decreased H3K27ac level achieved by HDAC3 was insufficient to trigger transcriptional repression

- The RIOX1-dCas9 fusion, designed to remove H3K4me3, did not reduce H3K4me3 quantity in the analyzed regions nor altered gene expression when targeted to H3K4me3-enriched regions of the *FUT8* and *B4GALT1* promoter. This tool requires further optimization to effectively remove H3K4me3 mark with hopeful effect on expression of target genes.
- Targeting the *FUT8* and *B4GALT1* promoter regions using G9a-dCas9 resulted in the downregulation of *B4GALT1*, but not *FUT8*. Concurrently, significant changes in H3K9me2 levels were not detected in either promoter. While attributing the observed transcriptional change in *B4GALT1* solely to G9a methyltransferase activity necessitates analysis of a broader targeted region, the G9a-dCas9 and HDAC3-dCas9 fusions stay promising tools in studies of epigenetic regulation of protein *N*-glycosylation.
- Targeting the *MGAT3* promoter with p300-dCas9 led to significant increase in quantity of H3K27ac mark without influencing *MGAT3* transcriptional activity. These results imply that either *MGAT3* is not regulated by H3K27ac, or that higher levels of histone acetylation are necessary to trigger its transcriptional reactivation.
- Targeting the proximal TSS region of the *MGAT3* gene using PRDM9-dCas9 significantly upregulated gene transcription but did not increase H3K4me3 level in its analyzed regions. Establishing a direct link between PRDM9's methyltransferase activity, the H3K4me3 levels and gene transcriptional activity necessitates the analysis of a broader region for H3K4me3 occupancy.
- Epigenetic manipulation by the HDAC3-dCas9, G9a-dCas9, p300-dCas9, or PRDM9-dCas9 fusions did not affect DNA methylation in the targeted regions of the *B4GALT1*, *FUT8*, and *MGAT3* genes, thus it was not possible to draw conclusions about interplay between DNA methylation and specific histone modifications.

Collectively, the results obtained in this doctoral dissertation provide strong evidence that DNA methylation has a regulatory role in glyco-gene expression and consequently in protein *N*-glycosylation. Furthermore, the findings from the experiments concerning epigenetic manipulation of histone modifications suggest that, with further optimization, dCas9-fusions with histone modifiers represent powerful molecular tools for further elucidating the epigenetic regulation of protein *N*-glycosylation.

7. REFERENCES

1. Kim JK, Samaranyake M, Pradhan S. Epigenetic mechanisms in mammals. *Cell Mol Life Sci.* 2009;66(4):596–612.
2. Tollervy JR, Lunyak VV. Judge, jury and executioner of stem cell fate. *Epigenetics.* 2012;7(8):823–40.
3. Li E, Zhang Y. DNA methylation in mammals. *Cold Spring Harb Perspect Biol.* 2014;6(5):a019133.
4. Larsen F, Gundersen G, Lopez R, Prydz H. CpG islands as gene markers in the human genome. *Genomics.* 1992;13(4):1095–107.
5. Stadler MB, Murr R, Burger L, Ivanek R, Lienert F, Schöler A, et al. DNA-binding factors shape the mouse methylome at distal regulatory regions. *Nature.* 2011;480(7378):490–5.
6. Greenberg MVC, Bourc'his D. The diverse roles of DNA methylation in mammalian development and disease. *Nat Rev Mol Cell Biol.* 2019;20(10):590–607.
7. Smith J, Sen S, Weeks RJ, Eccles MR, Chatterjee A. Promoter DNA hypermethylation and paradoxical gene activation. *Trends Cancer.* 2020;6(5):392–406.
8. Bestor TH, Edwards JR, Boulard M. Notes on the role of dynamic DNA methylation in mammalian development. *Proc Natl Acad Sci U S A.* 2015;112(22):6796–9.
9. Dhar GA, Saha S, Mitra P, Nag Chaudhuri R. DNA methylation and regulation of gene expression: Guardian of our health. *Nucleus.* 2021;64(3):259–270.
10. Okano M, Bell DW, Haber DA, Li E. DNA methyltransferases Dnmt3a and Dnmt3b are essential for de novo methylation and mammalian development. *Cell.* 1999;99(3):247–57.
11. Lyko F. The DNA methyltransferase family: A versatile toolkit for epigenetic regulation. *Nat Rev Genet.* 2018;19(2):81–92.
12. He YF, Li BZ, Li Z, Liu P, Wang Y, Tang Q, et al. Tet-mediated formation of 5-carboxylcytosine and its excision by TDG in mammalian DNA. *Science.* 2011;333(6047):1303–7.

13. Maiti A, Drohat AC. Thymine DNA glycosylase can rapidly excise 5-formylcytosine and 5-carboxylcytosine: Potential implications for active demethylation of CpG sites. *J Biol Chem*. 2011;286(41):35334–35338.
14. Michalak EM, Burr ML, Bannister AJ, Dawson MA. The roles of DNA, RNA and histone methylation in ageing and cancer. *Nat Rev Mol Cell Biol*. 2019;20(3):573–589.
15. Jung M, Pfeifer GP. Aging and DNA methylation. *BMC Biol*. 2015;13:7.
16. Zhao Z, Shilatifard A. Epigenetic modifications of histones in cancer. *Genome Biol*. 2019;20(1):245.
17. Zhao Y, Garcia BA. Comprehensive catalog of currently documented histone modifications. *Cold Spring Harb Perspect Biol*. 2015;7(9):a025065.
18. Marmorstein R, Zhou MM. Writers and readers of histone acetylation: Structure, mechanism, and inhibition. *Cold Spring Harb Perspect Biol*. 2014;6(7):a018762.
19. Sanaei M, Kavooosi F. Histone deacetylases and histone deacetylase inhibitors: Molecular mechanisms of action in various cancers. *Adv Biomed Res*. 2019;8:63.
20. Greer EL, Shi Y. Histone methylation: A dynamic mark in health, disease, and inheritance. *Nat Rev Genet*. 2012;13(5):343–57.
21. Padeken J, Methot SP, Gasser SM. Establishment of H3K9-methylated heterochromatin and its functions in tissue differentiation and maintenance. *Nat Rev Mol Cell Biol*. 2022;23(9):623–40.
22. Tachibana M, Sugimoto K, Nozaki M, Ueda J, Ohta T, Ohki M, et al. G9a histone methyltransferase plays a dominant role in euchromatic histone H3 lysine 9 methylation and is essential for early embryogenesis. *Genes Dev*. 2002;16(14):1779–81.
23. Kim TS, Buratowski S. Dimethylation of H3K4 by Set1 recruits the Set3 histone deacetylase complex to 5' transcribed regions. *Cell*. 2009;137(2):261–72.
24. Heintzman ND, Stuart RK, Hon G, Fu Y, Ching CW, Hawkins RD, et al. Distinct and predictive chromatin signatures of transcriptional promoters and enhancers in the human genome. *Nat Genet*. 2007;39(3):311–8.
25. Zhang Y, Sun Z, Jia J, Du T, Zhang N, Tang Y, et al. Overview of histone modification. In: *Advances in Experimental Medicine and Biology*. 2021;1267:1–20.

26. Baudat F, Buard J, Grey C, Fledel-Alon A, Ober C, Przeworski M, et al. PRDM9 is a major determinant of meiotic recombination hotspots in humans and mice. *Science*. 2010;327(5967):836–40.
27. Sinha KM, Yasuda H, Coombes MM, Dent SYR, De Crombrughe B. Regulation of the osteoblast-specific transcription factor Osterix by NO66, a Jumonji family histone demethylase. *EMBO J*. 2010;29(1):57–66.
28. Du J, Johnson LM, Jacobsen SE, Patel DJ. DNA methylation pathways and their crosstalk with histone methylation. *Nat Rev Mol Cell Biol*. 2015 Aug 21;16(9):519–32.
29. Otani J, Nankumo T, Arita K, Inamoto S, Ariyoshi M, Shirakawa M. Structural basis for recognition of H3K4 methylation status by the DNA methyltransferase 3A ATRX-DNMT3-DNMT3L domain. *EMBO Rep*. 2009;10(11):1243–9.
30. Guo X, Wang L, Li J, Ding Z, Xiao J, Yin X, et al. Structural insight into autoinhibition and histone H3-induced activation of DNMT3A. *Nature*. 2015;517(7536):640–4.
31. Epsztejn-Litman S, Feldman N, Abu-Remaileh M, Shufaro Y, Gerson A, Ueda J, et al. De novo DNA methylation promoted by G9a prevents reprogramming of embryonically silenced genes. *Nat Struct Mol Biol*. 2008;15(11):1176–83.
32. Meilinger D, Fellingner K, Bultmann S, Rothbauer U, Bonapace IM, Klinkert WEF, et al. Np95 interacts with de novo DNA methyltransferases, Dnmt3a and Dnmt3b, and mediates epigenetic silencing of the viral CMV promoter in embryonic stem cells. *EMBO Rep*. 2009;10(11):1273–9.
33. Xin Z, Tachibana M, Guggiari M, Heard E, Shinkai Y, Wagstaff J. Role of histone methyltransferase G9a in CpG methylation of the Prader-Willi syndrome imprinting center. *J Biol Chem*. 2003;278(17):14423–9.
34. Leung DC, Dong KB, Maksakova IA, Goyal P, Appanah R, Lee S, et al. Lysine methyltransferase G9a is required for de novo DNA methylation and the establishment, but not the maintenance, of proviral silencing. *Proc Natl Acad Sci USA*. 2011;108(14):5799–804.
35. Dong KB, Maksakova IA, Mohn F, Leung D, Appanah R, Lee S, et al. DNA methylation in ES cells requires the lysine methyltransferase G9a but not its catalytic activity. *EMBO J*. 2008;27(20):2927–39.

36. Estève PO, Hang GC, Smallwood A, Feehery GR, Gangisetty O, Karpf AR, et al. Direct interaction between DNMT1 and G9a coordinates DNA and histone methylation during replication. *Genes Dev.* 2006;20(22):3089-103.
37. Reily C, Stewart TJ, Renfrow MB, Novak J. Glycosylation in health and disease. *Nat Rev Nephrol.* 2019;15(6):346–66.
38. Pinho SS, Reis CA. Glycosylation in cancer: Mechanisms and clinical implications. *Nat Rev Cancer.* 2015;15(10):540–55.
39. Stowell SR, Ju T, Cummings RD. Protein glycosylation in cancer. *Annu Rev Pathol.* 2015; 10:473-510.
40. Lauc G, Vojta A, Zoldoš V. Epigenetic regulation of glycosylation is the quantum mechanics of biology. *Biochim Biophys Acta - Gen Subj.* 2014;1840(1):65–70.
41. Zoldoš V, Horvat T, Novokmet M, Cuenin C, Mužinić A, Pučić M, et al. Epigenetic silencing of HNF1A associates with changes in the composition of the human plasma N-glycome. *Epigenetics.* 2012;7(2):164–72.
42. Klasić M, Markulin D, Vojta A, Samaržija I, Biruš I, Dobrinić P, et al. Promoter methylation of the MGAT3 and BACH2 genes correlates with the composition of the immunoglobulin G glycome in inflammatory bowel disease. *Clin Epigenetics.* 2018;10:75.
43. Lauc G, Essafi A, Huffman JE, Hayward C, Knežević A, Kattla JJ, et al. Genomics meets glycomics—the first GWAS study of human N-glycome identifies HNF1A as a master regulator of plasma protein fucosylation. *PLoS Genet.* 2010;6(12):e1001256.
44. Vojta A, Samaržija I, Bočkor L, Zoldoš V. Glyco-genes change expression in cancer through aberrant methylation. *Biochim Biophys Acta Gen Subj.* 2016;1860(8):1776–85.
45. Klasić M, Krištić J, Korać P, Horvat T, Markulin D, Vojta A, et al. DNA hypomethylation upregulates expression of the MGAT3 gene in HepG2 cells and leads to changes in N-glycosylation of secreted glycoproteins. *Sci Rep.* 2016;6:24363.
46. Esmail S, Manolson MF. Advances in understanding N-glycosylation structure, function, and regulation in health and disease. *Eur J Cell Biol.* 2021 Sep 1;100(7–8):151–63.
47. Stanley P. Golgi glycosylation. *Cold Spring Harb Perspect Biol.* 2011;3(4):a005199.

48. Yan G, Li Y, Zhan L, Sun S, Yuan J, Wang T, et al. Decreased miR-124-3p promoted breast cancer proliferation and metastasis by targeting MGAT5. *Am J Cancer Res.* 2019;9(3):585–596.
49. Vaiana CA, Kurcon T, Mahal LK. MicroRNA-424 predicts a role for β -1,4 branched glycosylation in cell cycle progression. *J Biol Chem.* 2016;291(3):1529–37.
50. Tao Y, Zhao Z, Ma J, Dong L, Liang Y, Li S, et al. MiR-214-3p regulates the viability, invasion, migration, and EMT of TNBC cells by targeting ST6GAL1. *Cytotechnology.* 2019;71(6): 1155–1165.
51. Wang M, Wang J, Kong X, Chen H, Wang Y, Qin M, et al. MiR-198 represses tumor growth and metastasis in colorectal cancer by targeting fucosyl transferase 8. *Sci Rep.* 2014;1:4:6145.
52. Bernardi C, Soffientini U, Piacente F, Tonetti MG. Effects of microRNAs on fucosyltransferase 8 (FUT8) expression in hepatocarcinoma cells. *PLoS One.* 2013;8(10):e76540.
53. Poeta ML, Massi E, Parrella P, Pellegrini P, De Robertis M, Copetti M, et al. Aberrant promoter methylation of beta-1,4 galactosyltransferase 1 as potential cancer-specific biomarker of colorectal tumors. *Genes Chromosomes Cancer.* 2012;51(12): 1133-43.
54. Greville G, McCann A, Rudd PM, Saldova R. Epigenetic regulation of glycosylation and the impact on chemo-resistance in breast and ovarian cancer. *Epigenetics.* 2016; 11(12):845-857
55. Greville G, Llop E, Howard J, Madden SF, Perry AS, Peracaula R, et al. 5-AZA-dC induces epigenetic changes associated with modified glycosylation of secreted glycoproteins and increased EMT and migration in chemo-sensitive cancer cells. *Clin Epigenetics.* 2021;13(1):34.
56. Pulecio J, Verma N, Mejía-Ramírez E, Huangfu D, Raya A. CRISPR/Cas9-Based Engineering of the Epigenome. *Cell Stem Cell.* 2017;21(4):431–47.
57. Pickar-Oliver A, Gersbach CA. The next generation of CRISPR–Cas technologies and applications. *Nat Rev Mol Cell Biol.* 2019;20(8):490–507.

58. Qi LS, Larson MH, Gilbert LA, Doudna JA, Weissman JS, Arkin AP, et al. Repurposing CRISPR as an RNA-guided platform for sequence-specific control of gene expression. *Cell*. 2013;152(5):1173–83.
59. Goell JH, Hilton IB. CRISPR/Cas-based epigenome editing: Advances, applications, and clinical utility. *Trends Biotechnol*. 2021;39(7):678–91.
60. Liu XS, Wu H, Krzisch M, Wu X, Graef J, Muffat J, et al. Rescue of Fragile X Syndrome neurons by DNA methylation editing of the FMR1 gene. *Cell*. 2018;172(5):864–71.
61. Vojta A, Dobrinic P, Tadić V, Bockor L, Korac P, Julg B, et al. Repurposing the CRISPR-Cas9 system for targeted DNA methylation. *Nucleic Acids Res*. 2016;44(12):e116.
62. Josipović G, Tadić V, Klasić M, Zanki V, Bečeheli I, Chung F, et al. Antagonistic and synergistic epigenetic modulation using orthologous CRISPR/dCas9-based modular system. *Nucleic Acids Res*. 2019;47(18):9237–49.
63. O'Geen H, Ren C, Nicolet CM, Perez AA, Halmai J, Le VM, et al. dCas9-based epigenome editing suggests acquisition of histone methylation is not sufficient for target gene repression. *Nucleic Acids Res*. 2017;45(17):9826–39.
64. Cano-Rodriguez D, Gjaltema RAF, Jilderda LJ, Jellema P, Dokter-Fokkens J, Ruiters MHJ, et al. Writing of H3K4Me3 overcomes epigenetic silencing in a sustained but context-dependent manner. *Nat Commun*. 2016;7:11838.
65. Kwon DY, Zhao YT, Lamonica JM, Zhou Z. Locus-specific histone deacetylation using a synthetic CRISPR-Cas9-based HDAC. *Nat Commun*. 2017;8:15310.
66. Hilton IB, D'Ippolito AM, Vockley CM, Thakore PI, Crawford GE, Reddy TE, et al. Epigenome editing by a CRISPR-Cas9-based acetyltransferase activates genes from promoters and enhancers. *Nat Biotechnol*. 2015;33(5):510–7.
67. O'geen H, Tomkova M, Combs JA, Tilley EK, Segal DJ. Determinants of heritable gene silencing for KRAB-dCas9 + DNMT3 and Ezh2-dCas9 + DNMT3 hit-and-run epigenome editing. *Nucleic Acids Res*. 2022;50(6): 3239-3253.
68. Allis CD, Caparros ML, Jenuwein T, Reinberg D, editors. Epigenetics. 2nd ed. Cold Spring Harbor (NY): Cold Spring Harbor Laboratory Press; 2015.

69. Luger K, Dechassa ML, Tremethick DJ. New insights into nucleosome and chromatin structure: An ordered state or a disordered affair? *Nat Rev Mol Cell Biol.* 2012;13(7):436–47.
70. Hauer MH, Gasser SM. Chromatin and nucleosome dynamics in DNA damage and repair. *Genes Dev.* 2017;31(12):1151–61.
71. Allshire RC, Madhani HD. Ten principles of heterochromatin formation and function. *Nat Rev Mol Cell Biol.* 2018;19(4):229–44.
72. Bannister AJ, Kouzarides T. Regulation of chromatin by histone modifications. *Cell Res.* 2011;21(3):381–95.
73. Yadav T, Quivy JP, Almouzni G. Chromatin plasticity: A versatile landscape that underlies cell fate and identity. *Science.* 2018;361(6409):1332–1336.
74. Jambhekar A, Dhall A, Shi Y. Roles and regulation of histone methylation in animal development. *Nat Rev Mol Cell Biol.* 2019;20(10):625–41.
75. Avgustinova A, Benitah SA. Epigenetic control of adult stem cell function. *Nat Rev Mol Cell Biol.* 2016;17(10):643–58.
76. Kimmins S, Sassone-Corsi P. Chromatin remodelling and epigenetic features of germ cells. *Nature.* 2005;438(7068):1078–84.
77. Lee HJ, Hore TA, Reik W. Reprogramming the methylome: Erasing memory and creating diversity. *Cell Stem Cell.* 2014;14(6):710–9.
78. Kojima-Kita K, Kuramochi-Miyagawa S, Nagamori I, Ogonuki N, Ogura A, Hasuwa H, et al. MIWI2 as an effector of DNA methylation and gene silencing in embryonic male germ cells. *Cell Rep.* 2016;16(11):2819–28.
79. Klattenhoff C, Xi H, Li C, Lee S, Xu J, Khurana JS, et al. The Drosophila HP1 homolog Rhino is required for transposon silencing and piRNA production by dual-strand clusters. *Cell.* 2009;138(6):1137–49.
80. Sullivan LL, Maloney KA, Towers AJ, Gregory SG, Sullivan BA. Human centromere repositioning within euchromatin after partial chromosome deletion. *Chromosome Res.* 2016;24(4):451–66.

81. Nonaka N, Kitajima T, Yokobayashi S, Xiao G, Yamamoto M, Grewal SIS, et al. Recruitment of cohesin to heterochromatic regions by Swi6/HP1 in fission yeast. *Nat Cell Biol.* 2002;4(1):89–93.
82. Zhao J, Sun BK, Erwin JA, Song JJ, Lee JT. Polycomb proteins targeted by a short repeat RNA to the mouse X chromosome. *Science.* 2008;322(5902):750–3.
83. Xu Q, Xiang Y, Wang Q, Wang L, Brind'Amour J, Bogutz AB, et al. SETD2 regulates the maternal epigenome, genomic imprinting, and embryonic development. *Nat Genet.* 2019 May 1;51(5):844–56.
84. Kaneda M, Okano M, Hata K, Sado T, Tsujimoto H, Li E, et al. Essential role for de novo DNA methyltransferase Dnmt3a in paternal and maternal imprinting. *Nature.* 2004;429(6994):900–3.
85. Ziller MJ, Gu H, Müller F, Donaghey J, Tsai LTY, Kohlbacher O, et al. Charting a dynamic DNA methylation landscape of the human genome. *Nature.* 2013; 500 (7463):477–81.
86. Schultz MD, He Y, Whitaker JW, Hariharan M, Mukamel EA, Leung D, et al. Human body epigenome maps reveal noncanonical DNA methylation variation. *Nature.* 2015; 523(7559):212–6.
87. Watt F, Molloy PL. Cytosine methylation prevents binding to DNA of a HeLa cell transcription factor required for optimal expression of the adenovirus major late promoter. *Genes Dev.* 1988;2(9):1136–43.
88. Feng Q, Zhang Y. The MeCP1 complex represses transcription through preferential binding, remodeling, and deacetylating methylated nucleosomes. *Genes Dev.* 2001;15(7):829–43.
89. Tsuboi K, Nagatomo T, Gohn T, Higuchi T, Sasaki S, Fujiki N, et al. Single CpG site methylation controls estrogen receptor gene transcription and correlates with hormone therapy resistance. *J Steroid Biochem Mol Biol.* 2017;171:209–217.
90. Zou B, Chim CS, Zeng H, Leung SY, Yang Y, Tu SP, et al. Correlation between the single-site CpG methylation and expression silencing of the XAF1 gene in human gastric and colon cancers. *Gastroenterology.* 2006;131(6):1835–43.

91. Sproul D, Nestor C, Culley J, Dickson JH, Dixon JM, Harrison DJ, et al. Transcriptionally repressed genes become aberrantly methylated and distinguish tumors of different lineages in breast cancer. *Proc Natl Acad Sci U S A*. 2011;108(11):4364–9.
92. Guillaumet-Adkins A, Richter J, Odero MD, Sandoval J, Agirre X, Catala A, et al. Hypermethylation of the alternative AWT1 promoter in hematological malignancies is a highly specific marker for acute myeloid leukemias despite high expression levels. *J Hematol Oncol*. 2014;7:4.
93. Guilleret I, Yan P, Grange F, Braunschweig R, Bosman FT, Benhattar J. Hypermethylation of the human telomerase catalytic subunit (hTERT) gene correlates with telomerase activity. *Int J Cancer*. 2002;101(4):335–41.
94. Lee DD, Leão R, Komosa M, Gallo M, Zhang CH, Lipman T, et al. DNA hypermethylation within TERT promoter upregulates TERT expression in cancer. *J Clin Invest*. 2019;129(1):223–229.
95. Flavahan WA, Drier Y, Liao BB, Gillespie SM, Venteicher AS, Stemmer-Rachamimov AO, et al. Insulator dysfunction and oncogene activation in IDH mutant gliomas. *Nature*. 2016;529(7584):110–4.
96. Hon GC, Song CX, Du T, Jin F, Selvaraj S, Lee AY, et al. 5mC oxidation by Tet2 modulates enhancer activity and timing of transcriptome reprogramming during differentiation. *Mol Cell*. 2014;56(2):286–297.
97. Lee S, Park YS, Rhee JH, Chu H, Frost JM, Choi Y. Insights into plant regeneration: cellular pathways and DNA methylation dynamics. *Plant Cell Rep*. 2024;43(5):120.
98. Du Q, Luu PL, Stirzaker C, Clark SJ. Methyl-CpG-binding domain proteins: Readers of the epigenome. *Epigenomics*. 2015;7(6):1051–73.
99. Ooi SKT, Qiu C, Bernstein E, Li K, Jia D, Yang Z, et al. DNMT3L connects unmethylated lysine 4 of histone H3 to de novo methylation of DNA. *Nature*. 2007;448(7154):714–7.
100. Jia D, Jurkowska RZ, Zhang X, Jeltsch A, Cheng X. Structure of Dnmt3a bound to Dnmt3L suggests a model for de novo DNA methylation. *Nature*. 2007; 449 (7159): 248–51.

101. Lorsback RB, Moore J, Mathew S, Raimondi SC, Mukatira ST, Downing JR. TET1, a member of a novel protein family, is fused to MLL in acute myeloid leukemia containing the t(10;11)(q22;23). *Leukemia*. 2003; 17(3):637-41.
102. Ono R, Taki T, Taketani T, Taniwaki M, Kobayashi H, Hayashi Y. LCX, leukemia-associated protein with a CXXC domain, is fused to MLL in acute myeloid leukemia with trilineage dysplasia having t(10;11)(q22;q23). *Cancer Res*. 2002;62(14):4075–4080.
103. Ito S, Shen L, Dai Q, Wu SC, Collins LB, Swenberg JA, et al. Tet proteins can convert 5-methylcytosine to 5-formylcytosine and 5-carboxylcytosine. *Science*. 2011; 333 (6047):1300–3.
104. Ambrosi C, Manzo M, Baubec T. Dynamics and context-dependent roles of DNA methylation. *J Mol Biol*. 2017;429(10):1459–75.
105. Ko M, An J, Bandukwala HS, Chavez L, Äijö T, Pastor WA, et al. Modulation of TET2 expression and 5-methylcytosine oxidation by the CXXC domain protein IDAX. *Nature*. 2013;497(7447):122–6.
106. Deniz Ö, Frost JM, Branco MR. Regulation of transposable elements by DNA modifications. *Nat Rev Genet*. 2019;20(7):417–31.
107. Walsh CP, Chaillet JR, Bestor TH. Transcription of IAP endogenous retroviruses is constrained by cytosine methylation. *Nat Genet*. 1998;20(2):116–7.
108. Lock LF, Takagi N, Martin GR. Methylation of the Hprt gene on the inactive X occurs after chromosome inactivation. *Cell*. 1987;48(1):39–46.
109. Barlow DP, Bartolomei MS. Genomic imprinting in mammals. *Cold Spring Harb Perspect Biol*. 2014;6(2):a018382.
110. Monk D, Mackay DJG, Eggermann T, Maher ER, Riccio A. Genomic imprinting disorders: lessons on how genome, epigenome and environment interact. *Nat Rev Genet*. 2019;20(4):235–48.
111. Sanli I, Feil R. Chromatin mechanisms in the developmental control of imprinted gene expression. *Int J Biochem Cell Biol*. 2015;67:139–47.

112. Kim M, Costello J. DNA methylation: An epigenetic mark of cellular memory. *Exp Mol Med*. 2017; 49(4):e322.
113. Luo C, Hajkova P, Ecker JR. Dynamic DNA methylation: In the right place at the right time. *Science*. 2018; 361(6409):1336-1340.
114. Abdel-Wahab O, Mullally A, Hedvat C, Garcia-Manero G, Patel J, Wadleigh M, et al. Genetic characterization of TET1, TET2, and TET3 alterations in myeloid malignancies. *Blood*. 2009;114(1):144–7.
115. Shlush LI, Zandi S, Mitchell A, Chen WC, Brandwein JM, Gupta V, et al. Identification of pre-leukaemic haematopoietic stem cells in acute leukaemia. *Nature*. 2014;506(7488):328–33.
116. Zhao S, Allis CD, Wang GG. The language of chromatin modification in human cancers. *Nat Rev Cancer*. 2021;21(7):413–30.
117. Strahl BD, Allis CD. The language of covalent histone modifications. *Nature*. 2000;403(6765):41–5.
118. Wendong Ma, Xiaofan Ding, Jiajia Xu, Terence Chuen Wai Poon. CHHM: a Manually Curated Catalogue of Human Histone Modifications Revealing Hotspot Regions and Unique Distribution Patterns. *Int J Biol Sci*. 2024;20(10):3760–72.
119. Millán-Zambrano G, Burton A, Bannister AJ, Schneider R. Histone post-translational modifications—cause and consequence of genome function. *Nat Rev Genet*. 2022;23(9):563–80.
120. Josling GA, Selvarajah SA, Petter M, Duffy MF. The role of bromodomain proteins in regulating gene expression. *Genes (Basel)*. 2012;3(2):320–43.
121. Parbin S, Kar S, Shilpi A, Sengupta D, Deb M, Rath SK, et al. Histone deacetylases: A saga of perturbed acetylation homeostasis in cancer. *J Histochem Cytochem*. 2014;62(1):11–33.
122. Heintzman ND, Hon GC, Hawkins RD, Kheradpour P, Stark A, Harp LF, et al. Histone modifications at human enhancers reflect global cell-type-specific gene expression. *Nature*. 2009;459(7243):108–12.

123. Benton CB, Fiskus W, Bhalla KN. Targeting histone acetylation: readers and writers in leukemia and cancer. *Cancer J*. 2017;23(5):286–91.
124. Jin Q, Yu LR, Wang L, Zhang Z, Kasper LH, Lee JE, et al. Distinct roles of GCN5/PCAF-mediated H3K9ac and CBP/p300-mediated H3K18/27ac in nuclear receptor transactivation. *EMBO J*. 2011;30(2):249–62.
125. Lee CY, Grant PA. Role of histone acetylation and acetyltransferases in gene regulation. *BioEssays*. 1998; 20(8):615-26.
126. Lo WS, Trievel RC, Rojas JR, Duggan L, Hsu JY, Allis CD, et al. Phosphorylation of serine 10 in histone H3 is functionally linked in vitro and in vivo to Gcn5-mediated acetylation at lysine 14. *Mol Cell*. 2000;5(6):917–26.
127. Cheung P, Tanner KG, Cheung WL, Sassone-Corsi P, Denu JM, Allis CD. Synergistic coupling of histone H3 phosphorylation and acetylation in response to epidermal growth factor stimulation. *Mol Cell*. 2000;5(6):905–15.
128. Zippo A, Serafini R, Rocchigiani M, Pennacchini S, Krepelova A, Oliviero S. Histone crosstalk between H3S10ph and H4K16ac generates a histone code that mediates transcription elongation. *Cell*. 2009;138(6):1122–36.
129. Martire S, Gogate AA, Whitmill A, Tafessu A, Nguyen J, Teng YC, et al. Phosphorylation of histone H3.3 at serine 31 promotes p300 activity and enhancer acetylation. *Nat Genet*. 2019;51(7):941–946.
130. Rea S, Eisenhaber F, O’Carroll D, Strahl BD, Sun ZW, Schmid M, et al. Regulation of chromatin structure by site-specific histone H3 methyltransferases. *Nature*. 2000;406(6796):593–9.
131. Lachner M, O’Carroll D, Rea S, Mechtler K, Jenuwein T. Methylation of histone H3 lysine 9 creates a binding site for HP1 proteins. *Nature*. 2001;410(6824):116–20.
132. Bannister AJ, Zegerman P, Partridge JF, Miska EA, Thomas JO, Allshire RC, et al. Selective recognition of methylated lysine 9 on histone H3 by the HP1 chromo domain. *Nature*. 2001;410(6824):120–4.
133. Sampath SC, Marazzi I, Yap KL, Sampath SC, Krutchinsky AN, Mecklenbräuker I, et al. Methylation of a histone mimic within the histone methyltransferase G9a regulates protein complex assembly. *Mol Cell*. 2007;27(4):596–608.

134. Maksakova IA, Thompson PJ, Goyal P, Jones SJM, Singh PB, Karimi MM, et al. Distinct roles of KAP1, HP1 and G9a/GLP in silencing of the two-cell-specific retrotransposon MERVL in mouse ES cells. *Epigenetics Chromatin*. 2013;6(1):15.
135. Jiang Q, Ang JYJ, Lee AY, Cao Q, Li KY, Yip KY, et al. G9a plays distinct roles in maintaining DNA methylation, retrotransposon silencing, and chromatin looping. *Cell Rep*. 2020;33(4):108315.
136. Xiao Y, Li J, Liao X, He Y, He T, Yang C, et al. RIOX1-demethylated cGAS regulates ionizing radiation-elicited DNA repair. *Bone Res*. 2022;10(1):22.
137. Morgan MAJ, Shilatifard A. Reevaluating the roles of histone-modifying enzymes and their associated chromatin modifications in transcriptional regulation. *Nat Genet*. 2020;52(12):1271–81.
138. Plath K, Fang J, Mlynarczyk-Evans SK, Cao R, Worringer KA, Wang H, et al. Role of histone H3 lysine 27 methylation in X inactivation. *Science*. 2003;300(5616):131–5.
139. Inoue A, Jiang L, Lu F, Zhang Y. Genomic imprinting of Xist by maternal H3K27me3. *Genes Dev*. 2017;31(19):1927–32.
140. Inoue A, Jiang L, Lu F, Suzuki T, Zhang Y. Maternal H3K27me3 controls DNA methylation-independent imprinting. *Nature*. 2017;547(7664):419–24.
141. Piunti A, Shilatifard A. Epigenetic balance of gene expression by polycomb and compass families. *Science*. 2016;352(6290):aad9780.
142. Li Y, Chen X, Lu C. The interplay between DNA and histone methylation: molecular mechanisms and disease implications. *EMBO Rep*. 2021;22(5):e51803.
143. Meissner A, Mikkelsen TS, Gu H, Wernig M, Hanna J, Sivachenko A, et al. Genome-scale DNA methylation maps of pluripotent and differentiated cells. *Nature*. 2008;454(7205):766–70.
144. Zhang Y, Jurkowska R, Soeroes S, Rajavelu A, Dhayalan A, Bock I, et al. Chromatin methylation activity of Dnmt3a and Dnmt3a/3L is guided by interaction of the ADD domain with the histone H3 tail. *Nucleic Acids Res*. 2010;38(13):4246–53.

145. Ciccone DN, Su H, Hevi S, Gay F, Lei H, Bajko J, et al. KDM1B is a histone H3K4 demethylase required to establish maternal genomic imprints. *Nature*. 2009;461(7262):415–8.
146. Stewart KR, Veselovska L, Kim J, Huang J, Saadeh H, Tomizawa SI, et al. Dynamic changes in histone modifications precede de novo DNA methylation in oocytes. *Genes Dev*. 2015;29(23):2449–62.
147. Vlachogiannis G, Niederhuth CE, Tuna S, Stathopoulou A, Viiri K, de Rooij DG, et al. The Dnmt3L ADD Domain Controls Cytosine Methylation Establishment during Spermatogenesis. *Cell Rep*. 2015;10(6): 944-956.
148. Noh KM, Wang H, Kim HR, Wenderski W, Fang F, Li CH, et al. Engineering of a Histone-Recognition Domain in Dnmt3a Alters the Epigenetic Landscape and Phenotypic Features of Mouse ESCs. *Mol Cell*. 2015;59(1): 89-103.
149. Fu K, Bonora G, Pellegrini M. Interactions between core histone marks and DNA methyltransferases predict DNA methylation patterns observed in human cells and tissues. *Epigenetics*. 2020;15(3): 272-282.
150. Baubec T, Colombo DF, Wirbelauer C, Schmidt J, Burger L, Krebs AR, et al. Genomic profiling of DNA methyltransferases reveals a role for DNMT3B in genic methylation. *Nature*. 2015;520(7546) :243-7.
151. Dhayalan A, Rajavelu A, Rathert P, Tamas R, Jurkowska RZ, Ragozin S, et al. The Dnmt3a PWWP domain reads histone 3 lysine 36 trimethylation and guides DNA methylation. *J Biol Chem*. 2010;285(34): 26114-20.
152. Morselli M, Pastor WA, Montanini B, Nee K, Ferrari R, Fu K, et al. In vivo targeting of de novo DNA methylation by histone modifications in yeast and mouse. *Elife*. 2015;4: e06205.
153. Weinberg DN, Papillon-Cavanagh S, Chen H, Yue Y, Chen X, Rajagopalan KN, et al. The histone mark H3K36me2 recruits DNMT3A and shapes the intergenic DNA methylation landscape. *Nature*. 2019;573(7773): 281-286.
154. Fuks F, Hurd PJ, Deplus R, Kouzarides T. The DNA methyltransferases associate with HP1 and the SUV39H1 histone methyltransferase. *Nucleic Acids Res*. 2003;31(9):2305-12.

155. Lehnertz B, Ueda Y, Derijck AAHA, Braunschweig U, Perez-Burgos L, Kubicek S, et al. Suv39h-mediated histone H3 lysine 9 methylation directs DNA methylation to major satellite repeats at pericentric heterochromatin. *Curr Biol.* 2003;13(14):1192-200.
156. Leung D, Du T, Wagner U, Xie W, Lee AY, Goyal P, et al. Regulation of DNA methylation turnover at LTR retrotransposons and imprinted loci by the histone methyltransferase Setdb1. *Proc Natl Acad Sci U S A.* 2014;111(18):6690-5.
157. Auclair G, Borgel J, Sanz LA, Vallet J, Guibert S, Dumas M, et al. EHMT2 directs DNA methylation for efficient gene silencing in mouse embryos. *Genome Res.* 2016;26(2) :92-202.
158. Chang Y, Sun L, Kokura K, Horton JR, Fukuda M, Espejo A, et al. MPP8 mediates the interactions between DNA methyltransferase Dnmt3a and H3K9 methyltransferase GLP/G9a. *Nat Commun.* 2011;2:533.
159. Li T, Wang L, Du Y, Xie S, Yang X, Lian F, et al. Structural and mechanistic insights into UHRF1-mediated DNMT1 activation in the maintenance DNA methylation. *Nucleic Acids Res.* 2018;46(6):3218-3231.
160. Ishiyama S, Nishiyama A, Saeki Y, Moritsugu K, Morimoto D, Yamaguchi L, et al. Structure of the Dnmt1 Reader Module Complexed with a Unique Two-Mono-Ubiquitin Mark on Histone H3 Reveals the Basis for DNA Methylation Maintenance. *Mol Cell.* 2017;68(2):350-360.
161. Rajakumara E, Wang Z, Ma H, Hu L, Chen H, Lin Y, et al. PHD Finger Recognition of Unmodified Histone H3R2 Links UHRF1 to Regulation of Euchromatic Gene Expression. *Mol Cell.* 2011;43(2):275-284.
162. Rottach A, Frauer C, Pichler G, Bonapace IM, Spada F, Leonhardt H. The multi-domain protein Np95 connects DNA methylation and histone modification. *Nucleic Acids Res.* 2009;38(6):1796-804.
163. Ren W, Fan H, Grimm SA, Guo Y, Kim JJ, Yin J, et al. Direct readout of heterochromatic H3K9me3 regulates DNMT1-mediated maintenance DNA methylation. *Proc Natl Acad Sci U S A.* 2020;117(31):18439-18447.

164. Ming X, Zhang Z, Zou Z, Lv C, Dong Q, He Q, et al. Kinetics and mechanisms of mitotic inheritance of DNA methylation and their roles in aging-associated methylome deterioration. *Cell Res.* 2020;30(11):980-996.
165. Lauc G, Pezer M, Rudan I, Campbell H. Mechanisms of disease: The human N-glycome. *Biochim Biophys Acta Gen Subj.* 2016;1860(8):1574–82.
166. Lee HS, Qi Y, Im W. Effects of N-glycosylation on protein conformation and dynamics: Protein Data Bank analysis and molecular dynamics simulation study. *Sci Rep.* 2015;5:8926.
167. Esmail S, Yao Y, Kartner N, Li J, Reithmeier RAF, Manolson MF. N-Linked Glycosylation Is Required for Vacuolar H⁺-ATPase (V-ATPase) α 4 Subunit Stability, Assembly, and Cell Surface Expression. *J Cell Biochem.* 2016;117(10):2757-2768.
168. Xu C, Ng DTW. Glycosylation-directed quality control of protein folding. *Nat Rev Mol Cell Biol.* 2015;16(12):742–752.
169. Kobayashi K, Morishita A, Iwama H, Fujita K, Okura R, Fujihara S, et al. Galectin-9 suppresses cholangiocarcinoma cell proliferation by inducing apoptosis but not cell cycle arrest. *Oncol Rep.* 2015;34(4):1761–1770.
170. Maverakis E, Kim K, Shimoda M, Gershwin ME, Patel F, Wilken R, et al. Glycans in the immune system and The Altered Glycan Theory of Autoimmunity: A critical review. *J Autoimmun.* 2015;57:1–13.
171. Zhou JY, Oswald DM, Oliva KD, Kreisman LSC, Cobb BA. The Glycoscience of Immunity. *Trends Immunol.* 2018;39(7):523–535.
172. Ahmed AA, Giddens J, Pincetic A, Lomino JV, Ravetch JV, Wang LX, et al. Structural characterization of anti-inflammatory immunoglobulin G Fc proteins. *J Mol Biol.* 2014;426(18):3166–3179.
173. Dekkers G, Treffers L, Plomp R, Bentlage AEH, de Boer M, Koeleman CAM, et al. Decoding the human immunoglobulin G-glycan repertoire reveals a spectrum of Fc-receptor- and complement-mediated-effector activities. *Front Immunol.* 2017;8:877.
174. Anumula KR. Quantitative glycan profiling of normal human plasma derived immunoglobulin and its fragments Fab and Fc. *J Immunol Methods.* 2012;382(1–2):167–176.

175. Shkunnikova S, Mijakovac A, Sironic L, Hanic M, Lauc G, Kavur MM. IgG glycans in health and disease: Prediction, intervention, prognosis, and therapy. *Biotechnol Adv.* 2023;67: 108169.
176. Wu Y, Zhang Z, Chen L, Sun S. Immunoglobulin G glycosylation and its alterations in aging-related diseases. *Acta Biochim Biophys Sin (Shanghai).* 2024; 56(8):1221-1233.
177. Biermann MHC, Griffante G, Podolska MJ, Boeltz S, Stürmer J, Muñoz LE, et al. Sweet but dangerous - The role of immunoglobulin G glycosylation in autoimmunity and inflammation. *Lupus.* 2016;25(8):934-42.
178. Taniguchi N, Kizuka Y. Glycans and cancer: Role of N-Glycans in cancer biomarker, progression and metastasis, and therapeutics. *Adv Cancer Res.* 2015;126:11–51.
179. Pinho SS, Reis CA. Glycosylation in cancer: Mechanisms and clinical implications. *Nat Rev Cancer.* 2015;15(9):540–555.
180. Meany DL, Chan DW. Aberrant glycosylation associated with enzymes as cancer biomarkers. *Clin Proteomics.* 2011;8(1):7.
181. Andergassen U, Liesche F, Kölbl AC, Ilmer M, Hutter S, Friese K, et al. Glycosyltransferases as Markers for Early Tumorigenesis. *Biomed Res Int.* 2015;2015:792672.
182. Nagae M, Yamaguchi Y. Function and 3D structure of the N-glycans on glycoproteins. *Int J Mol Sci.* 2012;13(7):8398–8429.
183. Ohtsubo K, Taniguchi N. Mannosyl (alpha-1,3-)-glycoprotein beta-1,4-N-acetylglucosaminyltransferase, isozyme A, B (MGAT4A, B). *Handb Glycosyltransferases Relat Genes.* 2014;1–12.
184. Harrus D, Khoder-Agha F, Peltoniemi M, Hassinen A, Ruddock L, Kellokumpu S, et al. The dimeric structure of wild-type human glycosyltransferase B4GalT1. *PLoS One.* 2018;13(10):e0204864.
185. Kuhn B, Benz J, Greif M, Engel AM, Sobek H, Rudolph MG. The structure of human α -2,6-sialyltransferase reveals the binding mode of complex glycans. *Acta Crystallogr D Biol Crystallogr.* 2013;69(Pt 9):1826–1838.

186. Nagae M, Yamaguchi Y, Taniguchi N, Kizuka Y. 3D structure and function of glycosyltransferases involved in N-glycan maturation. *Int J Mol Sci.* 2020;21(2):437.
187. Krištić J, Sharapov SZ, Aulchenko YS. Quantitative Genetics of Human Protein N-Glycosylation. *Adv Exp Med Biol.* 2021;1325: 151-171.
188. Yamaguchi Y, Fujii J, Inoue S, Uozumi N, Yanagidani S, Ikeda Y, et al. Mapping of the α -1,6-fucosyltransferase gene, FUT8, to human chromosome 14q24.3. *Cytogenet Cell Genet.* 1999;84(1–2):58-60.
189. García-García A, Ceballos-Laita L, Serna S, Artschwager R, Reichardt NC, Corzana F, et al. Structural basis for substrate specificity and catalysis of α 1,6-fucosyltransferase. *Nat Commun.* 2020;11(1):973.
190. Yang Q, Wang LX. Mammalian α -1,6-fucosyltransferase (FUT8) is the sole enzyme responsible for the N-acetylglucosaminyltransferase I-independent core fucosylation of high-mannose N-glycans. *J Biol Chem.* 2016;291(21):11064-71.
191. Fujii H, Shinzaki S, Iijima H, Wakamatsu K, Iwamoto C, Sobajima T, et al. Core fucosylation on T cells, required for activation of T-cell receptor signaling and induction of colitis in mice, is increased in patients with inflammatory bowel disease. *Gastroenterology.* 2016;150(7):1620-1632.
192. Fukuda T, Hashimoto H, Okayasu N, Kameyama A, Onogi H, Nakagawasai O, et al. α 1,6-fucosyltransferase-deficient mice exhibit multiple behavioral abnormalities associated with a schizophrenia-like phenotype: Importance of the balance between the dopamine and serotonin systems. *J Biol Chem.* 2011;286(21):18434-43.
193. Wang X, Inoue S, Gu J, Miyoshi E, Noda K, Li W, et al. Dysregulation of TGF- β 1 receptor activation leads to abnormal lung development and emphysema-like phenotype in core fucose-deficient mice. *Proc Natl Acad Sci U S A.* 2005;102(44): 15791-6.
194. Bastian K, Scott E, Elliott DJ, Munkley J. Fut8 alpha-(1,6)-fucosyltransferase in cancer. *Int J Mol Sci.* 2021;22(1):455.
195. Osumi D, Takahashi M, Miyoshi E, Yokoe S, Lee SH, Noda K, et al. Core fucosylation of E-cadherin enhances cell-cell adhesion in human colon carcinoma WiDr cells. *Cancer Sci.* 2009;100(5):888-95.

196. Zhao Y, Itoh S, Wang X, Isaji T, Miyoshi E, Kariya Y, et al. Deletion of core fucosylation on $\alpha 3\beta 1$ integrin down-regulates its functions. *J Biol Chem*. 2006;281(50):38343-50.
197. Tu CF, Wu MY, Lin YC, Kannagi R, Yang RB. FUT8 promotes breast cancer cell invasiveness by remodeling TGF- β receptor core fucosylation. *Breast Cancer Res*. 2017;19(1):111.
198. Wang X, Gu J, Ihara H, Miyoshi E, Honke K, Taniguchi N. Core fucosylation regulates epidermal growth factor receptor-mediated intracellular signaling. *J Biol Chem*. 2006;281(5):2572-7.
199. Chen CY, Jan YH, Juan YH, Yang CJ, Huang MS, Yu CJ, et al. Fucosyltransferase 8 as a functional regulator of nonsmall cell lung cancer. *Proc Natl Acad Sci U S A*. 2013;110(2):630-5.
200. Lin H, Wang D, Wu T, Dong C, Shen N, Sun Y, et al. Blocking core fucosylation of TGF- $\beta 1$ receptors downregulates their functions and attenuates the epithelial-mesenchymal transition of renal tubular cells. *Am J Physiol Renal Physiol*. 2011;300(4):F1017-25.
201. Shinkawa T, Nakamura K, Yamane N, Shoji-Hosaka E, Kanda Y, Sakurada M, et al. The absence of fucose but not the presence of galactose or bisecting N-acetylglucosamine of human IgG1 complex-type oligosaccharides shows the critical role of enhancing antibody-dependent cellular cytotoxicity. *J Biol Chem*. 2003;278(5): 3466-73.
202. Lee JH, Sundaram S, Shaper NL, Raju TS, Stanley P. Chinese hamster ovary (CHO) cells may express six β 4-galactosyltransferases ($\beta 4$ GalTs). Consequences of the loss of functional $\beta 4$ GalT-1, $\beta 4$ GalT-6, or both in CHO glycosylation mutants. *J Biol Chem*. 2001;276(17):13924-34.
203. Bydlinski N, Maresch D, Schmieder V, Klanert G, Strasser R, Borth N. The contributions of individual galactosyltransferases to protein specific N-glycan processing in Chinese Hamster Ovary cells. *J Biotechnol*. 2018;282:101–10.
204. Ramakrishnan B, Ramasamy V, Qasba PK. Structural snapshots of β -1,4-galactosyltransferase-1 along the kinetic pathway. *J Mol Biol*. 2006;357(5):1619-33.
205. Ramakrishnan B, Boeggeman E, Ramasamy V, Qasba PK. Structure and catalytic cycle of β -1,4-galactosyltransferase. *Curr Opin Struct Biol*. 2004;14(5):593-600.

206. Forrest ARR, Kawaji H, Rehli M, Baillie JK, De Hoon MJL, Haberle V, et al. A promoter-level mammalian expression atlas. *Nature*. 2014;507(7493):462-70.
207. Al-Obaide MAI, Alobydi H, Abdelsalam AG, Zhang R, Srivenugopal KS. Multifaceted roles of 5'-regulatory region of the cancer associated gene B4GALT1 and its comparison with the gene family. *Int J Oncol*. 2015;47(4):1393-404.
208. Ren Z, Huang X, Lv Q, Lei Y, Shi H, Wang F, et al. High expression of B4GALT1 is associated with poor prognosis in acute myeloid leukemia. *Front Genet*. 2022;13:882004.
209. Tang W, Weng S, Zhang S, Wu W, Dong L, Shen X, et al. Direct interaction between surface β 1,4-galactosyltransferase 1 and epidermal growth factor receptor (EGFR) inhibits EGFR activation in hepatocellular carcinoma. *Biochem Biophys Res Commun*. 2013;434(3):449-54.
210. Choi HJ, Chung TW, Kim CH, Jeong HS, Joo M, Youn BH, et al. Estrogen induced β -1,4-galactosyltransferase 1 expression regulates proliferation of human breast cancer MCF-7 cells. *Biochem Biophys Res Commun*. 2012;426(4):620-5.
211. Wang P, Li X, Xie Y. B4GalT1 regulates apoptosis and autophagy of glioblastoma in vitro and in vivo. *Technol Cancer Res Treat*. 2020;19:1533033820980104.
212. Khoder-Agha F, Harrus D, Brysbaert G, Lensink MF, Harduin-Lepers A, Glumoff T, et al. Assembly of B4GALT1/ST6GAL1 heteromers in the Golgi membranes involves lateral interactions via highly charged surface domains. *J Biol Chem*. 2019 Sep 27;294(39):14383-14393.
213. Dorsett KA, Marciel MP, Hwang J, Ankenbauer KE, Bhalerao N, Bellis SL. Regulation of ST6GAL1 sialyltransferase expression in cancer cells. *Glycobiology*. 2021;31(5):530-9.
214. Xu L, Kurusu Y, Takizawa K, Tanaka J, Matsumoto K, Taniguchi A. Transcriptional regulation of human β -galactoside α 2,6-sialyltransferase (hST6Gal I) gene in colon adenocarcinoma cell line. *Biochem Biophys Res Commun*. 2003;307(4):1070-4.
215. Dall'Olio F, Chiricolo M, D'Errico A, Gruppioni E, Altimari A, Fiorentino M, et al. Expression of β -galactoside α 2,6 sialyltransferase and of α 2,6-sialylated glycoconjugates

- in normal human liver, hepatocarcinoma, and cirrhosis. *Glycobiology*. 2004;14(1): 39-49.
216. Lu J, Gu J. Significance of β -galactoside α 2,6 sialyltransferase 1 in cancers. *Molecules*. 2015;20(5):7509–7527.
 217. de-Souza-Ferreira M, Ferreira ÉE, de-Freitas-Junior JCM. Aberrant N-glycosylation in cancer: MGAT5 and β 1,6-GlcNAc branched N-glycans as critical regulators of tumor development and progression. *Cell Oncol*. 2023;46(3):481–501.
 218. Kizuka Y, Taniguchi N. Enzymes for N-Glycan branching and their genetic and nongenetic regulation in cancer. *Biomolecules*. 2016;6(2):25.
 219. Chen L, Zhang W, Fregien N, Pierce M. The her-2/neu oncogene stimulates the transcription of N-acetylglucosaminyltransferase V and expression of its cell surface oligosaccharide products. *Oncogene*. 1998;17(16):2087–93.
 220. Nishikawa A, Ihara Y, Hatakeyama M, Kangawa K, Taniguchi N. Purification, cDNA cloning, and expression of UDP-N-acetylglucosamine: β -D-mannoside β -1,4-N-acetylglucosaminyltransferase III from rat kidney. *Journal of Biological Chemistry*. 1992;267(25):18199–204.
 221. Nakano M, Mishra SK, Tokoro Y, Sato K, Nakajima K, Yamaguchi Y, et al. Bisecting GlcNAc is a general suppressor of terminal modification of N-glycan. *Molecular and Cellular Proteomics*. 2019;18(10):2044–2057.
 222. Schedin-Weiss S, Gaunitz S, Sui P, Chen Q, Haslam SM, Blennow K, et al. Glycan biomarkers for Alzheimer disease correlate with T-tau and P-tau in cerebrospinal fluid in subjective cognitive impairment. *FEBS Journal*. 2020;287(15):3221–3234.
 223. Yoshimura M, Ihara Y, Nishiura T, Okajima Y, Ogawa M, Yoshida H, et al. Bisecting GlcNAc structure is implicated in suppression of stroma-dependent haemopoiesis in transgenic mice expressing N-acetylglucosaminyltransferase III. *Biochemical Journal*. 1998;331(3):733–42.
 224. Takamatsu S, Katsumata T, Inoue N, Watanabe T, Fujibayashi Y, Takeuchi M. Abnormal biantennary sugar chains are expressed in human chorionic gonadotropin produced in the choriocarcinoma cell line, JEG-3. *Glycoconjugate Journal*. 2003;20(7–8):473–81.

225. Chen Q, Tan Z, Guan F, Ren Y. The essential functions and detection of bisecting GlcNAc in cell biology. *Frontiers in Chemistry*. 2020;8:511.
226. Iijima J, Zhao Y, Isaji T, Kameyama A, Nakaya S, Wang X, et al. Cell-cell interaction-dependent regulation of N-acetylglucosaminyltransferase III and the bisected N-glycans in GE11 epithelial cells: involvement of E-cadherin-mediated cell adhesion. *Journal of Biological Chemistry*. 2006;281(19):13038–13046.
227. Yoshimura M, Ihara Y, Matsuzawa Y, Taniguchi N. Aberrant glycosylation of E-cadherin enhances cell-cell binding to suppress metastasis. *Journal of Biological Chemistry*. 1996;271(23):13811–5.
228. Li S, Mo C, Peng Q, Kang X, Sun C, Jiang K, et al. Cell surface glycan alterations in epithelial mesenchymal transition process of Huh7 hepatocellular carcinoma cell. *PLoS One*. 2013;8(8):e71273.
229. Osada N, Nagae M, Nakano M, Hirata T, Kizuka Y. Examination of differential glycoprotein preferences of N-acetylglucosaminyltransferase-IV isozymes a and b. *Journal of Biological Chemistry*. 2022;298(9):102400.
230. Takamatsu S, Antonopoulos A, Ohtsubo K, Ditto D, Chiba Y, Le DT, et al. Physiological and glycomic characterization of N-acetylglucosaminyltransferase-IVa and -IVb double deficient mice. *Glycobiology*. 2010;20(4): 485–497.
231. Oguri S, Yoshida A, Minowa MT, Takeuchi M. Kinetic properties and substrate specificities of two recombinant human N-acetylglucosaminyltransferase-IV isozymes. *Glycoconj J*. 2006;23(7–8):473–80.
232. Ohtsubo K, Takamatsu S, Minowa MT, Yoshida A, Takeuchi M, Marth JD. Dietary and genetic control of glucose transporter 2 glycosylation promotes insulin secretion in suppressing diabetes. *Cell*. 2005;123(7):1307–21.
233. Ohtsubo K, Chen MZ, Olefsky JM, Marth JD. Pathway to diabetes through attenuation of pancreatic beta cell glycosylation and glucose transport. *Nat Med*. 2011;17(9):1067–75.
234. Fan J, Wang S, Yu S, He J, Zheng W, Zhang J. N-acetylglucosaminyltransferase IVa regulates metastatic potential of mouse hepatocarcinoma cells through glycosylation of CD147. *Glycoconj J*. 2012;29(5–6):323–34.

235. Ide Y, Miyoshi E, Nakagawa T, Gu J, Tanemura M, Nishida T, et al. Aberrant expression of N-acetylglucosaminyltransferase-IVa and IVb (GnT-IVa and b) in pancreatic cancer. *Biochem Biophys Res Commun.* 2006;341(2):478–82.
236. Niimi K, Yamamoto E, Fujiwara S, Shinjo K, Kotani T, Umezu T, et al. High expression of N-acetylglucosaminyltransferase IVa promotes invasion of choriocarcinoma. *Br J Cancer.* 2012;107(12):1969–77.
237. Indelicato R, Trinchera M. Epigenetic regulation of glycosylation in cancer and other diseases. *Int J Mol Sci.* 2021;22(6):2980.
238. Lauc G, Huffman JE, Pučić M, Zgaga L, Adamczyk B, Mužinić A, et al. Loci associated with N-glycosylation of human immunoglobulin G show pleiotropy with autoimmune diseases and haematological cancers. *PLoS Genet.* 2013;9(1):e1003225.
239. Wahl A, van den Akker E, Klaric L, Štambuk J, Benedetti E, Plomp R, et al. Genome-wide association study on immunoglobulin G glycosylation patterns. *Front Immunol.* 2018;26:9:277.
240. Klarić L, Tsepilov YA, Stanton CM, Mangino M, Sikka T, Esko T, et al. Glycosylation of immunoglobulin G is regulated by a large network of genes pleiotropic with inflammatory diseases. *Sci Adv.* 2020; 6(8):eaax0301
241. Huffman JE, Knežević A, Vitart V, Kattla J, Adamczyk B, Novokmet M, et al. Polymorphisms in B3GAT1, SLC9A9, and MGAT5 are associated with variation within the human plasma N-glycome of 3533 European adults. *Hum Mol Genet.* 2011;20(24):5000–11.
242. Thu CT, Mahal LK. Sweet Control: MicroRNA Regulation of the Glycome. *Biochemistry.* 2020; 59(34):3098-3110.
243. Cheng L, Gao S, Song X, Dong W, Zhou H, Zhao L, et al. Comprehensive N-glycan profiles of hepatocellular carcinoma reveal association of fucosylation with tumor progression and regulation of FUT8 by microRNAs. *Oncotarget.* 2016;7(38): 61199-61214.
244. Sun Y, Yang X, Liu M, Tang H. B4GALT3 up-regulation by miR-27a contributes to the oncogenic activity in human cervical cancer cells. *Cancer Lett.* 2016;375(2):284–292.

245. Schliekelman MJ, Gibbons DL, Faca VM, Creighton CJ, Rizvi ZH, Zhang Q, et al. Targets of the tumor suppressor miR-200 in regulation of the epithelial–mesenchymal transition in cancer. *Cancer Res.* 2011;71(24):7670–82.
246. Minami A, Shimono Y, Mizutani K, Nobutani K, Momose K, Azuma T, et al. Reduction of the ST6 β -galactosamide α -2,6-sialyltransferase 1 (ST6GAL1)-catalyzed sialylation of nectin-like molecule 2/cell adhesion molecule 1 and enhancement of ErbB2/ErbB3 signaling by microRNA-199a. *J Biol Chem.* 2013;288(17): 11845–11853.
247. Anugraham M, Jacob F, Nixdorf S, Everest-Dass AV, Heinzelmann-Schwarz V, Packer NH. Specific glycosylation of membrane proteins in epithelial ovarian cancer cell lines: Glycan structures reflect gene expression and DNA methylation status. *Mol Cell Proteomics.* 2014;13(9):2213–32.
248. Picardo F, Romanelli A, Muinelo-Romay L, Mazza T, Fusilli C, Parrella P, et al. Diagnostic and prognostic value of B4GALT1 hypermethylation and its clinical significance as a novel circulating cell-free DNA biomarker in colorectal cancer. *Cancers (Basel).* 2019;11(10):1598.
249. Fleischer T, Edvardsen H, Solvang HK, Daviaud C, Naume B, Børresen-Dale AL, et al. Integrated analysis of high-resolution DNA methylation profiles, gene expression, germline genotypes and clinical end points in breast cancer patients. *Int J Cancer.* 2014;134(11):2615–25.
250. Kroes RA, Moskal JR. The role of DNA methylation in ST6Gal1 expression in gliomas. *Glycobiology.* 2016;26(12):1271–83.
251. Antony P, Rose M, Heidenreich A, Knüchel R, Gaisa NT, Dahl E. Epigenetic inactivation of ST6GAL1 in human bladder cancer. *BMC Cancer.* 2014;14:901.
252. Kaburagi T, Kizuka Y, Kitazume S, Taniguchi N. The inhibitory role of α 2,6-sialylation in adipogenesis. *J Biol Chem.* 2017;292(6):2278–2286.
253. Zoldoš V, Grgurević S, Lauc G. Epigenetic regulation of protein glycosylation. *Biomol Concepts.* 2010; 1(3-4):253-61.
254. Dall'Olio F, Trinchera M. Epigenetic bases of aberrant glycosylation in cancer. *Int J Mol Sci.* 2017;18(5):998.

255. Kizuka Y, Kitazume S, Yoshida M, Taniguchi N. Brain-specific expression of N-acetylglucosaminyltransferase IX (GnT-IX) is regulated by epigenetic histone modifications. *J Biol Chem*. 2011;286(36):31875–84.
256. Kizuka Y, Kitazume S, Okahara K, Villagra A, Sotomayor EM, Taniguchi N. Epigenetic regulation of a brain-specific glycosyltransferase N-acetylglucosaminyltransferase-IX (GnT-IX) by specific chromatin modifiers. *J Biol Chem*. 2014;289(16):11253–11261.
257. Miyazaki K, Ohmori K, Izawa M, Koike T, Kumamoto K, Furukawa K, et al. Loss of disialyl Lewis(a), the ligand for lymphocyte inhibitory receptor sialic acid-binding immunoglobulin-like lectin-7 (Siglec-7) associated with increased sialyl Lewis(a) expression on human colon cancers. *Cancer Res*. 2004;64(13):4498–505.
258. Dannenberg LO, Edenberg HJ. Epigenetics of gene expression in human hepatoma cells: Expression profiling the response to inhibition of DNA methylation and histone deacetylation. *BMC Genomics*. 2006;7:181.
259. Horvat T, Deželjin M, Redžić I, Barišić D, Herak Bosnar M, Lauc G, et al. Reversibility of membrane N-glycome of HeLa cells upon treatment with epigenetic inhibitors. *PLoS One*. 2013;8(1):e54672.
260. Horvat T, Mužinić A, Barišić D, Bosnar MH, Zoldoš V. Epigenetic modulation of the HeLa cell membrane N-glycome. *Biochim Biophys Acta Gen Subj*. 2012;1820(9):1412–9.
261. Jinek M, Chylinski K, Fonfara I, Hauer M, Doudna JA, Charpentier E. A programmable dual-RNA-guided DNA endonuclease in adaptive bacterial immunity. *Science*. 2012;337(6096):816–21.
262. Tadić V, Josipović G, Zoldoš V, Vojta A. CRISPR/Cas9-based epigenome editing: An overview of dCas9-based tools with special emphasis on off-target activity. *Methods*. 2019;164–165:109–119.
263. Cong L, Ran FA, Cox D, Lin S, Barretto R, Habib N, et al. Multiplex genome engineering using CRISPR/Cas systems. *Science*. 2013;339(6121):819–23.
264. Deltcheva E, Chylinski K, Sharma CM, Gonzales K, Chao Y, Pirzada ZA, et al. CRISPR RNA maturation by trans-encoded small RNA and host factor RNase III. *Nature*. 2011;471(7340):602–607.

265. Dominguez AA, Lim WA, Qi LS. Beyond editing: Repurposing CRISPR-Cas9 for precision genome regulation and interrogation. *Nat Rev Mol Cell Biol.* 2016;17(1):5–15.
266. Breunig CT, Köferle A, Neuner AM, Wiesbeck MF, Baumann V, Stricker SH. CRISPR tools for physiology and cell state changes: Potential of transcriptional engineering and epigenome editing. *Physiol Rev.* 2021;101(1):177–211.
267. Groner AC, Meylan S, Ciuffi A, Zangger N, Ambrosini G, Dénervaud N, et al. KRAB-zinc finger proteins and KAP1 can mediate long-range transcriptional repression through heterochromatin spreading. *PLoS Genet.* 2010;6(3):e1000869.
268. Yeo NC, Chavez A, Lance-Byrne A, Chan Y, Menn D, Milanova D, et al. An enhanced CRISPR repressor for targeted mammalian gene regulation. *Nat Methods.* 2018;15(8):611–616.
269. Chavez A, Tuttle M, Pruitt BW, Ewen-Campen B, Chari R, Ter-Ovanesyan D, et al. Comparison of Cas9 activators in multiple species. *Nat Methods.* 2016;13(7):563–567.
270. Chavez A, Scheiman J, Vora S, Pruitt BW, Tuttle M, Iyer EP, et al. Highly efficient Cas9-mediated transcriptional programming. *Nat Methods.* 2015;12(4):326–8.
271. McDonald JJ, Celik H, Rois LE, Fishberger G, Fowler T, Rees R, et al. Reprogrammable CRISPR/Cas9-based system for inducing site-specific DNA methylation. *Biol Open.* 2016;5(6):866–74.
272. Lei Y, Zhang X, Su J, Jeong M, Gundry MC, Huang YH, et al. Targeted DNA methylation in vivo using an engineered dCas9-MQ1 fusion protein. *Nat Commun.* 2017;8:16026.
273. Choudhury SR, Cui Y, Lubecka K, Stefanska B, Irudayaraj J. CRISPR-dCas9 mediated TET1 targeting for selective DNA demethylation at BRCA1 promoter. *Oncotarget.* 2016;7(29):46545–46556.
274. Kim JM, Kim K, Schmidt T, Punj V, Tucker H, Rice JC, et al. Cooperation between SMYD3 and PC4 drives a distinct transcriptional program in cancer cells. *Nucleic Acids Res.* 2015;43(18):8868–83.
275. Su J, Huang YH, Cui X, Wang X, Zhang X, Lei Y, et al. Homeobox oncogene activation by pan-cancer DNA hypermethylation. *Genome Biol.* 2018;19(1):108.

276. Pflueger C, Tan D, Swain T, Nguyen T, Pflueger J, Nefzger C, et al. A modular dCas9-SunTag DNMT3A epigenome editing system overcomes pervasive off-target activity of direct fusion dCas9-DNMT3A constructs. *Genome Res.* 2018;28(8):1193–1206.
277. Huang YH, Su J, Lei Y, Brunetti L, Gundry MC, Zhang X, et al. DNA epigenome editing using CRISPR-Cas SunTag-directed DNMT3A. *Genome Biol.* 2017;18(1):176.
278. Tanenbaum ME, Gilbert LA, Qi LS, Weissman JS, Vale RD. A protein-tagging system for signal amplification in gene expression and fluorescence imaging. *Cell.* 2014;159(3):635–46.
279. Amabile A, Migliara A, Capasso P, Biffi M, Cittaro D, Naldini L, et al. Inheritable silencing of endogenous genes by hit-and-run targeted epigenetic editing. *Cell.* 2016;167(1):219–232.e14.
280. Stepper P, Kungulovski G, Jurkowska RZ, Chandra T, Krueger F, Reinhardt R, et al. Efficient targeted DNA methylation with chimeric dCas9-Dnmt3a-Dnmt3L methyltransferase. *Nucleic Acids Res.* 2017;45(4):1703–1713.
281. Morita S, Noguchi H, Horii T, Nakabayashi K, Kimura M, Okamura K, et al. Targeted DNA demethylation in vivo using dCas9-peptide repeat and scFv-TET1 catalytic domain fusions. *Nat Biotechnol.* 2016;34(10):1060–1065.
282. Liu XS, Wu H, Ji X, Stelzer Y, Wu X, Czauderna S, et al. Editing DNA methylation in the mammalian genome. *Cell.* 2016;167(1):233–247.e17.
283. Okada M, Kanamori M, Someya K, Nakatsukasa H, Yoshimura A. Stabilization of Foxp3 expression by CRISPR-dCas9-based epigenome editing in mouse primary T cells. *Epigenetics Chromatin.* 2017;10:24.
284. Chen T, Gao D, Zhang R, Zeng G, Yan H, Lim E, et al. Chemically controlled epigenome editing through an inducible dCas9 system. *J Am Chem Soc.* 2017;139(33):11337–11340.
285. Shrimp JH, Grose C, Widmeyer SRT, Thorpe AL, Jadhav A, Meier JL. Chemical control of a CRISPR-Cas9 acetyltransferase. *ACS Chem Biol.* 2018;13(2):455–460.
286. Chen LF, Lin YT, Gallegos DA, Hazlett MF, Gómez-Schiavon M, Yang MG, et al. Enhancer histone acetylation modulates transcriptional bursting dynamics of neuronal activity-inducible genes. *Cell Rep.* 2019;26(5):1174–1188.e5.

287. Kearns NA, Pham H, Tabak B, Genga RM, Silverstein NJ, Garber M, et al. Functional annotation of native enhancers with a Cas9-histone demethylase fusion. *Nat Methods*. 2015;12(5):401–403.
288. Guilinger JP, Thompson DB, Liu DR. Fusion of catalytically inactive Cas9 to FokI nuclease improves the specificity of genome modification. *Nat Biotechnol*. 2014;32(6):577–582.
289. Ran FA, Cong L, Yan WX, Scott DA, Gootenberg JS, Kriz AJ, et al. In vivo genome editing using *Staphylococcus aureus* Cas9. *Nature*. 2015;520(7546):186–91.
290. Gao Y, Xiong X, Wong S, Charles EJ, Lim WA, Qi LS. Complex transcriptional modulation with orthogonal and inducible dCas9 regulators. *Nat Methods*. 2016;13(12):1043–1049.
291. Lin L, Liu Y, Xu F, Huang J, Dugaard TF, Petersen TS, et al. Genome-wide determination of on-target and off-target characteristics for RNA-guided DNA methylation by dCas9 methyltransferases. *Gigascience*. 2018;7(3):1–19.
292. Cao J, Wu L, Zhang SM, Lu M, Cheung WKC, Cai W, et al. An easy and efficient inducible CRISPR/Cas9 platform with improved specificity for multiple gene targeting. *Nucleic Acids Res*. 2016;44(19):e149.
293. Ranganathan V, Wahlin K, Maruotti J, Zack DJ. Expansion of the CRISPR-Cas9 genome targeting space through the use of H1 promoter-expressed guide RNAs. *Nat Commun*. 2014;5:4516.
294. Pattanayak V, Lin S, Guilinger JP, Ma E, Doudna JA, Liu DR. High-throughput profiling of off-target DNA cleavage reveals RNA-programmed Cas9 nuclease specificity. *Nat Biotechnol*. 2013;31(9):839–43.
295. Hsu PD, Scott DA, Weinstein JA, Ran FA, Konermann S, Agarwala V, et al. DNA targeting specificity of RNA-guided Cas9 nucleases. *Nat Biotechnol*. 2013;31(9):827–32.
296. Concordet JP, Haeussler M. CRISPOR: Intuitive guide selection for CRISPR/Cas9 genome editing experiments and screens. *Nucleic Acids Res*. 2018;46(W1):W242–W245.
297. Monti M. Epigenetics protocols. *Eur J Histochem*. 2012;56(2):e20.

298. Schmittgen TD, Livak KJ. Analyzing real-time PCR data by the comparative CT method. *Nat Protoc.* 2008;3(6):1101–8.
299. Ye J, Coulouris G, Zaretskaya I, Cutcutache I, Rozen S, Madden TL. Primer-BLAST: a tool to design target-specific primers for polymerase chain reaction. *BMC Bioinformatics.* 2012;13:134.
300. Ceroni A, Maass K, Geyer H, Geyer R, Dell A, Haslam SM. GlycoWorkbench: A tool for the computer-assisted annotation of mass spectra of glycans. *J Proteome Res.* 2008;7(4):1650–9.
301. Cooper CA, Gasteiger E, Packer NH. GlycoMod - A software tool for determining glycosylation compositions from mass spectrometric data. *Proteomics.* 2001;1(2):340–9.
302. Štambuk T, Klasić M, Zoldoš V, Lauc G. N-glycans as functional effectors of genetic and epigenetic disease risk. *Mol Aspects Med.* 2021;79:100891
303. Stanley P. What Have We Learned from Glycosyltransferase Knockouts in Mice? *J Mol Biol.* 2016;428(16):3166-3182.
304. Michailidi C, Soudry E, Brait M, Maldonado L, Jaffe A, Ili-Gangas C, et al. Genome-wide and gene-specific epigenomic platforms for hepatocellular carcinoma biomarker development trials. *Gastroenterol Res Pract.* 2014;2014:597164.
305. Yang G, Wang Q, Chen L, Betenbaugh MJ, Zhang H. Glycoproteomic characterization of FUT8 knock-out CHO cells reveals roles of FUT8 in the glycosylation. *Front Chem.* 2021;9: 755238.
306. López-Cortés R, Muinelo-Romay L, Fernández-Briera A, Gil Martín E. High-throughput mass spectrometry analysis of N-glycans and protein markers after FUT8 knockdown in the syngeneic SW480/SW620 colorectal cancer cell model. *J Proteome Res.* 2024;23(4): 1379-1398.
307. Jia Z, Liao P, Yan B, Lei P. Comprehensive pan-cancer analysis of FUTs family as prognostic and immunity markers based on multi-omics data. *Discov Oncol* [Internet]. 2024 Oct 16;15(1):567.
308. Marx N, Dhiman H, Schmieder V, Freire CM, Nguyen LN, Klanert G, et al. Enhanced targeted DNA methylation of the CMV and endogenous promoters with dCas9-

- DNMT3A3L entails distinct subsequent histone modification changes in CHO cells. *Metab Eng.* 2021;66: 268-282.
309. Kizuka Y, Nakano M, Miura Y, Taniguchi N. Epigenetic regulation of neural N-glycomics. *Proteomics.* 2016;16(22):2854–2863.
 310. Chakraborty AK, de Frietas Sousa J, Chakraborty D, Funasaka Y, Bhattacharya M, Chatterjee A, et al. GnT-V expression and metastatic phenotypes in macrophage-melanoma fusion hybrids is down-regulated by 5-Aza-dC: Evidence for methylation sensitive, extragenic regulation of GnT-V transcription. *Gene.* 2006;374: 166-73.
 311. Marx N, Grünwald-Gruber C, Bydlinski N, Dhiman H, Ngoc Nguyen L, Klanert G, et al. CRISPR-based targeted epigenetic editing enables gene expression modulation of the silenced beta-galactoside alpha-2,6-sialyltransferase 1 in CHO cells. *Biotechnol J.* 2018;13(10):e1700217.
 312. Frkatović-Hodžić A, Mijakovac A, Miškeć K, Nostaeva A, Sharapov SZ, Landini A, et al. Mapping of the gene network that regulates glycan clock of ageing. *Aging.* 2023;15(24): 14509-14552.
 313. Galonska C, Charlton J, Mattei AL, Donaghey J, Clement K, Gu H, et al. Genome-wide tracking of dCas9-methyltransferase footprints. *Nat Commun.* 2018;9(1):597.
 314. Fu Y, Foden JA, Khayter C, Maeder ML, Reyon D, Joung JK, et al. High-frequency off-target mutagenesis induced by CRISPR-Cas nucleases in human cells. *Nat Biotechnol.* 2013;31(9):822–6.
 315. Kuscu C, Arslan S, Singh R, Thorpe J, Adli M. Genome-wide analysis reveals characteristics of off-target sites bound by the Cas9 endonuclease. *Nat Biotechnol.* 2014;32(7):677–83.
 316. Emmett MJ, Lazar MA. Integrative regulation of physiology by histone deacetylase 3. *Nat Rev Mol Cell Biol.* 2019;20(2):102–115.
 317. Guenther MG, Barak O, Lazar MA. The SMRT and N-CoR corepressors are activating cofactors for histone deacetylase 3. *Mol Cell Biol.* 2001;21(18):6091–101.
 318. Rahman MM, Tollefsbol TO. dCas9-HDAC8-EGFP fusion enables epigenetic editing of breast cancer cells by H3K9 deacetylation. *Eur J Cell Biol.* 2024;103(4):151463.

319. Guhathakurta S, Kim J, Adams L, Basu S, Song MK, Adler E, et al. Targeted attenuation of elevated histone marks at SNCA alleviates α -synuclein in Parkinson's disease. *EMBO Mol Med*. 2021;13(2):e12188.
320. See K, Kiseleva AA, Smith CL, Liu F, Li J, Poleshko A, et al. Histone methyltransferase activity programs nuclear peripheral genome positioning. *Dev Biol*. 2020;466(1–2): 90–98.
321. Wu Q, Wu J, Karim K, Chen X, Wang T, Iwama S, et al. Massively parallel characterization of CRISPR activator efficacy in human induced pluripotent stem cells and neurons. *Mol Cell*. 2023;83(7): 1125–1139.e8.
322. Kostyushev D, Brezgin S, Kostyusheva A, Ponomareva N, Bayurova E, Zakirova N, et al. Transient and tunable CRISPRa regulation of APOBEC/AID genes for targeting hepatitis B virus. *Mol Ther Nucleic Acids*. 2023;32: 478–493.
323. Parvanov ED, Tian H, Billings T, Saxl RL, Spruce C, Aithal R, et al. PRDM9 interactions with other proteins provide a link between recombination hotspots and the chromosomal axis in meiosis. *Mol Biol Cell*. 2017;28(3):488–499.
324. Smagulova F, Gregoret IV, Brick K, Khil P, Camerini-Otero RD, Petukhova GV. Genome-wide analysis reveals novel molecular features of mouse recombination hotspots. *Nature*. 2011;472(7343):375–8.
325. Baker CL, Walker M, Kajita S, Petkov PM, Paigen K. PRDM9 binding organizes hotspot nucleosomes and limits Holliday junction migration. *Genome Res*. 2014;24(5):724–32.
326. Kang JG, Park JS, Ko JH, Kim YS. Regulation of gene expression by altered promoter methylation using a CRISPR/Cas9-mediated epigenetic editing system. *Sci Rep*. 2019;9(1):11960.
327. O'Geen H, Bates SL, Carter SS, Nisson KA, Halmai J, Fink KD, et al. Ezh2-dCas9 and KRAB-dCas9 enable engineering of epigenetic memory in a context-dependent manner. *Epigenetics Chromatin*. 2019;12(1):26.
328. Wang Q, Chung CY, Chough S, Betenbaugh MJ. Antibody glycoengineering strategies in mammalian cells. *Biotechnol Bioeng*. 2018;115(6):1378–1393.

8. CURRICULUM VITAE

Ana Vujić was born on October 18, 1995, in Subotica, Serbia. In 2001, she moved with her family to the island of Rab, Croatia, where she completed her primary and secondary education, graduating from a general gymnasium. She earned her Bachelor's degree in Biology from the Faculty of Science, University of Zagreb in 2017, and continued at the same institution to obtain a Master's degree in Molecular Biology, graduating in 2019. During her studies, she was engaged in various student jobs, notably at AnimaLabs, a laboratory within the company InovaGen d.o.o., which specialized in DNA testing for hereditary diseases and traits in pets and domestic animals.

In January 2020, Ana began working in the Epigenetics research group led by Professor Vlatka Zoldoš at the Faculty of Science, University of Zagreb. She was employed as a project associate on the project CEKOM – Molecular Diagnostics. That same year, she commenced her PhD in Biology under Professor Zoldoš's mentorship. Her doctoral research focused on the application of the CRISPR/dCas9 system to investigate epigenetic regulation of genes involved in protein *N*-glycosylation. From 2020 to 2024, Ana was an active member of the Epigenetics group, with a brief break in 2023 during which she worked as a researcher at Genos d.o.o. In addition to her work on the CEKOM project, she also contributed as a project associate to the CardioMetabolic project. In April 2024, Ana transitioned to the pharmaceutical industry and is currently employed as a Quality Control Analyst at Pfizer in Zagreb.

During her PhD, Ana presented her work at two international conferences—one as a poster presentation and one as a short oral presentation. She is the first author of one original research article and co-author of another, published in a highly ranked scientific journal. In parallel with her research, Ana also contributed to teaching, assisting in practical classes for two university courses: Genetics and Epigenetics.

Published papers:

Vujić A, Klasić M, Lauc G, Polašek O, Zoldoš V, Vojta A. Predicting Biochemical and Physiological Parameters: Deep Learning from IgG Glycome Composition. *Int J Mol Sci.* 2024;25(18):9988.

Vičić Bočkor V, Foglar N, Josipović G, Klasić M, Vujić A, Plavša B, et al. Transcription Factors HNF1A, HNF4A, and FOXA2 Regulate Hepatic Cell Protein N-Glycosylation. *Engineering.* 2024;32:57-68.